To N.C.L. Library

Prof F Brown (U.S.A).

Certified Copy

Ph.D. Awarded

28.3.1968

COMPUTERISED

SEMICONDUCTING PROPERTIES OF DOPED BARIUM TITANATE

COMPUTERISED

A THESIS

SUBMITTED TO

THE UNIVERSITY OF POONA

FOR

THE DEGREE OF DOCTOR OF PHILOSOPHY

IN PHYSICS

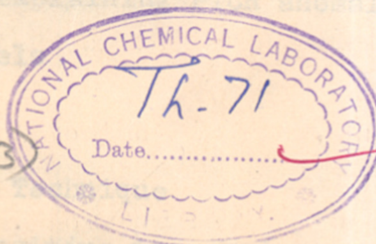

537.311.33 (043)
BRA

By

BHAGCHAND GULABCHAND BRAHMECHA, M.Sc.,

Solid State & Molecular Physics Group,

National Chemical Laboratory

Poona 8, (India)

MARCH - 1968

CONTENTS

Page

Acknowledgements

Synopsis

CHAPTER - 1 Introduction

1.1 General Introduction 1

1.2 Structure of $BaTiO_3$ 3

1.3 The Origin of Ferroelectricity 6

1.4 Survey of Semiconducting properties of $PaTiO_3$ 10
1.4.1 Polycrystalline data 10
1.4.2 Single crystal data 13

1.5 Practical Applications of Semiconducting $BaTiO_5$ 15

1.6 Mechanisms for explaining PTCR anomaly 17

1.7 Comments on Models 22

References 24

CHAPTER - 2 Experimental Technique

2.1 Processing of positive temperature coefficient thermistors ("Posistors") 29

2.2 Electrical resistivity (D.C.) Measurements 33

2.3 A. C. Measurements 34

2.4 Thermo-electric power measurements 38

2.5 V-I characteristics Measurements 39
References 40

CHAPTER - 3 Experimental Results and Discussion of Semiconducting properties of $BaTiO_3$

3.1 Ceramic Properties of Semiconducting BaTio3 41

3.2 D.C. Electric Properties 41

3.2.1 Voltage current relation 41
3.2.2 D.C. Resistivity 43
PTCR anomaly of several systems 46
3.2.3 Effect of frequency on PTCR 58

3 .3 A.C.Characteristics

3.3.1 Variation of Dielectric constant (Є) with temperature 59
3.3.2 Dispersion of (Є) and (e) at audio frequencies 62

3.4 Thermoelectric Effect 67

3.5 Nonohmic Metal-Semiconductor contact behaviour 73
References 82

CHAPTER - 4 A Theoretical Analysis of Resistively Anomaly

Introduction 84

Mathematical formulation 85

Estimates and discussion 93

References 97

ACKNOWLEDGEMENTS

I take this opportunity to express my deep sense of gratitude to Dr.K.P.Sinha for his meticulous planning, methodical and inspiring guidance during the pursuit of this work.

I am grateful to Dr.A.B.Biswas for his valuable guidance and keen interest in the initial stage of the work.

Further I wish to thank Dr.N.Kumar for stimulating discussions relating to the work of the Chapter IV. Thanks are due to all my colleagues for their ungrudging help.

Finally I am thankful to the Director, National Chemical Laboratory, Poona, for permission to submit this work in the form of a thesis.

Poona
1968

BGBrahmecha
(B.G.Brahmecha)

S Y N O P S I S

In contradistinction to the well known negative temperature coefficient of resistivity of usual thermistors, semiconducting $BaTiO_3$ is characterised by its PTCR (positive temperature coefficient of resistivity) anomaly beyond its transition temperature. It exhibits a phenomenal increase in resistance by more than thousand times within a short termperature interval. This unique property of semiconducting $BaTiO_3$ has opened up numerous avenues of practical applications and theoretical considerations.

During the past decade, continuing and extensive efforts have been made to understand the phenomenon of PTCR and its anomaly. Several mechanisms have been put forward. Inspite of some measure of success, they do not seem to explain all features of the experimental results. In the present work, an attempt has been made to explain the anomalous behaviour in terms of a new mechanism based on the idea of scattering of an electron by polarization fluctuations.

The thesis starts with an introductory survey of the origin of ferroelectricity in $BaTiO_3$. An account of various theories about the origin has been given. Then in the next section the work done to date on polycrystalline as well as single crystal semiconducting $BaTiO_3$ has been summarised. A critical analysis of the mechanisms proposed so far to explain PTCR anomaly has been given.

The second chapter deals with the details of experimental techniques. A detailed account of the preparation of semiconducting $BaTiO_3$ and techniques employed for studying several parameters has been given.

In the succeeding chapters the results and discussion of electrical conductivity, thermoelectric power, a.c. characteristics, rectification, barrier-layer capacitance phenomenon etc. of the following are given

1. $Ba_{1-x}La_xTiO_3$
2. $Ba_{1-x}Dy_xTiO_3$
3. $Ba(Ti_{1-x}Nb_x)O_3$
4. $Ba_{1-x}Tb_xTiO_3$
5. $Ba_{1-x}Er_xTiO_3$
6. (Ba, Sr) TiO_3 + 0.5 % Er.
7. (Ba, Ca) TiO_3 + 0.5 % Er.

The temperature range of study was 25°C to 200°C. X-ray analysis of typical compositions was performed at room temperatures. The contacts used for the study of electrical conductivity proved to be perfect ohmic throughout the temperature range. So the resistivity characteristic can be assumed to represent the bulk property of polycrystalline samples.

Among the compositions noted above, those having semiconducting properties exhibit PTCR anomaly. However, the resistivity at room temperature and the magnitude of PTCR anomaly are different for each additive.

Thermoelectric measurements and rectification study show that semiconducting $BaTiO_3$ is an n-type semiconductor. However, the thermoelectric power changes its sigh suddently and becomes positive above the transition temperature. Barrier-layer capacitance phenomenon shows that the type of junction formed between the semiconductor and the metal is Schottky type with the carrier concentration remaining nearly constant throughout the PTCR range. Therefore PTCR anomaly may be considered to be a mobility activated process.

The study of a.c. characteristics gives the following information: (1) dielectric behaviour of semiconducting samples of $BaTiO_3$ with temperature is similar to ferroelectric undoped ceramic $BaTiO_3$, i.e. above the Curie point they obey the Curie-Weiss law, (2) dispersion of dielectric constant and resistivity takes place in the audio-frequency region (i.e. from 500 c/s - 100 kc/s). Above the Curie point, a sharp rise in resistivity against temperature is observed at low frequencies. However, as the frequency is increased, the value falls off and tends to a constant value. This clearly shows that the sample (i.e. semiconducting $BaTiO_3$) consists of well conducting grains separated by low conducting layers.

X-ray analysis shows that there is no change in lattice constants of $BaTiO_3$ due to small percentage of doping.

The physical properties described above are relevant to the exposition of anomaly. In the light of above findings, the existing theories are suitably modified so as to conform with the experimental results.

C H A P T E R - I

CHAPTER - I

1.1 General Introduction

We have made remarkable progress in understanding quantitative details of many complex properties of semiconductors in terms of such concepts as energy bands, electrons and holes, phonons, polarons, excitons and a wide variety of interactions between them. These include scattering processes, recombination and trapping and so forth. In most cases, parameters such as energy gaps, effective masses and mobilities are determined empirically. Much ingenuity has gone into devising experiments to measure these quantities and great progress has been made in the theoretical interpretations of associated transport phenomena.

Creation and annihilation of the electron-hole pair in a semiconductor is associated with the introduction or evolution of a small quantity of energy. Therefore prospects for the application of semiconductors as energy transducers are rather attractive. Also, the corresponding devices are marked by their simplicity. For example semiconductors have led to new applications of energy conversion of heat, light or sound into electricity and

vice versa, to a control of temperature conditions, and various kinds of automatic devices. Semiconductors will, perhaps, fulfil the dream of centuries for the utilisation of solar energy.

Among semiconducting elements, "Thermistors" occupy an important position in view of their numerous practical applications and the fundamental electronic processes involved. The present work relates to a new type of thermistors having a positive temperature coefficient of resistivity (PTCR), also known as "Posistors". In contradistinction to the well-known negative temperature characteristics of usual thermistors, the posistors are characterised by their PTCR anomaly beyond a transition temperature. This feature opens up numerous avenues of practical applications and theoretical concepts.

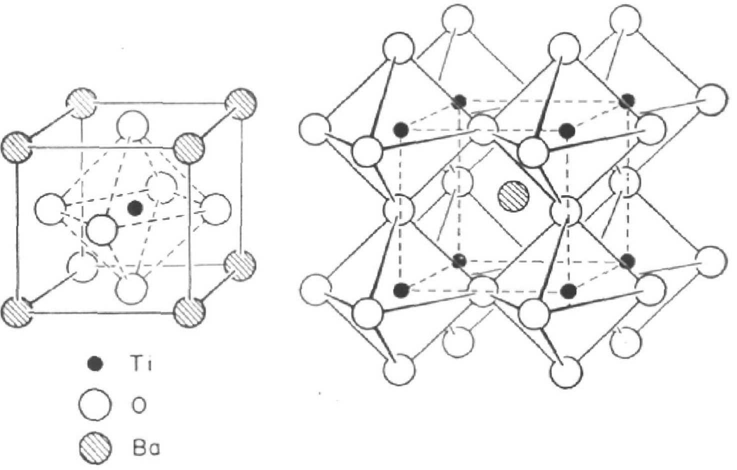

Fig. 1 Ideal perovskite structure.

1.2 Structure of $BaTiO_3$

Many compounds having the general formula ABO_3 are isomorphic with the structure of mineral perovskite $CaTiO_3$, the unit cell of which is ideally cubic with cell edge of about 4Å.

$BaTiO_3$ belongs to this family. It has the ideal perovskite structure[1] above the Curie Temperature as shown in Fig.1. All the atoms are in special positions

Ba at (0, 0, 0,) cube corners.

Ti at ($\frac{1}{2}$, $\frac{1}{2}$, $\frac{1}{2}$,) body centre

3 O's at ($\frac{1}{2}$, $\frac{1}{2}$, 0) ($\frac{1}{2}$, 0, $\frac{1}{2}$) (0, $\frac{1}{2}$, $\frac{1}{2}$) face centre.

a = 4.0Å with space group Pm 3m, and one formula unit per unit cell.

In order to visualize the continuity of structure, it is convenient to describe it by taking the origin at the Ti atom (cf. fig. 1). Thus each Ti atom is at the centre of 6 O-atoms, which are in turn placed at the corners of a regular octahedron. The octahedra are linked by their corners into a three dimensional framework, enclosing large holes which are occupied by the Ba atoms. The structure may also be looked upon as a face - centred

cubic close - packed arrangement of Ba^{2+} ion O^{2-} ions, every available octahedral hole between six O^{2-} ions being filled with a Ti^{4+} ion.

Below the Curie point the structure is tetragonal with a = 3.992 Å and c = 4.036 Å. This structure was worked out by Evans[2] using x-ray and by Frazer et. al.[3] using neutron diffraction methods. The oxygen octahedra are only slightly distorted. However, the Ti atoms are displaced relative to the centres of their octahedra by 0.13 Å, so that Ti-O bond lengths are altered by the Ti shift, whereas no large change occurs in the Ba-O bond length.

Below 0°C the structure becomes orthorhombic[4,5,6] with a = 5.682 Å, b = 5.669 Å, c = 3.990 Å. The unit cell is thus twice as large as the cubic cell and contains two formula units. The Ti atom is displaced from its symmetrical position by 0.06 Å.

Below - 90°C, the symmetry of the phase was found to be rhombohedral[7] (a = 3.998 Å) but the structure has not yet been determined. When $BaTiO_3$ is quenched from high temperatures ($\approx$ 1600°C), a hexagonal form is obtained. It is not ferroelectric.

In both the tetragonal and the orthorhombic phases, the slight distortion of the oxygen octahedra can be looked upon as being the result of the displacement of Ti and Ba along the polar axis. Thus the structure analysis clearly indicates the essential role played by the Ti atoms in the ferroelectric phenomenon.

1.3 The Origin of Ferroelectricity

Despite a considerable amount of experimental and theoretical investigations on ferroelectric crystals, our knowledge of the origin of phase transformation to the ferro-electric phase is still incomplete.

The earlier theoretical considerations were based on the close analogy between ferromagnetism and ferroelectricity. Following the work of Weiss[8] one can postulate for the internal field for ferroelectric system the relation:

$$F = E + \frac{4\pi}{3} P$$

where E = the external field, P = polarization of sublattice per unit volume, $\frac{4\pi P}{3}$ is the Lorentz term.

Adopting the view that polarization results on account of a displacive motion of the ions in $BaTiO_3$, the first successful attempt to describe the ferroelectricity was made by Devonshire.[9] He proposed a phenomenological theory of ferro-electric transition in $BaTiO_3$. In his theory emphasis has been given on the occurrence of multiple minima in the free energy function. He expressed the free energy of the crystal per unit volume by expressing it as a function of stress and polarization. This could explain the dielectric, piezoelectric and elastic behaviour of the crystal at any temperature by means of a 'single' free energy polynomial involving a limited number of terms.

Inspite of this, it is an approximation in the sense that a finite number of terms are used in the free energy. Secondly the same free energy expansion for both the cubic and tetragonal phase is used. Also the assumed complete ionic character of $BaTiO_3$ is doubtful. Various investigations including X-ray, neutron diffraction and infrared spectra reveal that $BaTiO_3$ has an intermediate character.[10,11-13]

Slater[14] modified Devonshire's theory by taking into account polarization of ions by distortion and the Lorentz correction for the values of the internal field at the ion sites.

Wigner[15] and Jaynes[16] extended Slater's work. They introduced an electronic theory in which the electronic states of the entire TiO_6 octahedra are considered rather than the electronic polarizabilities of the individual ions. On the supposition that excited electronic states lie close to the ground state, crystal field mixing was considered on account of dipole moment operator. It was a step in the right direction.

Further work on the properties of $BaTiO_3$ type ferroelectric crystals explored the possibilities of relating these properties in terms of Born and Von Karaman's[17] theory of lattice dynamics. The actual incorporation of the concept of time varying polarization instead of static one,[18] and its

relation to lattice dynamics was done by Cochran,[19] Anderson,[20] Landauer[21] et al. The main point in this approach is that the structure should become unstable with respect to certain vibrational modes at some temperature. Accordingly, the region where $\underline{K} = 0$, is responsible for the ferroelectric phase and the region where $\underline{K} = \pi/a$ is responsible for antiferroelectric phase, $\underline{K}$ being the propagation vector of transverse lattice vibrational modes. The temperature dependence of the frequency ω_T is given by $\omega_T^2 \, . \propto . \, (T - T_c)$, where T_c is a characteristic temperature. This could also explain the Curie-Weiss behaviour of the dielectric constant.

However, the above approach suffers from two drawbacks. Firstly below T_c , ω_T^2 is negative which, in turn, implies that the system is unstable in the harmonic approximation. Secondly it is not possible to predict the transition. Also they assumed that the electronic excited states are far removed from the ground state and are accordingly ignored in the lattice dynamics of the system. This is questionable.

These adhoc aspects are done away by Shukla and Sinha[22] by taking into account the role of electron-phonon coupling.

It will be noted from Section (1.2) that the octahedral structure is of paramount importance in the understanding of various ferroelectric properties of $BaTiO_3$. Von Hippel[23]

has remarked that in $BaTiO_3$ the ferroelectricity arises from a feed back coupling between the titanium and oxygen sublattices.

A quantum mechanical justification of the above has been given by Shukla and Sinha.[22] It has been shown that electron-vibration coupling in each elementary octahedron leads to the formation of permanent electric dipoles. These dipoles get ordered below T_c. However, the long-range order breaks down above the transition temperature. One can visualize fluctuations in these polarizations. In semiconducting $BaTiO_3$, the carriers (electrons) will undergo scattering by these spatial polarization fluctuations. In the last chapter, a theoretical formulation in terms of such scattering of carriers will be given.

1.4 Survey of Semiconducting Properties of $BaTiO_3$

1.4.1 Polycrystalline data:

The unique phenomenon of positive temperature coefficient of resistivity in semiconducting $BaTiO_3$ attracted the attention of many workers and a considerable amount of work on the properties of semiconducting $BaTiO_3$ has been performed. The work todate on polycrystalline $BaTiO_3$ may be summarised by the following points:

1) By the incorporation of trivalent rare earth ions[24-27] into the lattice of $BaTiO_3$ an n-type semiconducting system is obtained. Similar results are also obtained by reduction[26] of the titanate or by incorporation of certain other ions (Sb, Nb . . .)[26,47]

2) Semiconductivity is restricted within a short range of doping (0.1 - 0.5 mole %).

3) The resistivity is sensitive to the concentration of trace additives, to undesirable impurities in the raw materials and to sintering and maturing conditions.[30]

4) Room temperature resistivity in the case of high temperature equilibration with differing oxygen partial pressures of doped $BaTiO_3$ semiconductor is proportional to the doping concentration over a limited concentration range.

MacChesney's[46] explanation for this is based on Kroger's[62] generalised solution to the defect equilibria in terms of the concentration of imperfection.

5) Well below the ferroelectric Curie point of the host lattice the resistivity of these materials behaves 'normally' i.e. a slight negative temperature coefficient of resistivity is observed. However, several degrees below the Curie point the resistivity begins to increase and within a short interval of temperature at Curie point it suddenly jumps up by order of several hundreds. It continues increasing until a temperature of 50° to 100°C above the Curie point is achieved. At this point the materials again show normal behaviour. (Fig. 11).

6) The phenomenon of PTCR is sensitive to oxidation under certain non-equilibrium conditions.[45,46,52] Accompanying the enhanced PTCR, the room-temperature resistivity is increased by cooling in atmospheres of relatively high oxygen partial pressure. The formation of high resistivity surface layers could produce both these effects. The stability of Ti^{3+} which is associated with the semiconducting phase is reduced at high oxygen pressures and at low temperatures.[46] Therefore a concentration gradient of Ti^{3+} is established from the surface to the interior of such grain.[39]

7) The effect of non-stoichiometry is also observed on resistivity.[26,47]

8) The resistivity in the PTCR range is very sensitive to hydrostatic pressure or to uniaxial stress. The hydrostatic effects seem to be related to the stress-induced shift of the Curie temperature. There is some disagreement between workers regarding the sign of resistivity change. Saburi[29] found a decrease whereas Sauer et al.[28] observed an increase in resistivity with hydrostatic pressure.

9) D.C. resistivity is sensitive to the voltage applied during the measurement.[25,26]

10) Dielectric constant and resistance show dispersion effects in audiofrequency range.[26,36,46]

11) The sign of thermo-e.m.f., Hall coefficient clearly shows that it is an n-type semiconductor. Saburi[26] observed that the thermo-e.m.f. in semiconductor $BaTiO_3$ is independent of the temperature and the sign of the Seebeck coefficient does not change above the transition temperature. But according to Tennery and Cook,[31] the thermoelectric power and hence the Seebeck coefficient changes sign and becomes +ve at the transition temperature.

12) According to Saburi[54] and Ikushima[47] the carrier concentration is unchanged throughout the entire temperature range (including the Curie region) and PTCR is a mobility activated process. On the other hand Rayan and Subbarao[37] report that the carrier concentration decreases at the transition temperature. This is also observed by Tekster.[55]

13) The semiconductor - metal contact study shows that the Schottky type barrier layer is formed at the junction between semiconducting $BaTiO_3$ and metal[47,53].

14) The study of optical properties by Saburi[54] indicates that semiconducting $BaTiO_3$ shows an absorption ranging from 420 mμ upto infrared region, and this absorption characteristic is temperature independent. From this he concluded that band conduction does not take place here.

1.4.2: Single Crystal Data:

At present there is no unambiguous evidence that the PTCR is a property of homogeneous single crystals or that it is necessarily associated with the rare earth or similar ions incorporated into Barium titanate lattice. Divergent views have been expressed by different workers.

Goodman[40] has demonstrated that suitably doped single crystals, grown by a variant of the Czochralski technique, fail to show a PTCR, even though ceramic specimens made from these crystals do exhibit it. Similarly, Saburi[26] and Waku[63] also found no evidence of the PTCR anomaly in crystals grown from potassium fluoride flux, and doped by either lanthanum or tantalum. Also MacChesney[46] could not observe PTCR in single crystals of $(Ba, Sr)TiO_3$ doped with La and grown by Czochralski technique. However, after surface oxidation PTCR is developed. On the contrary

Bodanov and Rassustin[64)] reported PTCR in single crystals doped with lanthanum. Brown[42)] also observed PTCR effect in $BaTiO_3$ single crystals grown by the floating zone method, and doped with niobium. According to Takesh Tukeda,[51)] high electrical resistivity of $BaTiO_3$ single crystals grown by KF flux method, with low Gd^{+3} doping, is due to K^{+1} trap. However, when Gd^{+3} is heavily doped to exceed K^{+1}, the crystals become semi-conducting.

The PTCR effect is clearly observed in the case of reduced $BaTiO_3$ single crystals grown by KF flux.[26,38,41)] But the magnitude of the change was quite small as compared to polycrystalline samples.

1.5: Practical Applications:

The unique phenomenon of positive temperature coefficient of resistivity anomaly in semiconductor $BaTiO_3$ has led to several interesting applications in the electronic engineering field.[66-68] A few of these are briefly mentioned here.

Several examples of applications according to characteristics are listed in Table-1.

TABLE - 1

Group	Characteristic	Applications
A	Flat upto the transition temperature and very steep rise of resistance above T_c (High PTCR)	As a Sensing element: Thermal indicator, thermal regulator, fire alarm, very sensitive measurements of low pressures (10^{-6} mm./Hg) and high air velocities (10^{-2} mm/sec), overheat protector, contactless relay. As a heat dissipator Current limiter, current stabilizer, voltage stabilizer, automatic volume control, relay protection etc.
B	Flat upto the transition temperature T_c and fairly steep resistance rise above T_c (Low PTCR)	As a sensing element Temperature compensation of electronic apparatus, voltage stabiliser, thermometer, humidity meter, etc. As a heat dissipator as in the case of (A)

Besides the above applications, two more novel applications have been recently developed:

1) Using the technique of valence compensation, a part of the semiconducting $BaTiO_3$ sample may be converted into an insulator. Thus a certain number of resistors and capacitors, may be produced in one ceramic piece. This is similar to the integration circuit in TV receivers.[66]

2) Recently a new type of Capacitor having high dielectric constant and low loss factor has been developed by the diffusion of thin monovalent ionic layer into the semiconducting $BaTiO_3$.[69,70]

1.6: Mechanisms for explaining PTCR anomaly:

During the past decade continuing and extensive efforts have been made to understand the phenomenon of PTCR and its anomaly. Several mechanisms have been put forth. Sufficient information for deciding in the favour of any one model is, however, not yet available.

An account of various models is given below:

1) SABURI'S LOCAL FIELD MODEL:[54)]

According to him doping with a rare earth and other impurities leads to the formation of the Ti^{3+} ions. Comparison of the ionization potential values, viz.

2nd	ionization	potential	of Ba	= 9.95 eV.
3rd	"	"	" rare earths	= 20.5 eV.
4th	"	"	" Ti ~~ion~~	= 42.98 eV.

shows that a 3d electron is exchanged between Ti^{4+} and Ti^{3+} ions in the lattice of a compound such as $Ba^{2+}_{1-x}\ La^{3+}_{x}\ Ti^{4+}_{1-x}\ Ti^{3+}_{x}\ O^{2-}_{3}$. The exchange or hopping probability of electrons is large in the ferroelectric region owing to local field consideration, but becomes very small in the paraelectric region when the local field is negligible. This leads to the sudden decrease of carrier mobility and hence to the resistivity anomaly above the Curie point.

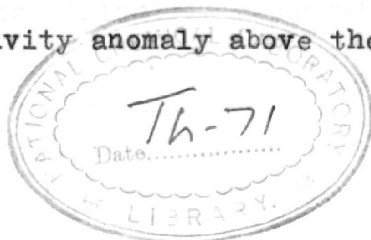
Th-71
Date.........

537.311.33(043)
BRA

By making use of the value of local field at Ti ion (3.8×10^8 volts/cm as reported by Kinase[56,57]) Saburi has worked out the model quantitatively. The field E_{Ti} is assumed to exist in a very short range near Ti ions (= 0.03 A°). Thus he derived a numerical value for the relative change in resistivity at the transition point which agrees well with the observed one.

The above model predicts an abrupt change of resistivity at the Curie point, whereas, in practice, the change is continuous in the range from 90°C to 175°C. To explain this discrepancy Saburi took into consideration the fact that the tetragonality of $BaTiO_3$ crystal is maintained upto 200°C at grain surfaces as reported by Kanzig.[60)]

2. HEYWANG'S GRAIN BOUNDARY MODEL[36)]

Heywang ascribed the origin of the PTCR anomaly to the grain boundary between the two n-type semiconducting crystals. The grain boundary consists of a number of surface states in which electrons can be trapped and hence a space charge is set up at the grain boundary. This space charge constitutes a potential barrier for conduction electrons and the barrier width, i.e. its tailing off distance into grains on either side, is assumed to be a function of its dielectric constant.

According to Heywang the relation for conductivity turns out to be

$$\sigma = \alpha\sigma_v \exp. (- \phi_o/kT),$$

where

σ_v = conductivity of the interior of grains

ϕ_o = Potential barrier at the grain boundary.

k = Boltzmann constant

T = Temperature ^oK

α = a geometrical factor.

The potential barrier

$$\phi_o = \frac{e^2 n_d r^2}{2\epsilon\epsilon_o} ,$$

where

e = electronic charge,

n_d = number of donors,

ϵ = dielectric constant of boundary layer,

ϵ_o = dielectric constant of vacuum.

Thus it appears that above the Curie temperature the decrease of (ϵ), according to Curie-Weiss law, produces

an increase in ϕ_o and hence the conductivity decreases above the Curie point. This increase in the potential barriers, with decreasing dielectric constant, continues only until the surface states reach the Fermi level at which point normal semiconductor behavior is resumed.

3. PERIA'S PIEZOELECTRIC STRESS-STRAIN MODEL:[61)]

The strong influence of composition and processing on the PTCR anomaly suggests that microstructures may play an important role in the behavior of these materials. Several of the proposed mechanisms for the anomaly, in fact, are based on the character of ceramic microstructure. Peria et al.[61)] postulate that the electrical resistance of the inter-grain contacts in such titanate ceramics is both non-ohmic and pressure sensitive. Consequently, the piezoelectric stress and strain generated at these grain boundaries when the unit-cell dimensions change discontinuously at the Curie point, causes their electrical resistivity to change abruptly. When the electrical resistivity of such a system is measured at a sufficiently high a.c. frequency the grain boundary capacitance shunts the high grain boundary resistance. One then finds a resistivity several orders of magnitude less than that of the d.c. case. This lower value represents the true or bulk resistivity of the grains.

The principal shortcoming of this model is that it does not account for the absence of large PTCR anomaly at the orthorhombic - tetragonal and rhombohedral - orthorhombic transitions, even though the accompanying changes in lattice constants are larger than that at the Curie point.[40)]

1.7 Comments on Models:-

All proposed mechanisms to-date describing PTCR phenomenon and its anomaly are essentially based either on Saburi's local field model or on Heywang's Grain Boundary model; a description of these was given in the previous section.

The two mechanisms are quite different from each other. Saburi's model is based on the principle of valence control[65] in which the conduction is by a hopping process. In this model, use has been made of the local field at Ti ion, which is a function of dipole interaction and spontaneous polarization. Therefore this model has linked the semiconducting and ferroelectric behaviour of $BaTiO_3$.

The observed experimental facts supporting this model are; (i) characteristic blue colour which proves the existence of Ti^{3+} ion, (ii) very low Hall mobiligy $\mu = 10^{-2}\ cm^2/v\text{-sec.}$, (iii) dependence of electric conductivity on crystal structure, (iv) PTCR phenomenon is not observed in any other pervoskite type crystals like $KNbO_3$, (Pb, Co) TiO_3 etc. where Ba^{2+} and Ti^{4+} are not present together.

The serious drawback in this model is that it permits the occurrence of the PTCR anomaly even in the absence of

grain boundaries. The anomaly is not observed in semiconducting $BaTiO_3$ doped with alkaline rare-earth oxides when fired in neutral atmosphere, when the surface states at the grain boundaries are absent.

As we have seen in the last section, Heywang has successfully described PTCR anomaly with the help of a model based on grain boundaries. It should, however, be pointed out that the idea of surface states, on which the model is based, has been introduced only phenomenologically and that only a scanty knowledge about their nature exists. Many questions concering the nature of surface states are still unanswered.

The pertinent question that cannot be answered by this model is as to why PTCR phenomenon is restricted to $BaTiO_3$ based ceramics. As pointed out by Jonker[44] even the highest value of the effective dielectric constant i.e. 10,000, is not high enough to account for the high conductivity exhibited by the doped titanate below the Curie point.

A critical study of the various mechanisms described reveals that inspite of some measures of success they cannot be accepted entirely. Thus there is scope for further work for the removal of these shortcomings. In the last chapter, an alternative mechanism based on the idea of scattering of an electron by spatial polarization fluctuations, has been given.

REFERENCES

1. H.D.Megaw, Proc. Roy. Soc. (London), 189, 261 (1947).
2. H.T.Evans, Tech. Report No.58, Laboratory for Insulation Research, Massachusetts Institute of Technology, (1953).
3. B.C.Frazer, H.Danner and R.Pepinsky, Phys. Rev., 100, 745 (1955).
4. H.F.Kay, Phil. Mag., 40, 1019 (1949).
5. F.Jona and R.Pepinsky, Phys. Rev., 105, 861 (1957).
6. R.G.Rhodes, Acta Cryst., 2, 417 (1949).
7. H.F.Kay and P.Vousden, Phil. Mag. Series, 7, 1019 (1949).
8. P.Weiss, J. de Physique, 6, 601 (1907).
9. A.F.Devonshire, Phil. Mag., 40, 1040 (1949); 42, 1065 (1951), Phil. Mag. Supplement 3, 85 (1954).
10. H.D.Megaw, 'Ferroelectricity in Crystal' (Methuen and Co.Ltd., London,1957).
11. M.A.Blokhin, Dokl. Akad. Nauk S.S.S.R., 95, 965, 1165 (1954).
12. G.A.Smolenskii, Zhur. Tekh. Fiz., 27, 1778 (1957).
13. L.E.Orgel, Discussion Far. Soc., 26, 138 (1958).
14. J.C.Slater, Phys. Rev., 78, 758 (1950).
15. E.P.Wigner, Unpublished, quoted by Jaynes, (1949).
16. E.T.Jayne, 'Ferroelectricity' [Princeton Univ. Press, London (1953)]
17. M.Born and K.Haung, 'Dynamical Theory of Crystal Lattice' (Oxford Univ. Press, N.Y. 1964).

18. H.R.Hagedorh, Z. Physik, 133, 394 (1952).

19. W.Cochran, Phys. Rev. Letter, 3, 1959; Adv. Phys., 9, 387 (1960).

20. P.W.Anderson, Fizika dielectrikov, Ed. G.I.Skanavi. Published by Akad. Nauk S.S.S.R. Moscow (1960) in Russian.

21. R.Landauer, H.Juretsche and P.Sorokin, (Unpublished manuscript, 1958).

22. G.C.Shukla and K.P.Sinha, J. Phys. Chem. Solids, 27, 1837 (1966).

23. A. Von Hippel, 'Dielectrics and Waves ' (John Wiley and Sons Inc. N.Y., 1954, pp.209)

24. P.W.Haayman et al. German Pat. 929350, (1955).

25. H.A.Sauer and S.S.Flaschen, Proc. Electronic Components Symposium, 7th Washington D.C., May (1956) p.41.

26. O. Saburi, Jr., Phys. Soc. Japan, 14 (9), 1159 (1959).

27. G.G.Harman, Phys. Rev., 106 (6), 1358 (1957).

28. H.A.Sauer and S.S.Flaschen, J.Am.Cer.Soc., 42 (8), 363 (1959).

29. O. Saburi, J. Phys. Soc., Japan, 15 (4) 733 (1960).

30. H.A.Sauer, J. Am. Cer.Soc., 43 (6) 297 (1960).

31. V.I.Tennery and R.L.Cook, J.Am.Cer.Soc., 44 (4) 187 (1961)

32. W.Heywang, Solid State Electronics 3, 51 (1961)

33. W.Heywang, Z. Angew. Phys., 16 (1) 1 (1963).

34. W.Heywant, Z. Angew. Phys., 18 (4), 316 (1965)

35. W.Heywang, Solid State Electronics, 8, 129 (1965).

36. W.Heywang, J. Am. Cer. Soc., 47 (10) 484 (1964).

37. F.M.Ryan and E.C.Subbarao, Appl. Phys. Lett. 1 (3), 69 (1962)

38. K.Kawabe and Y.Inuishi, Japan J.Appl.Phys., 2, 590 (1963)

39. T.Y.Tien and W.G.Carson, J.Am.Cer.Soc., 46 (6) 297 (1963)

40. G.Goodman, J.Am.Cer.Soc., 46 (1) 48 (1963)

41. S.I.Kegami and I.Udea, J.Phys.Soc. Japan, 19 (2) 1594 (1964)

42. F.Brown and C.E.Taylor, J. Appl. Phys., 35 (8) 2554 (1964)

43. G.Goodman, Japan J.Appl.Phys., 3, 123 (1964).

44. G.H.Jonker, Solidsstate electronics, 7, 895 (1964)

45. I.Udea and S.Ikegami, J. Phys. Soc. Japan, 20 (4) 546 (1965)

46. J.B.Macchesney and J.F.Potter, J.Am.Cer.Soc., 48 (2), 81 (1965).

47. H.Ikushima and S.Hayakawa, Japan Jr. Appl. Phys., 4 (5) 328 (1965).

48. C.R.Crowell et al., J. Appl. Phys., 36 (12), 3843 (1965).

49. P.Garthsen et al., Solid State Communication, 3, 165 (1965).

50. P. Gerthsen et al., Phys. Stat.Sold., 11 303 (1965) (German)

51. Takeshi Takeda et al., J. Phys. Soc. Japan, 21, 2414, (1966).

52. T.Ashida and H.Toyoda, Japan J. Appl. Phys., 5, (4) 269 (1966)

53. T.Murakami, Japan J. Appl. Phys., 5, 450 (1966)

54. O. Saburi, "An explanation of PTCR anomaly in semiconducting $BaTiO_3$". Presented at the Symposium on Dielectrics in the meeting of Phy. Soc. of Japan, Tokyo, April 2nd (1961).

55. G.N.Tekster, Fiz. Tverdogo Tela, 5, 3463 (1963).

56. W.Kinase and H.Takahashi, J. Phys. Soc. Japan, 10, 942, (1955).

57. W.Kinase and H.Takahashi, J. Phys. Soc. Japan, 12, 464 (1957)

58. F.J.Morin, Bell Syst. Tech. J., 37 (4) 1047 (1958)

59. Rees A.L.G., "Chemistry of the Defect Solid State", John Wiley Inc., N.Y. (1954), p. 68.

60. W.Kanzig, Phys. Rev., 98 (2) 549 (1955).

61. W.T.Peria et al., J. Am.Cer.Soc., 44 (5) 249 (1961).

62. F.A.Kroger and H.J.Vink, Phys. and Chem. Solids, 5, 208 (1958).

63. S.Wakui , Kogyo Kagaku Zasshi, 64, 1176 (1961).

64. S.V.Bodamov and Rassushin, Izv. Akad. Nauk SSSR, Ser. Fiz., 24 (10) 1247 (1960)

65. E.J.W.Verwey et al., Philips Res. Repts., 5 (6) 163 (1950).

66. Osamu Saburi, "Experimental Researches in Semiconducting $BaTiO_3$". Published by Murata Mfg. Co., 132 (1961). (Japan)

67. K.Kraus, Rev.Sci.Inst., 36, 1191 (1965).

68. E.Andrich and K.H.Hardtl, Philips Tech.Rev., 36, 119 (1965)

69. P.K.Gallagher, J.B.McChesney, U.S.Patent 3,292,062 (Cl. 317 - 258), Dec. 1966.

70. Toshio Ashida and Hiroo Toyoda, Japan J. Appl. Phys., 5, 269 (1966).

C H A P T E R - 2

CHAPTER - 2

EXPERIMENTAL TECHNIQUE

2.1 Processing of positive temperature coefficient Thermistors ("Posistors").

It was noted in Chapter 1 that there are a number of factors which affect the PTCR phenomenon. The resistivity in these systems is extremely sensitive to the concentration of additives, to undesirable impurities in the raw materials and to the sintering and maturing conditions. This fact is attested by the complex processing and composition procedures necessary to prepare an optimum "posistor".[1-3]

Here we will give an outline of the process followed by us for producing the posistor.

The first step in the process is the weighing out the ingredients in proper proportions to obtain the desired end composition e.g. an illustration of a particular composition is shown in Table-2. To compensate the deviation from the stoichiometry caused by impurities present, correction has been made as shown in Table-2. Phase equilibrium studies of the system BaO - TiO_2[4] indicate that compositions in which the TiO_2 concentration is greater than equimolar, an eutectic with barium metatitanate is formed which provides liquid phase above 1322°C. The presence

Table - 2

Typical Formulation of Erbium doped Barium-Strontium Titanate.

Compound	Mol.Wt.	Moles	Corrected for impurity	Wt.gms
$BaCO_3$	197.37	x 0.895	x 1/0.99	178.4
$SrCO_3$	147.63	x 0.100	x 1/0.991	14.896
TiO_2	79.9	x 1.005	x 1/0.99	80.7
Er_2O_3	382.4 x 1/2	x 0.005	x 1/0.99	0.9658

Fires to $Ba_{0.895}\ Sr_{0.1}\ Er_{0.005}\ TiO_3$ at $1400^{\circ}C$/1hr

of this liquid phase fosters the introduction of the dopant into the crystal lattice and also promotes the sintering process. To achieve this we have added a slight excess of TiO_2 (0.5 mole %).

Table-3 gives the information about the purity of raw materials used.

In order to achieve uniform dispersion of dopant throughout the bulk material a suitable ball milling process is employed, details of which are given in table No.4.

Table - 3

Raw Materials

Material	Supplies and grade	Major impurities (mole %)
$BaCO_3$	E.Merck (Germany) AR	$Cl = 0.002$, $NO_3 = 0.003$, $S = 0.0005$, $Pb = 0.001$ Calcium & alkaline sulphate = 0.1 $Fe = 0.001$
$SrCO_3$	Merck & Co.(N.J.USA) 99.1%	Insol.$HC_2H_3O = 0.025$ $Cl = 0.02$, $NO_3 = 0.01$, Alkali = 0.05, Salts = 0.3 $Ba = 0.02$, $Ca = 0.4$ $Pb = 0.002$, $Fe = 0.005$
$CaCO_3$	May and Baker (England) 98 %	-
TiO_2	Fluka (Switzerland) AG 99.5 %	-
Er_2O_3	Fluka (Switzerland) AG 99.9 %)	-

Table - 4

Mill Data

Type	- Porcelain Jar (Indian)
Size	- 1/2 lb (diameter = 2.5 in)
Grinding medium	- Hard glass balls (diameter = 0.65 in)
Number of balls	- 5 to 7
Wt. of balls	- 35 gms
Wt. of materials	- 6.8 gm substance + 20 c.c. water (double distilled)
Speed of revolution	- 60 r.p.m.
Duration	- 24 hours.

Mill size and type and size of grinding media are so chosen as to provide the lowest milling time, the most efficient mixing and grinding and the least contamination. The following flow sheet illustrates the outline of the salient features of the processing technique;

Raw materials (e.g. $BaCO_3$, $SrCO_3$, TiO_2 and doping element)

- Weighed in proper porportions
- mixed in ball mill
- Filtered and dried
- Calcined in air at 1100°C for one to two hours in platinum crucibles.

↓

White or yellowish crystalline, nonconducting blocks

- Crushed and mixed thoroughly in agate pestle and mortar.
- Dried and pressed into pellets at pressure of 10,000lbs/in^2 using polyvinal acetate binder 2%.
- Fired at 1350-1400°C in air for one hour on platinum lids at the rate of 100° to 200°C/hr

↓

Dark blue semiconducting $BaTiO_3$

FIG. 2. SAMPLE HOLDER ASSEMBLY FOR MEASURING D.C. RESISTIVITY

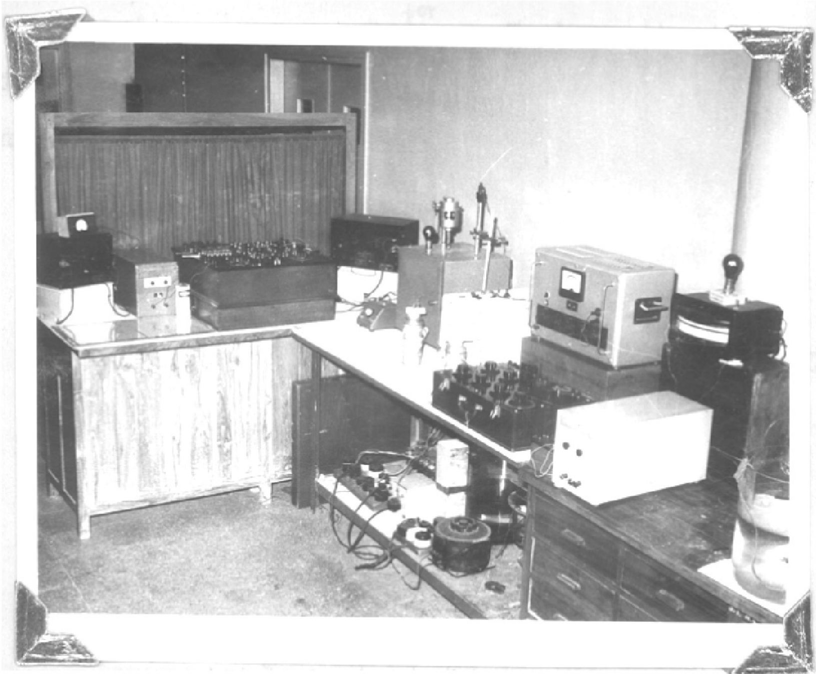

Experimental set up for D.C. resistivity measurements

2.2 Electrical Resistivity (D.C.) Measurements:

The pellet thus prepared was fixed between two electrodes of the sample holder shown in Fig.2. For heating the sample an air thermostat with a capacity of 5 litres was constructed. The temperature was controlled by using a 'Beckman' mercury regulator. To keep the temperature uniform inside the whole thermostate, a suitable rotating fan system was applied.

Technical Data

Temperature range	25°C to 200°C
Regulating accuracy	± 0.1°C
Voltage supply	230 volts
Heating capacity	1000 watts.

For measuring resistances of the order of 10^{-3} to 10^{8} ohms, Leeds and Northrup precision Jones conductivity bridge, which incorporates the Wheatstone's bridge circuit, was used. For D.C. supply external standard cells of 1.5 volts were used. A moving coil galvanometer of lamp and scale arrangement (sensitivity 10^{-8} amp/mm) was used as a detector.

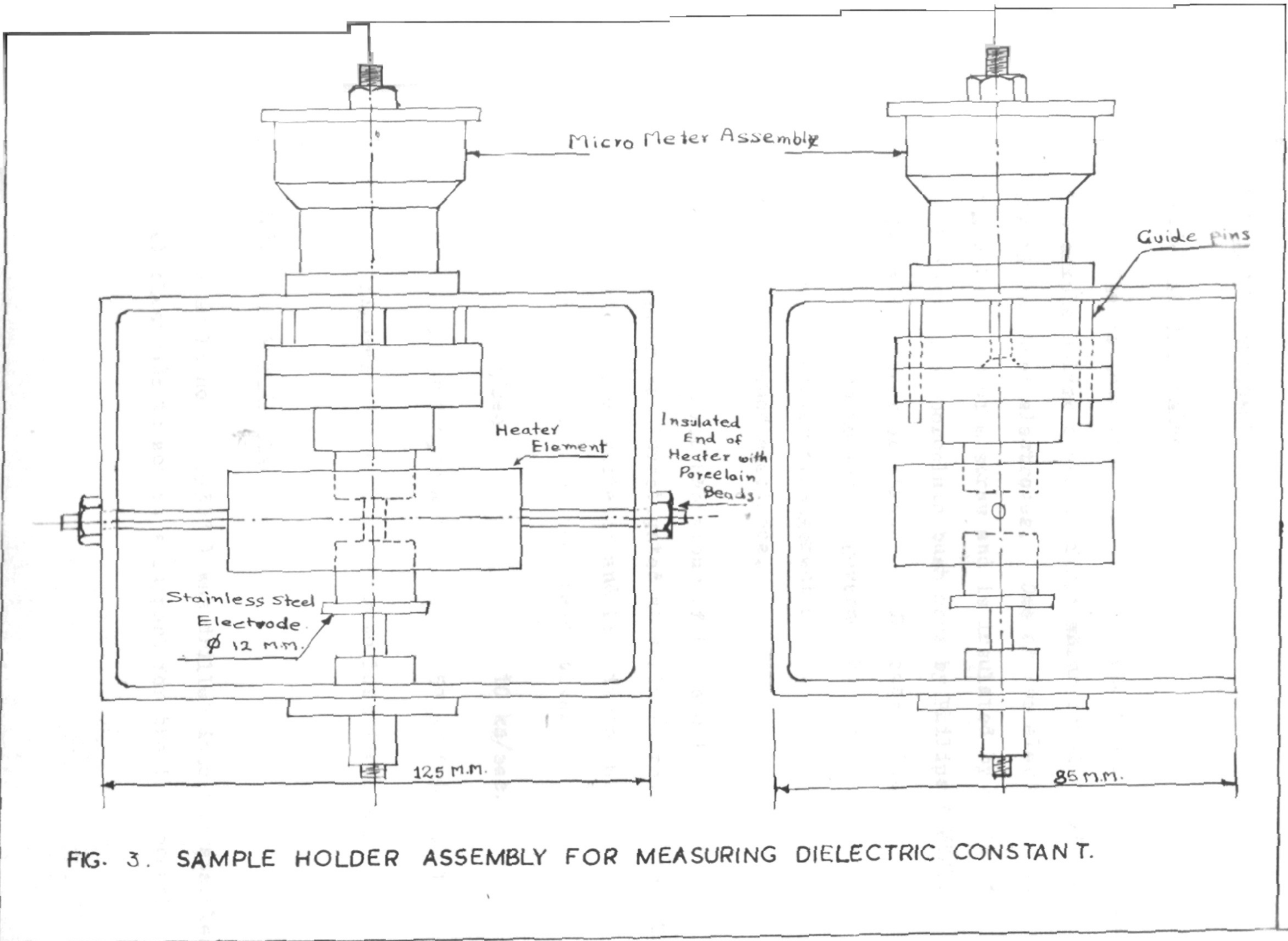

FIG. 3. SAMPLE HOLDER ASSEMBLY FOR MEASURING DIELECTRIC CONSTANT.

2.3 A/C Measurements:

2.3.1 Sample Holder

The pellets were fixed in between two electrodes of the sample holder shown in fig.3 which consists of two stainless steel electrodes. One of the electrodes is fixed by means of a screw and is insulated by means of a high insulation porcelain bush made by Philips (GMBH). This is the upper electrode. The other electrode is movable. The motion is governed by two guide pins, with the micrometer arrangement at the end of the electrode. This is the ground electrode.

The dielectric behaviour of the sample holder with air as medium was investigated at various frequencies. The contribution to capacitance and loss factor measured at 50v/cm is noted below at two frequencies.

1 kc/sec	10 kc/sec.
57 Pf (0.0034)	59 pf (0.0031)

(figures in brackets refer to loss factors)

2.3.2 Heating System

A small hole (3/32") was drilled into the stainless steel electrode to act as a support for the thermocouple tip.

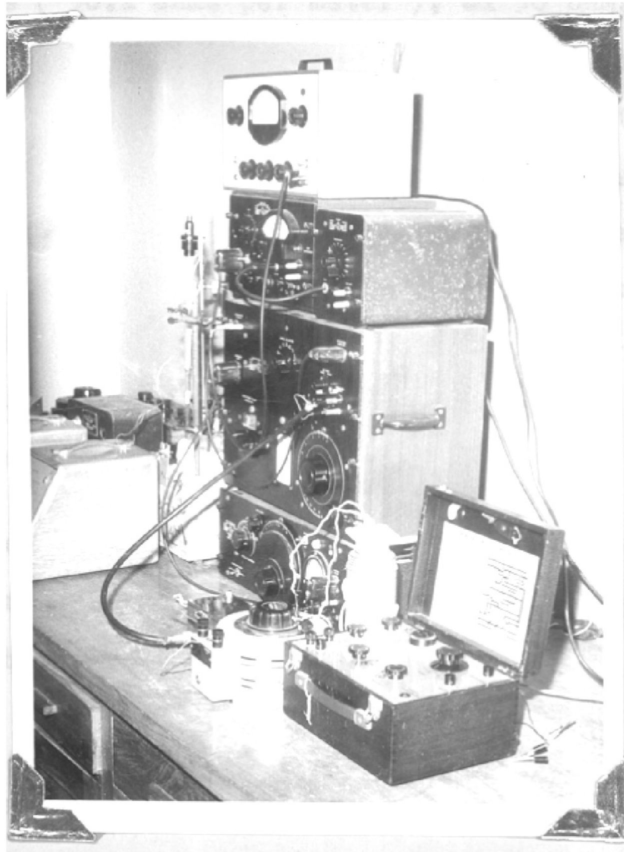

Experimental set up for A.C. measurements

A calibrated chromel-alumel thermocouple was used to measure the temperature with its cold junction placed in ice. The heating was done with the help of two circular band heaters (Sandwich type) encircling the electrodes. Kanthal tapes (30.2 ohms per meter), of 50 ohms resistance each, were used for heater. The sides of the sample holder box were lagged with MgO and asbestos powder to minimise heat losses. The temperature of the heater was fairly constant at the centre where the pellet was placed. As stainless steel is a fairly good thermal conductor and the thickness of the pellet being very small ($\sim$ 1 mm), the temperature of the pellet may be considered as uniform and recorded accurately by the thermocouple.

A variac (8 amperes, 220 volts) was used to control the temperature. The temperature remained constant within $\pm$ 2°C throughout the range i.e. upto 200°C.

A "PYE" (made in England) portable potentiometer was used to measure the thermocouple e.m.f.. The accuracy in this measurement was $\pm$ 0.2 % for voltages from 5 mv upwards.

2.3.3 Measurements of dielectric constant - A.C.resistivity their Dispersion and Barrier Layer Capacitance

For lower values of capacitance (from 100 PF to 1.0 μF at 1 KC and 100 PF to 1150 PF at other frequencies)

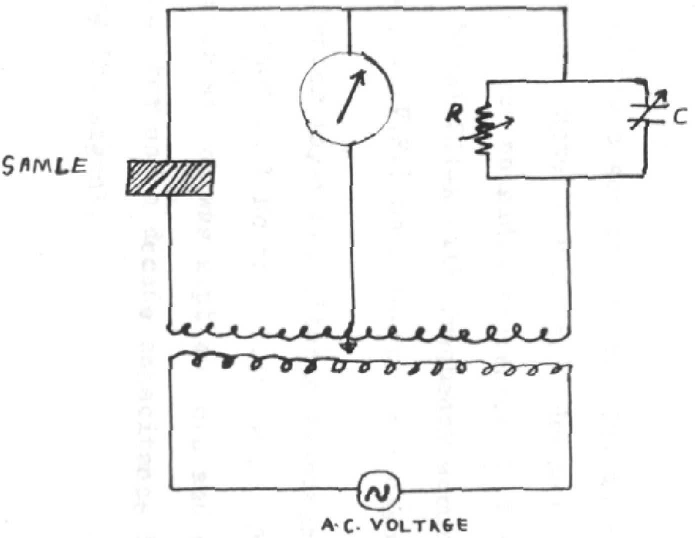

BLOCK DIAGRAM OF TRANSFORMER TYPE BRIDGE.

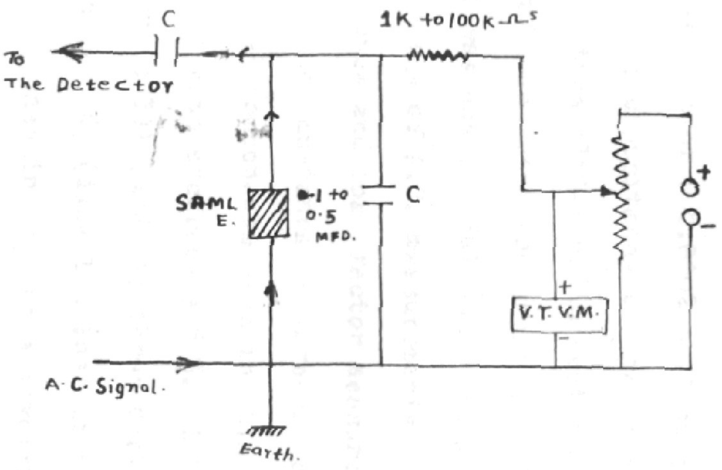

CIRCUIT USED FOR REVERSE BIAS SUPPLY.

Fig. No. 4.

and loss factor (0.0002 to 0.56); the general radio 716-C type capacitance bridge together with accessories such as type 1340-B audio beat frequency generator, 1231-B type null detector and amplifier with 1231-P_5 type variable filter was used. But this bridge could not cover the whole range of A.C. measurements. For higher values of capacitance and loss factor measurements, a "transformer type - wide impedance" bridge was constructed (Fig.4). Electrical components used in this bridge were (i) carbon resistors with accuracy ± 5 %, (ii) decade capacitor box 'OSAW Mo. 30391 (India); three dials of 0.001, 0.01, 0.1 mfd, accuracy ± 5 %, (iii) low loss iron core transformer giving linear response in the whole investigated audio frequency region.

The above generator was also used for dispersion measurements upto 40 kc/sec. However, in the range 50 kc/sec to 100 kc/sec, an audio generator [Forbes Cambel and Co. (India) Model 201-A with frequency accuracy ± 5 %] and Philips (V.T.V.M.) as detector were used.

Barrier layer capacitance measurements were done by direct method at 1 Kc on G.R.Bridge. The position of loss factor switch was kept on zero and an external standard resistance box and a decade capacitance box were used for balancing the signal.

The capacitance measurements of the non-ohmic barriers (metal - semiconductor junctions) were carried out with the help of an auxiliary circuit for reverse bias supply as shown in Fig.4.

FIG. 5.

Sample Holder for Measuring Thermo E.M.F.

2.4 Thermoelectric Power Measurements:

Specimens used for this were in the form of rectangular plates with dimensions $\sim 1.5 \times 0.5 \times 0.1$ cm. The specimen was held in a brass block sample holder shown in fig.5. Of the two methods used viz. differential and integral, the first was used for this measurements. The technique consists in establishing the temperature difference between two ends by heating one end with a microheater. The microheater is made of a spiral coil of nicrom wire ($\sim$ 30 ohms per meter) of 20 to 30 ohms resistance. This coil was inserted in a small thermocouple sheeth. A variac (8 ampers, 220 volts) was used to control the temperature.

The ambient temperature was varied by outer silica tube furnace surrounding the sample holder. Proper care was taken to avoid the sudden heat changes due to air flow.

The temperatures of both ends of the specimen were measured by embedded chromel-alumel thermocouples just under the ends of the recesses holding the ends of the specimen.

The thermo e.m.f. was mesured on a high precision vernier type D.C.potentiometer ["KAYCEE" Bajaj elec.(India)] capable of reading down to one microvolt. To determine the sign of the thermo.e.m.f. a high sensitive moving coil galvanometer with lamp and scale arrangement was used. (Sensivity of the galvanometer 10^{-8} amps/mm)

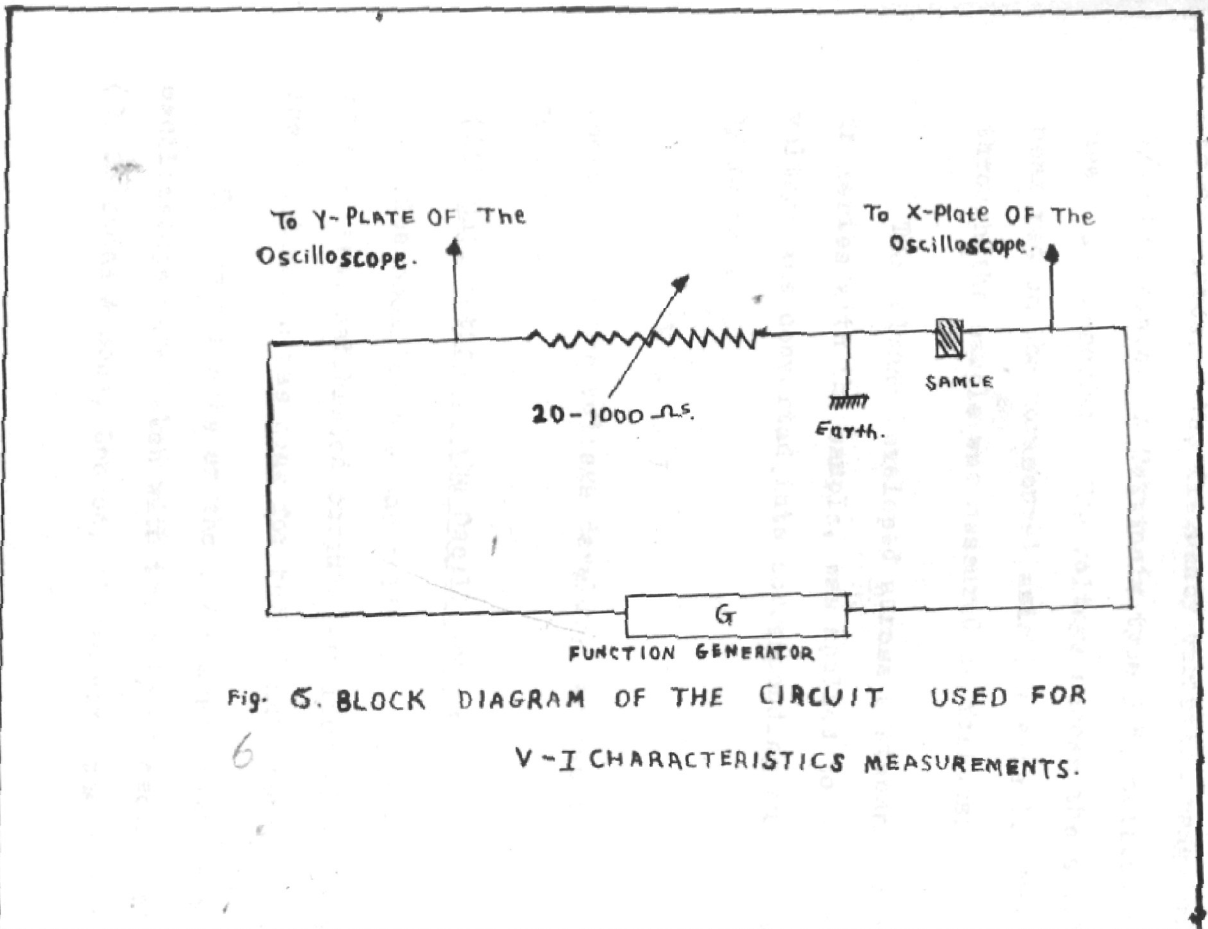

Fig. 6. BLOCK DIAGRAM OF THE CIRCUIT USED FOR V-I CHARACTERISTICS MEASUREMENTS.

2.5 V - I Characteristics Méasurement

(i) Circuit

A simple circuit as shown in Fig.6 was used. An APLAB low frequency generator type OS-1 was used as a power source. The frequency variation range was 1/400 to 1/.0004, c.p.s. A Tekttonix type 515 oscilloscope was used as a recorder. The voltage across the sample was measured on the horizontal axis (x axis). The current through the sample was measured as follows:

The voltage developed across a standard resistance, in series with the sample, was applied to Y -plates. This voltage was converted into corresponding current value 'I' by formula

$$V = R I$$

where 'V' is the voltage developed across the standard resistance R.

(ii) Calibration of the Oscilloscope:

The oscilloscope was calibrated with the help of the square wave, calibrated output, supplied with the oscilloscope. The calibration was done for both X axis as well as Y axis.

The photographs of the I-V characteristics on the oscilloscope were taken with the help of oscilloscope camera (D. Shackman & Sons, London) fitted with the oscilloscope.

REFERENCES

1. P.W.Haaijman, R.W.Dam and H.A.Klasens, Netherlands Pat. 84,015 Feb. (1957).

2. Yoshio Ichikkawa, U.S.Pat. 2,981,699 April (1961)

3. H.A.Sauer, J.R.Fisher, J.Am.Cer.Soc., 43, 297 (1960)

4. D.E.Rase and Rustum Roy, J.Am.Cer.Soc., 38, 102 (1955).

CHAPTER - 3

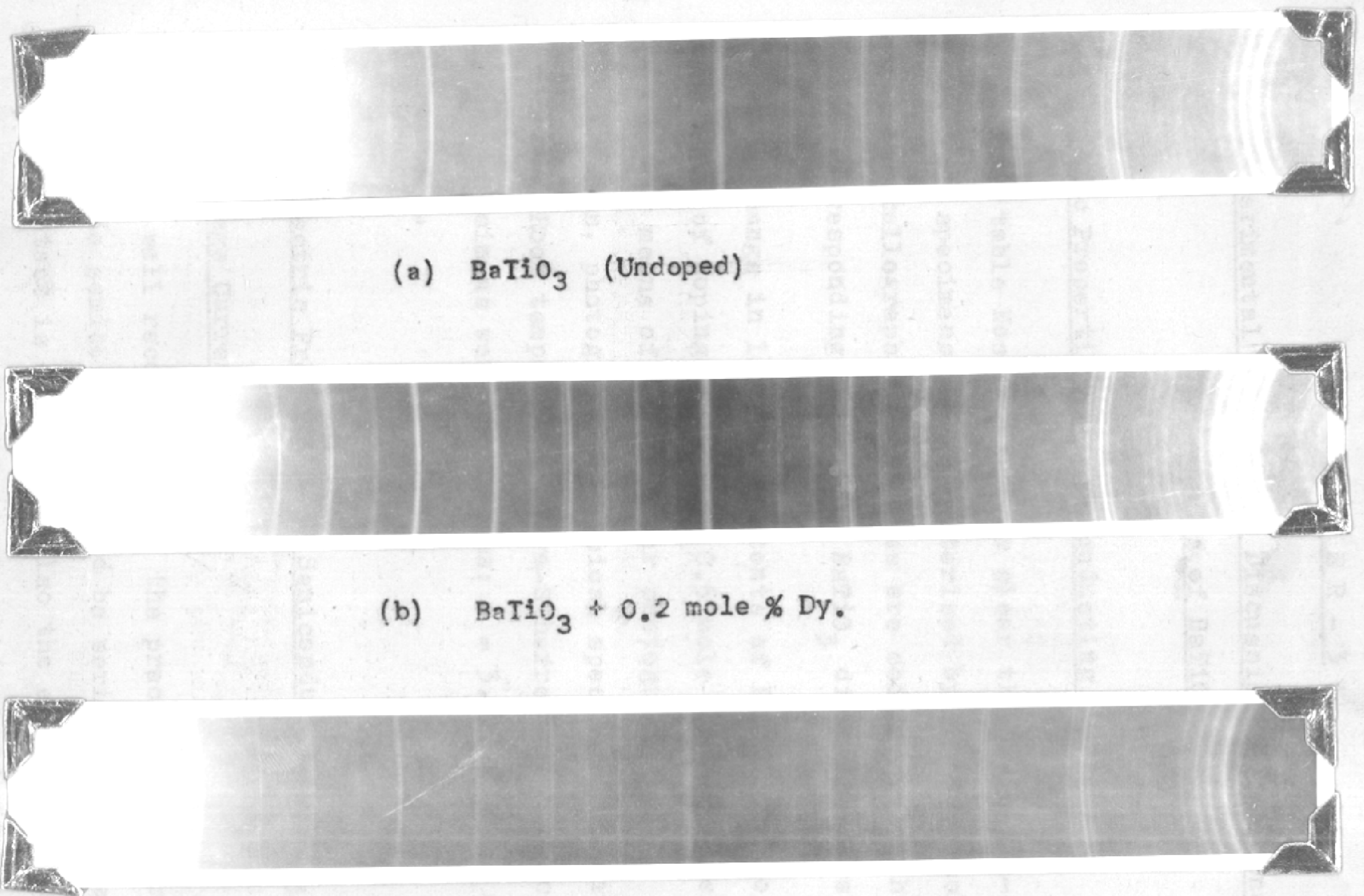

(a) $BaTiO_3$ (Undoped)

(b) $BaTiO_3$ + 0.2 mole % Dy.

(c) $BaTiO_3$ + 0.5 mole % Er.

Fig.7. Powder photographs of some typical materials at room temperature (CuKα radiation)

C H A P T E R - 3

Experimental Results and Discussion of Semiconducting Properties of $BaTiO_3$

3.1 Ceramic Properties of Semiconducting $BaTiO_3$

From table Nos. 5-11 it is clear that the semiconducting specimens are characterised by the blue colour. Their crystallographic properties are coincident with those of the corresponding members of $BaTiO_3$ dielectric systems.

No change in lattice constants of $BaTiO_3$ due to small percentage of dopings (0.05 to 0.5 mole %) could be observed by means of x-ray powder photographs. For illustration, photographs of typical specimens are given in Fig.7. Room temperature Debye-Scherrer lattice constants for all specimens were as follows: $a = 3.992$ Å , $C = 4.036$ Å $c/a = 1.011$.

3.2 D.C.Electric Properties of Semiconducting $BaTiO_3$

3.2.1 Voltage Current relation

It is well recognised that the practical applications of this oxide semiconductor would be seriously limited unless an ohmic contact is obtained. Also the electrode contact resistance effects act against the achievement of true bulk property determination.

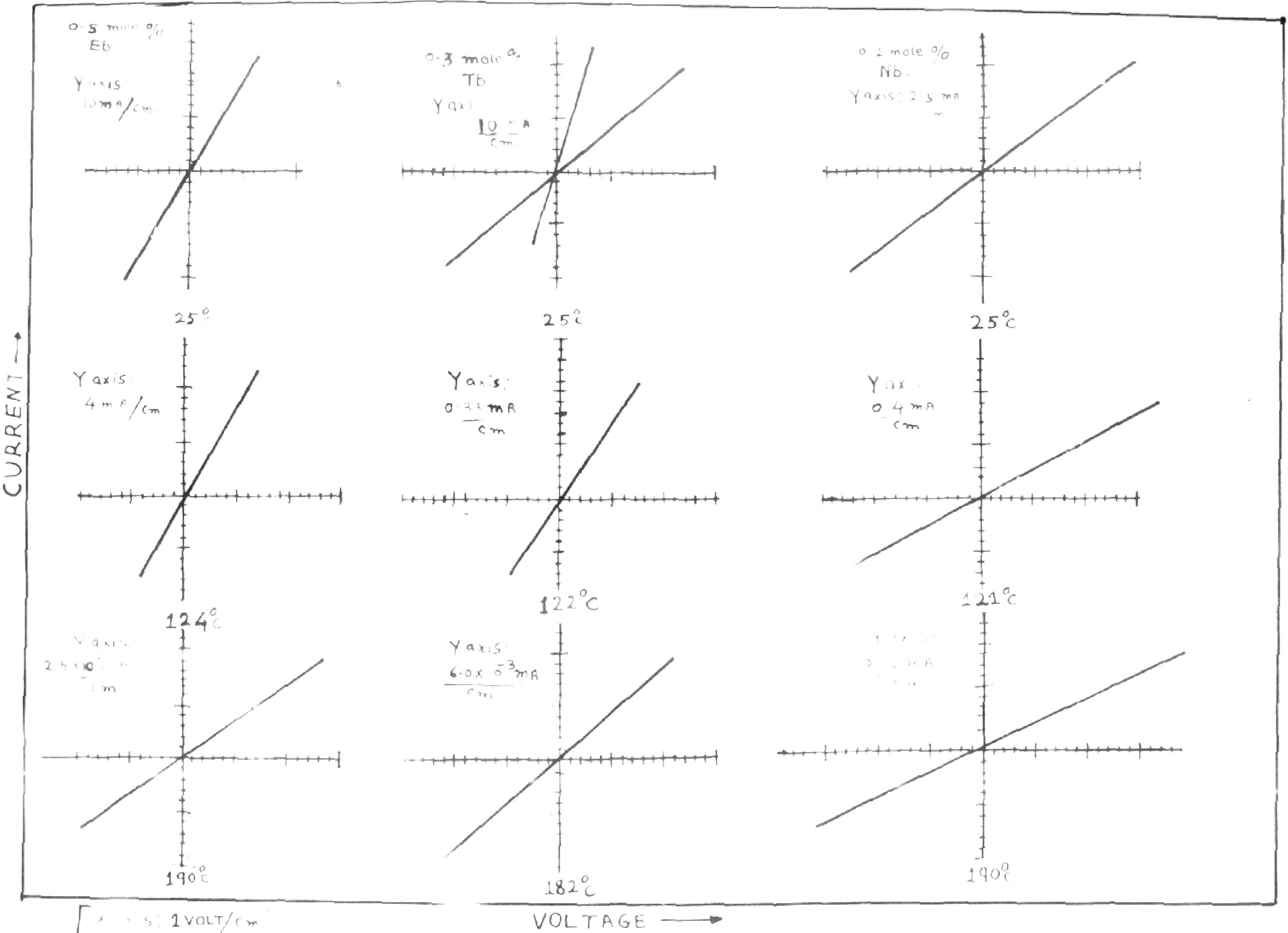

FIG 9 LTAGE RRENT CHA ERISTIC OF SEMIC NDUCTING $BaTiO_3$

Various models have been proposed theoretically from quantum mechanical considerations for explaining a dc ohmic contact between a metal and a semiconductor. Phenomenologically such a contact is, of course, defined by the fact that it obeys Ohm's law and fulfils the following criteria:[1] (1) the threshold voltage for zero current is negligible with respect to the applied voltage and (2) the proportionality factor between current and voltage (i.e. the conductivity) does not vary measurably with voltage. Both conditions (1) and (2) must be satisfied within a reasonable voltage range.

An exhaustive list of the materials and processes tried for semiconductor $BaTiO_3$ has been given by Sauer and Flachen.[2]). Flaschen and Van Uitert[3]) successfully studied the low contact resistance behaviour of indium alloys. Sauer and Turner[4]) showed that electroless as well as electroplated nickel contact with heat treatment proved to be ohmic.

In the present work, we have used indium-mercury electrodes. They were examined to ascertain whether they satisfied the above criteria for ohmic contacts throughout the temperature range of study. An example of the data obtained is shown in Fig.8. It shows clearly that the contacts are ohmic in the whole temperature region ($25^{\circ}C$ to $200^{\circ}C$). Thus the measured resistivity is the true bulk resistivity of the polycrystalline samples.

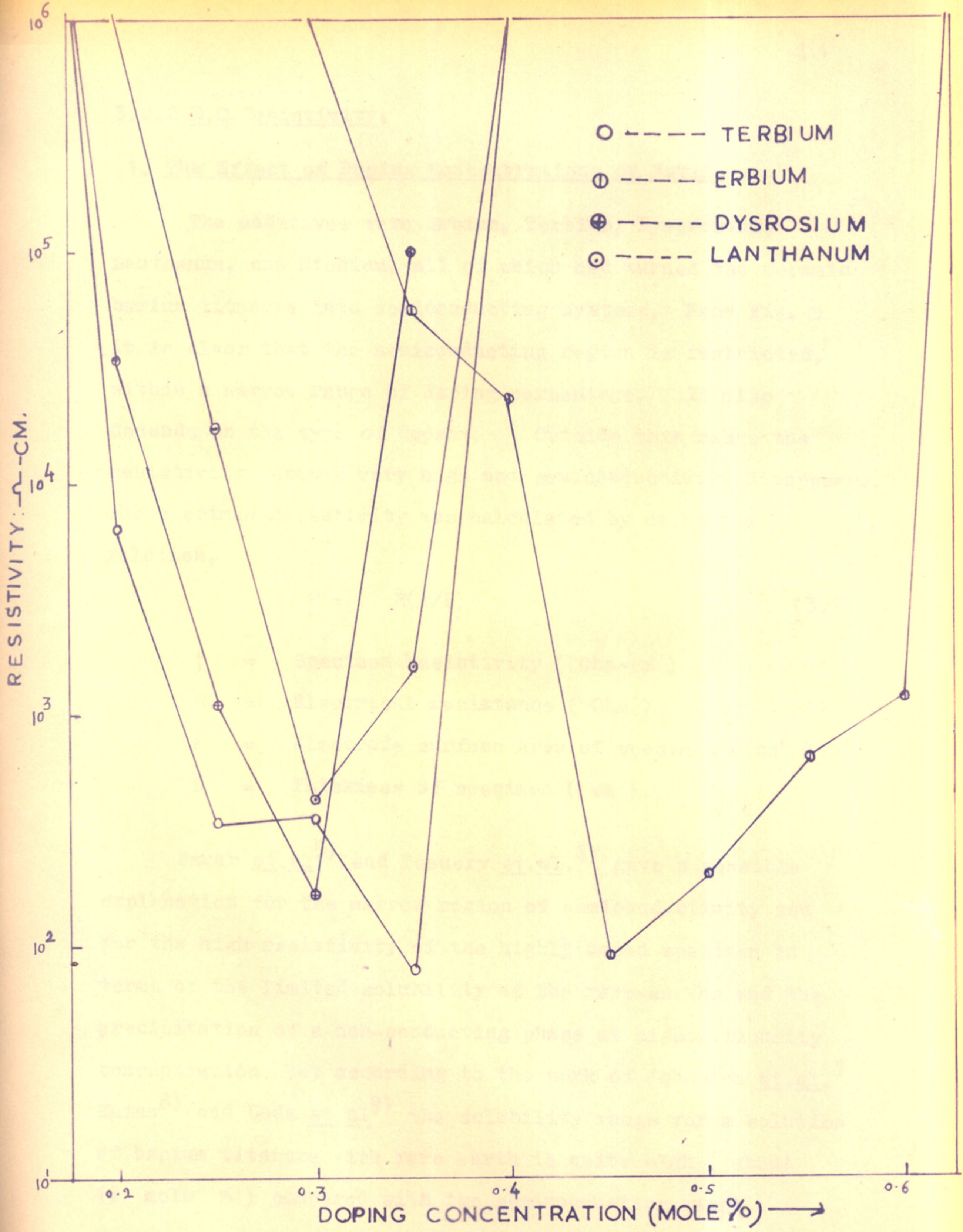

FIG. 9. DEPENDENCE OF RESISTIVITY ON % CONCENTRATION OF DOPINGS.

3.2.2 D.C.Resistivity:

1. The Effect of Doping Concentrations on $BaTiO_3$

The additives were Erbium, Terbium, Dysprosium, Lanthanum, and Niobium, all of which had turned the ceramic barium titanate into semiconducting systems. From Fig. 9 it is clear that the semiconducting region is restricted, within a narrow range of doping percentage. It also depends on the type of dopant. Outside this range the resistivity becomes very high and semiconductivity disappears. The specimen resistivity was calculated by using the relation,

$$\rho = R(A/L) \qquad (3.1)$$

ρ = Specimen resistivity (Ohm-cm)

R = Electrical resistance (Ohm)

A = Electrode surface area of specimen (cm^2)

L = Thickness of specimen (cm).

Sauer et.al.[5)] and Tennery et.al.[6)] gave a possible explanation for the narrow region of semiconductivity and for the high resistivity of the highly doped specimen in terms of the limited solubility of the rare-earths and the precipitation of a non-conducting phase at higher impurity concentration. But according to the work of Johnston et.al.[7] Kainz[8)] and Ueda et al[9)] the solubility range for a solution of barium titanate with rare earth is quite high (about 16 mole %) compared with the semiconducting range .

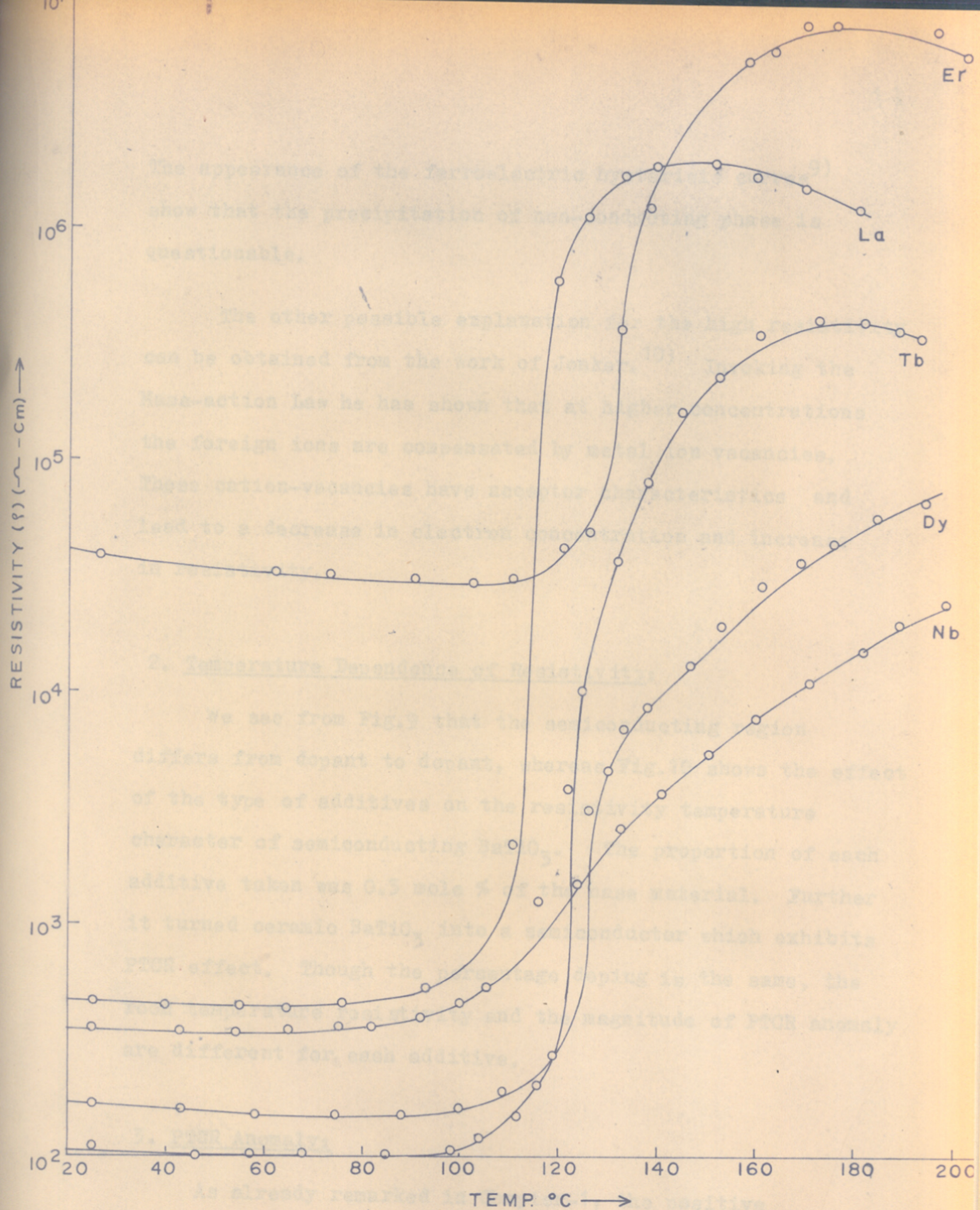

Fig. 10. Resistivity - Temperature characteristics of Semiconducting Barium Titanate containing 0·3 mole % additives.

The appearance of the ferroelectric hysterisis curves[9] show that the precipitation of non-conducting phase is questionable.

The other possible explanation for the high resistivity can be obtained from the work of Jonker.[10] Invoking the Mass-action Law he has shown that at higher concentrations the foreign ions are compensated by metal ion vacancies. These cation-vacancies have acceptor characteristics and lead to a decrease in electron concentration and increase in resistivity.

2. Temperature Dependence of Resistivity:

We see from Fig.9 that the semiconducting region differs from dopant to dopant, whereas Fig.10 shows the effect of the type of additives on the resistivity temperature character of semiconducting $BaTiO_3$. The proportion of each additive taken was 0.3 mole % of the base material. Further it turned ceramic $BaTiO_3$ into a semiconductor which exhibits PTCR effect. Though the percentage doping is the same, the room temperature resistivity and the magnitude of PTCR anomaly are different for each additive.

3. PTCR Anomaly:

As already remarked in Chapter-1, the positive temperature coefficient of resistivity (PTCR) anomaly is

10^6

10^5

$x = 0.35\ \%$

$x = 0.4\ \%$

RESISTIVITY (ρ) (Ω - Cm.) ⟶

10^4

$x = 0.6\ \%$

10^3

$x = 0.55\ \%$

$x = 0.5\ \%$

10^2

$x = 0.45\ \%$

20 40 60 80 100 120 140 160 180 200

TEMP. °C ⟶

Fig. 11 Dependence of resistivity-temp. characters on the content of Erbium.

Table No.5

Ceramic and Electric Data of Compositions in the system $Ba_{1-x}Er_xTiO_3$

Sample No.	Chemical formula	Firing Temp (°C)	Soaking time (hr)	Colour	Curie point °C	Resistivity at 25°C (Ω.cm)	Temp. of α_{max} °C	max temp. coefficient of α_{max} %/°C	ΔE_1 (eV)	ΔE_2 (eV)	Lattice Parameters at 25°C	
											a-axis Å	c-axis Å
E_1	$Ba_{0.9995}Er_{0.0005}TiO_3$	1400	2 hr	Yellowish gray	-	$>10^8$	-	-	-	-	-	-
E_2	$Ba_{0.999}Er_{.001}TiO_3$	"	"	Gray	-	"	-	-	-	-	-	-
E_3	$Ba_{.9985}Er_{.0015}TiO_3$	"	"	Gray	-	"	-	-	-	-	-	-
E_4	$Ba_{.998}Er_{.002}TiO_3$	"	"	Ivory gray	-	"	-	-	-	-	-	-
E_5	$Ba_{.0075}Er_{0.0025}TiO_3$	"	"	Gray	-	"	-	-	-	-	-	-
E_6	$Ba_{.997}Er_{0.003}TiO_3$	"	"	Bluish gray	-	1.2×10^8	-	-	-	-	3.992	4.036
E_7	$Ba_{.9965}Er_{.0035}GiO_3$	"	"	Light blue	122	56.58×10^3	123	36.13	0.085	0.099	"	"
E_8	$Ba_{.996}Er_{.004}TiO_3$	"	"	Blue	120	24.64×10^3	125	16.53	0.049	0.26	"	"
E_9	$Ba_{.9955}Er_{.0045}TiO_3$	"	"	Dark blue	120	90.0	130	42.13	0.039	0.13	"	"
E_{10}	$Ba_{.995}Er_{.005}TiO_3$	"	"	"	118	217.6	128	42.73	0.04	-	"	"
E_{11}	$Ba_{.9945}Er_{.0055}TiO_3$	"	"	"	120	696.0	126	16.5	0.058	-	"	"
E_{12}	$Ba_{.994}Er_{.006}TiO_3$	"	"	"	120	1.2×10^3	125	33.41	0.049	-	"	"

a specific property of semiconducting Barium titanate. It was first observed by Haayman et al.[12]

In the present series of investigations, several systems (Binary and Ternary) have been prepared to study the above property in detail.

System - 1: $Ba_{1-x}Er_xTiO_3$

Compositions containing erbium from 0.05 to 0.8 mole % were studied. Compositions and some physical properties for each sample in the system are listed in Table- 5. Upto E_6 (0.3 mole % Er), the systems were almost grey in colour. In the intermediate range (0.3 to 0.55 mole %), the compounds were blue in colour. This is the semiconducting region. The blue colour faded with increasing proportion of Er. X-ray data for all specimens were similar indicating that doping did not lead to any detectable change in lattice parameters.

Every composition in the system has the same value of Curie temperature ($\sim$ 120°C), (cf. Fig. 11) as observed in the case of undoped ceramic $BaTiO_3$. The PTCR anomaly starts at the Curie point for all systems.

The resistivity below the Curie point follows the relation of

$$\rho = \rho_0 \exp\left(\frac{\Delta E_1}{kT}\right) , \qquad (3.2)$$

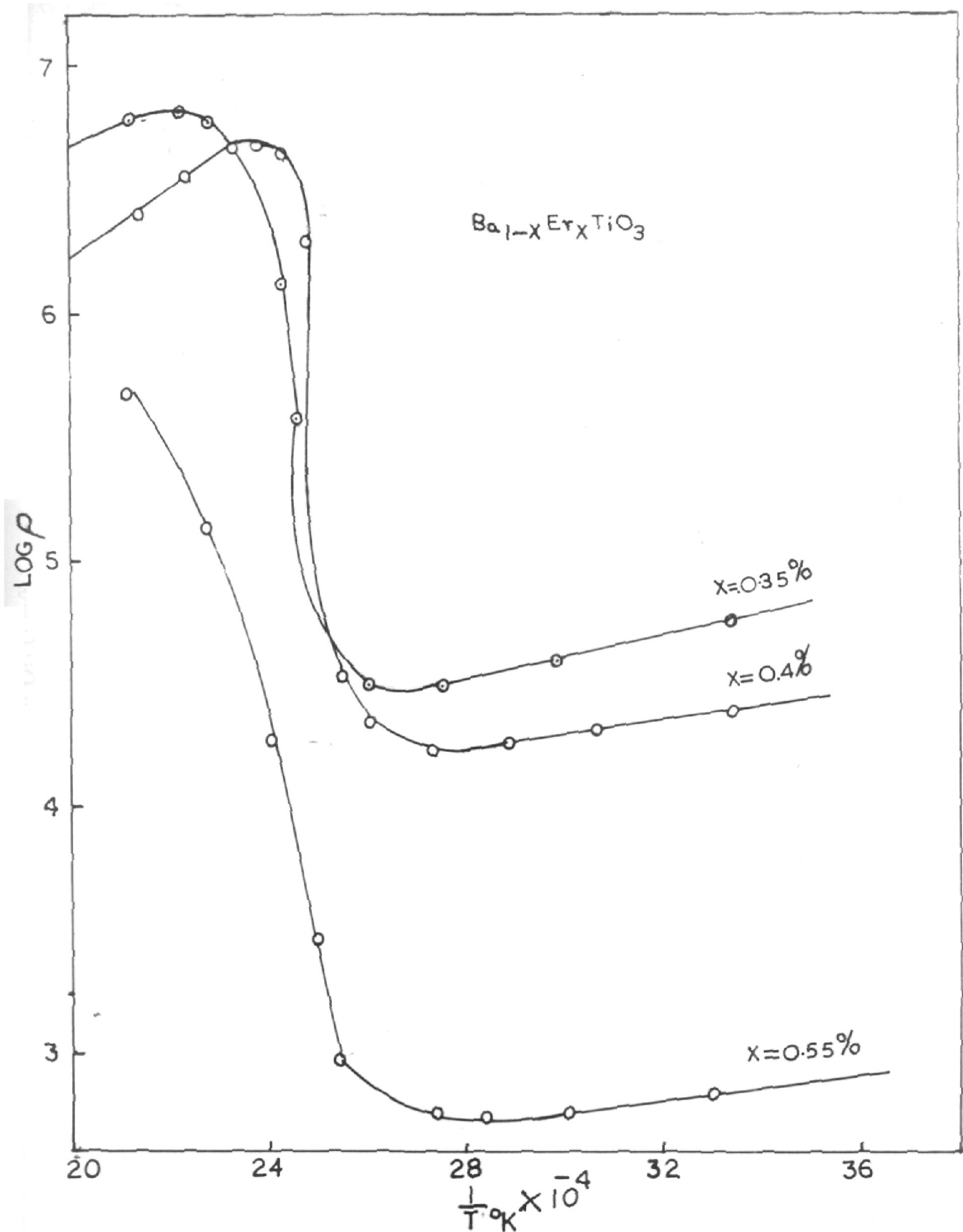

FIG·12 DEPENDENCE OF LOG ρ ON THE INVERSE OF ABSOLUTE TEMP.

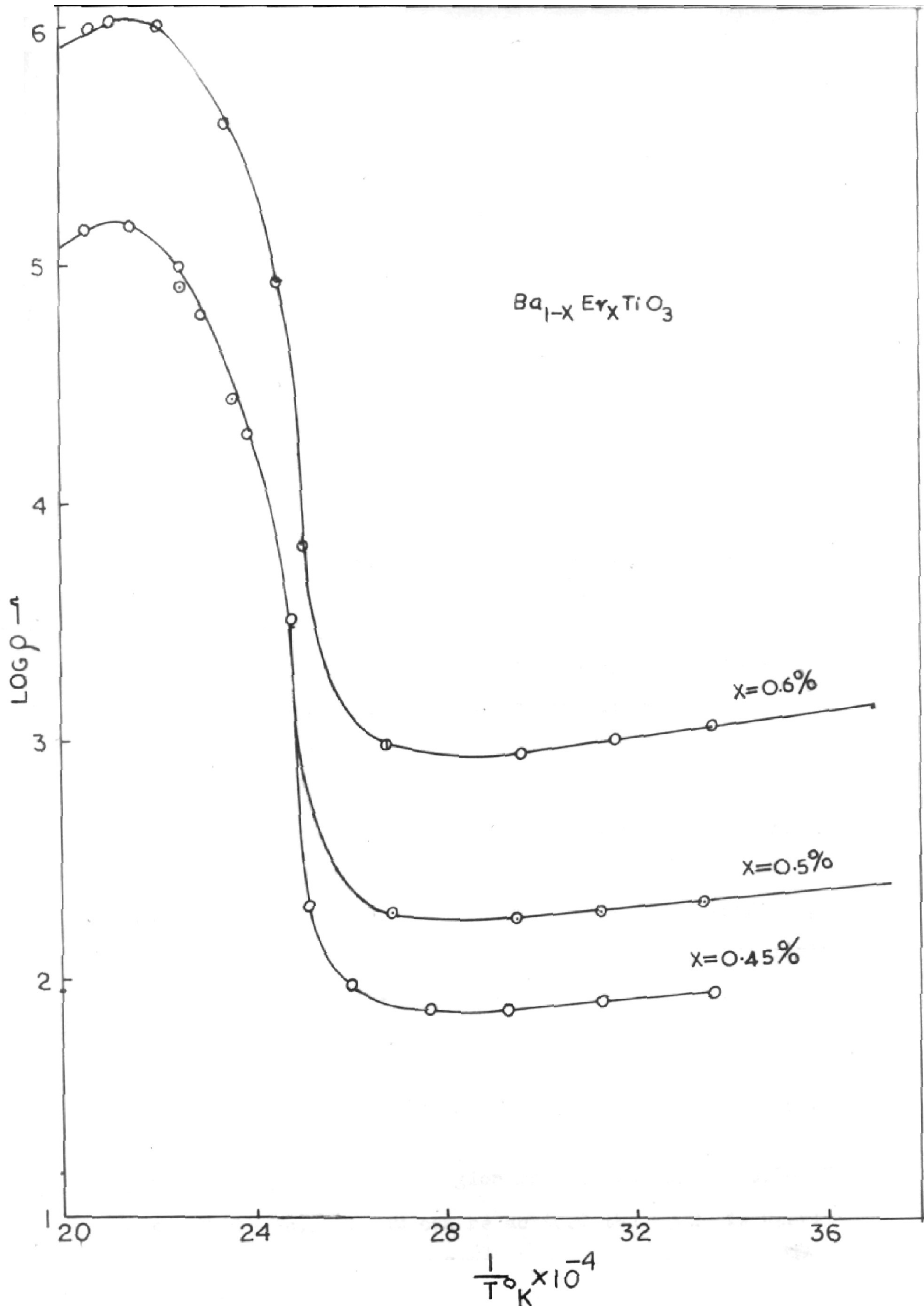

FIG-13. DEPENDENCE OF LOGρ ON THE INVERSE OF ABSOLUTE TEMP

where

ρ = resistivity (ohm-cm) at temperature T(^oK)

ρ_0 = resistivity intercept (extrapolated) at infinite temperature.

ΔE_1 = Activation energy

k = Boltzmann constant

The activation energy is calculated from the slope of the plot of $\frac{1}{T}$ Vs logρ . (cf. figs. 12, 13). The value of activation energy lies in the range of 0.039 eV to 0.085 eV.

Just below the Curie point the resistivity begins to increase and within a short range of temperature it shoots up by several orders. In some cases, it becomes more than hundred time higher than the value at room temperature. From the Figure 11 it is clear that in all cases the principal portion of the anomaly lies in a short range of temperature, restricted to Curie region. Then follows the region of continuous increase of resistivity. This is a broad range of temperature ($\sim$ 125°C to 180°C). As temperature is further increased, resistivity begins to decrease and it follows a relation similar to (3.2) i.e.

$$\rho = \rho_0 \exp (\Delta E_2/kT) , \qquad (3.3)$$

ΔE_2 in the paraelectric region ranges from 0.1 to 0.26 eV (cf. Table No.5). It can be noticed that ΔE_2 is nearly five times higher than ΔE_1.

The decrease in resistivity at higher temperatures is not common to all cases. In some cases resistivity goes on increasing continuously for relatively larger temperature range.

The temperature coefficient of resistivity is calculated from the following considerations:

The initial relation between α (α the temperature coefficient of resistivity) and the resistivity is given by

$$\rho = \rho_0 e^{\alpha \Delta T} \tag{3.4}$$

$$\Delta T = T_2 - T_1, \text{ the temperature difference.}$$

As

$$\frac{d\rho}{dT} = \rho_0 \alpha e^{\alpha \Delta T}$$

Therefore

$$\frac{1}{\rho} \frac{d\rho}{dT} = \frac{1}{\rho_0} e^{-\alpha \Delta T} \times \rho_0 \alpha e^{\alpha \Delta T} = \alpha \tag{3.5}$$

which by definition is the temperature coefficient of resistivity.

Now equation (3.4) can be written as

$$\ln \frac{\rho_2}{\rho_1} = \alpha \Delta T \tag{3.6}$$

Table No.6

Ceramic and Electric Data of compositions in the system (Ba, Sr) TiO_3 + 0.5 % Er

Sample	Chemical formula	Firing Temp. (°C)	Soaking time (hr)	Colour	Curie point °C	Resistivity at 25°C (Ω.cm)	Temp. of α_{max} °C	max temp. coefficient of α_{max} %/°C	ΔE1 (eV)	ΔE2 (eV)	Lattice Parameters at 25°C a-axis	Lattice Parameters at 25°C c-axis
S_1	$(Ba_{.945}Sr_{.05}Er_{.005})TiO_3$	1400	1 hr	Dark blue	105	963.0	112.5	32.21	0.044	0.198	3.998	4.035
S_2	$(Ba_{.895}Sr_{.10}Er_{.005})TiO_3$	"	"	Dark blue	70	72.0	100.0	8.5	0.065	-	3.994	4.026
S_3	$(Ba_{.795}Sr_{.20}Er_{.005})TiO_3$	"	"	Bluish gray	60	11.3×10^4	65	-	-	-	3.979	4.011
S_4	$(Ba_{0.695}Sr_{0.3}Er_{.005})TiO_3$	"	"	Ivory	-	5×10^6	-	-	-	-	-	-
S_5	$(Ba_{0.595}Sr_{0.4}Er_{.005})TiO_3$	"	"	Gray	-	$>10^6$	-	-	-	-	-	-
S_6	$(Ba_{0.495}Sr_{0.5}Er_{.005})TiO_3$	"	"	Gray	-	8.0×10^5	-	-	-	-	-	-

where

ρ_2 = resistivity at T_2 ^{o}K say

ρ_1 = resistivity at T_1 ^{o}K

Therefore

$$\frac{1}{\Delta T} \ln \frac{\rho_2}{\rho_1} = \alpha$$

or

$$\frac{1}{0.4343 \Delta T} \log \frac{\rho_2}{\rho_1} = \alpha \qquad (3.7)$$

The maximum temperature coefficient of resistivity (α_{max}) was calculated from equation (3.7) at the steepest portion of the plot.

<u>System - 2</u>: (Ba, Sr) TiO_3 + 0.5 mole % Er

Here the effect of the partial substitution of Ba^{2+} by Sr^{2+} on PTCR behaviour has been studied.

Compositions containing 5 to 50 mole % of strontium were prepared. Compositions and electrical properties are summarised in Table 6. Semiconductivity property was exhibited upto 20 mole % of strontium, afterwards as the proportion of strontium was increased, samples became non-semiconducting.

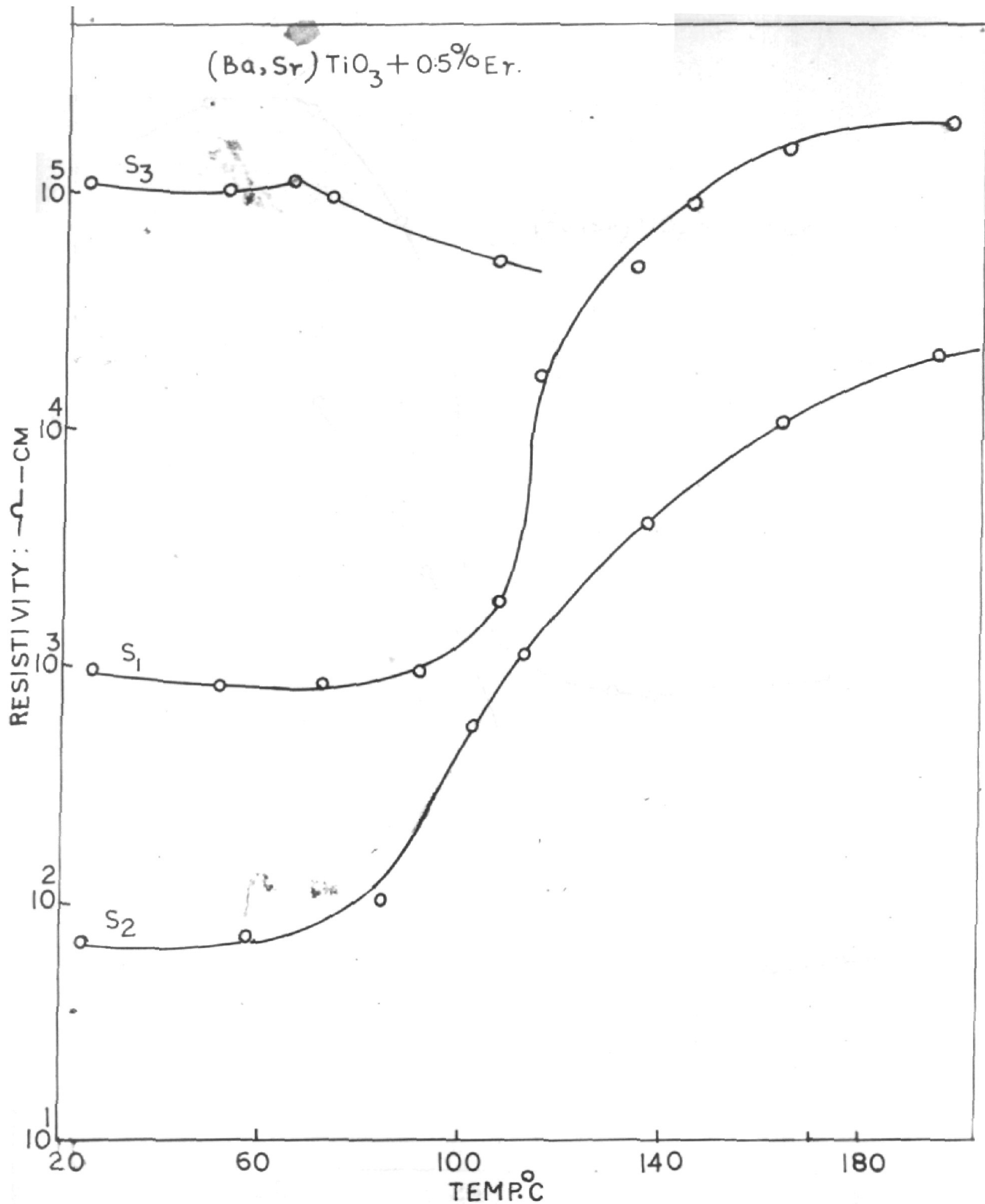

FIG 14. RESISTIVITY TEMP. CHARACTERISTICS OF THE BODIES IN THE SYSTEM $(Ba,Sr)TiO_3$

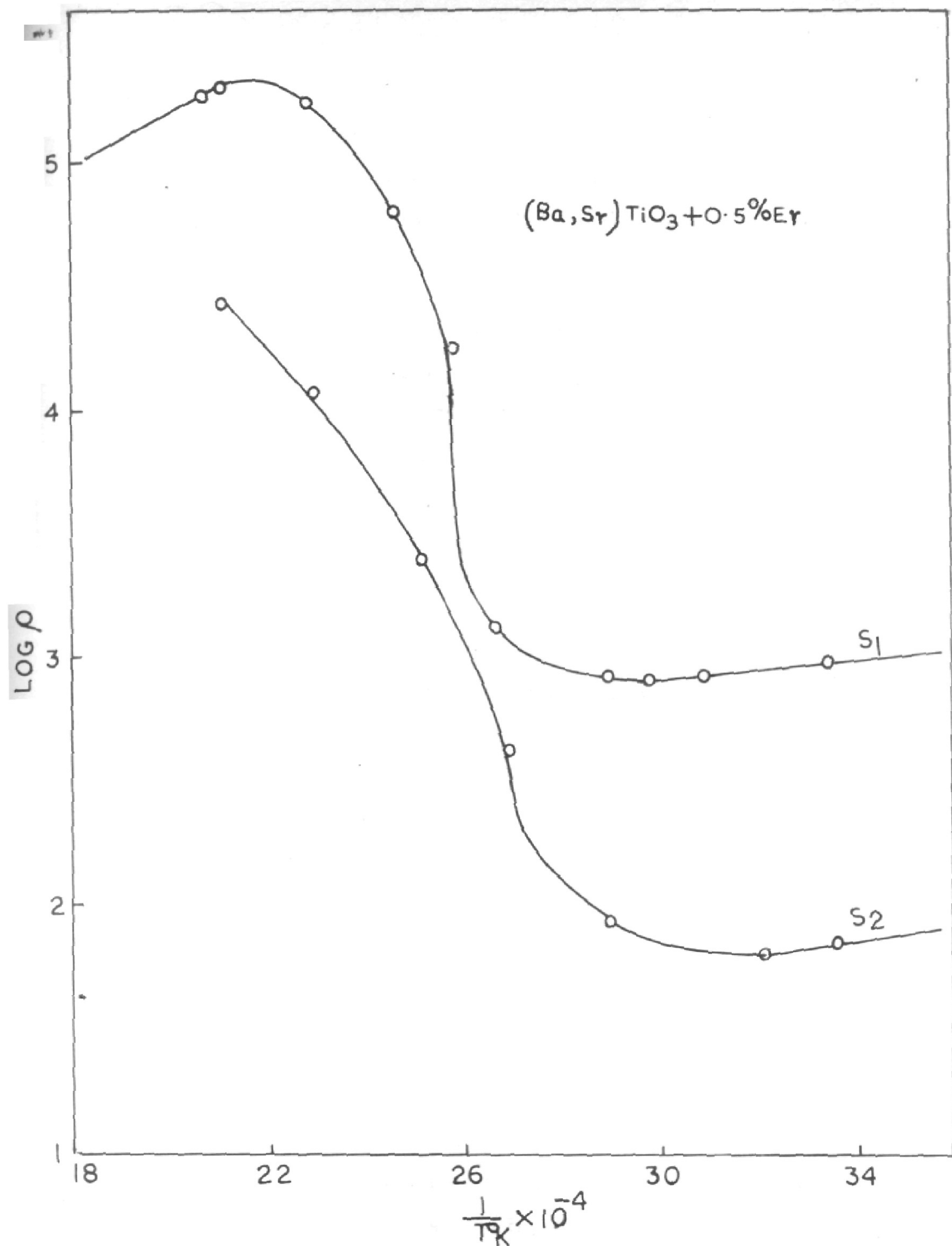

FIG.15. DEPENDENCE OF LOG ρ ON THE INVERSE OF ABSOLUTE TEMP.

With increasing strontium the Curie point shifted towards a lower temperature. The effect is similar to that reported by Dungan et al.[12] in the case of undoped system.

The resistivity versus temperature curves of semiconducting samples are shown in Fig. 14. Below the Curie region the behaviour is more or less similar to the system-1. In each sample of the system, the resistivity anomaly occurred in correspondence with the Curie point, therefore the resistivity anomaly temperature shifted to a lower temperature with an increase in strontium.

One can easily see the essential difference between the resistivity - temperature characteristics of the two systems (cf. Fig. 11 and Fig. 14). The PTCR anomaly in this system is not as sharp as in the system - 1. The increasing percentage of strontium seems to suppress the anomalous effect.

The values of activation energies in both paraelectric and ferroelectric regions are calculated from the slope of the plot of $\frac{1}{T}$ V_s $\log \rho$ (Fig.15). From table 6 it can be seen that ΔE_2 is nearly five times higher than ΔE_1. This change is similar to system-1.

<u>System - 3:</u> (Ba, Ca) TiO_3 + 0.5 mole % Er

Mcquerrie[13] and Roy et al[14] have reported about the dielectric properties of (Ba, Ca, Sr) TiO_3 system. Here system-3 has been made semiconducting by doping 0.5 mole % of erbium.

Table No.7

Ceramic and Electric Dat of Compositions in the sstem (Ba,Ca)TiO_3 + 0.5 % Er

Sample No.	Chemical formula	Firing Temp. (^oC)	Soaking time (hr)	olour	Curie point ^oC	Resisttivity at 25^oC (Ω cm)	Temp. of α_{max} ^oC	max temp coefficient α_{max} off (%/^oC)	ΔE_1 (eV)	ΔE_2 (eV)	Lattice Parameters at 25 C a-axis Å	c-axis Å
C_1	$(Ba_{0.945}Ca_{0.05}Er_{0.005})TiO_3$	1350	2 hr	ark lue	120	7.0×10^1	135	51.6	0.049	-	3.979	4.032
C_2	$(Ba_{0.845}Ca_{0.15}Er_{0.005})TiO_3$	"	"	rayish Blue	120	3.71×10^2	126	13.09	0.079	0.159	3.977	4.023
C_3	$(Ba_{0.795}Ca_{0.2}Er_{0.005})TiO_3$	"	"	"	120	3.71×10^2	122	26.57	0.079	0.139	3.963	4.009
C_4	$(Ba_{0.745}Ca_{0.25}Er_{0.005})TiO_3$	"	"	ellow	-	$>10^8$	-	-	-	-	-	-
C_5	$(Ba_{0.695}Ca_{0.3}Er_{0.005})TiO_3$	"	"	rayish iolet	-	$>10^8$	-	-	-	-	-	-

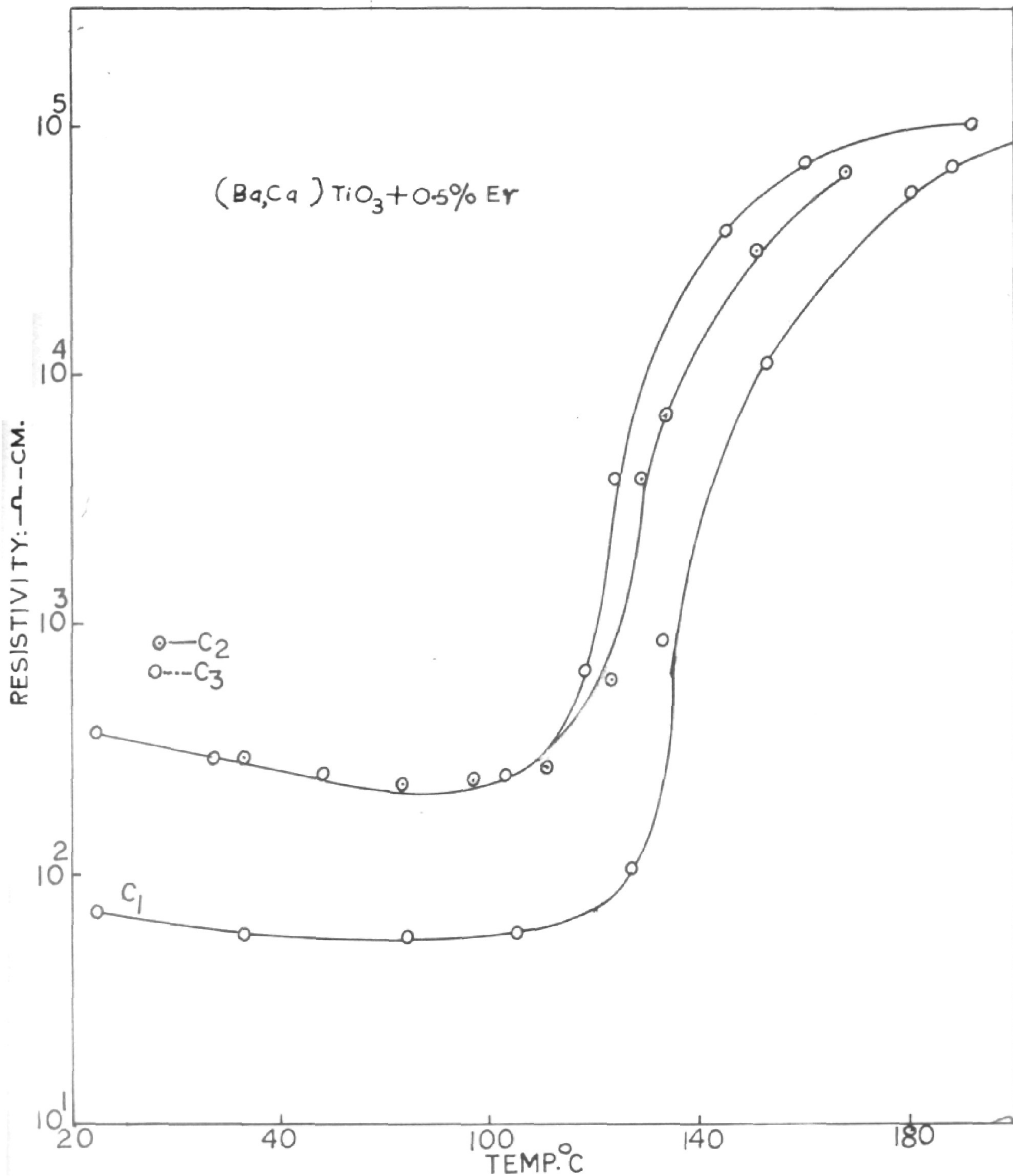

FIG.16. DEPENDENCE OF RESISTIVITY–TEMP. CHARACTERS ON THE CONTENT OF CALCIUM

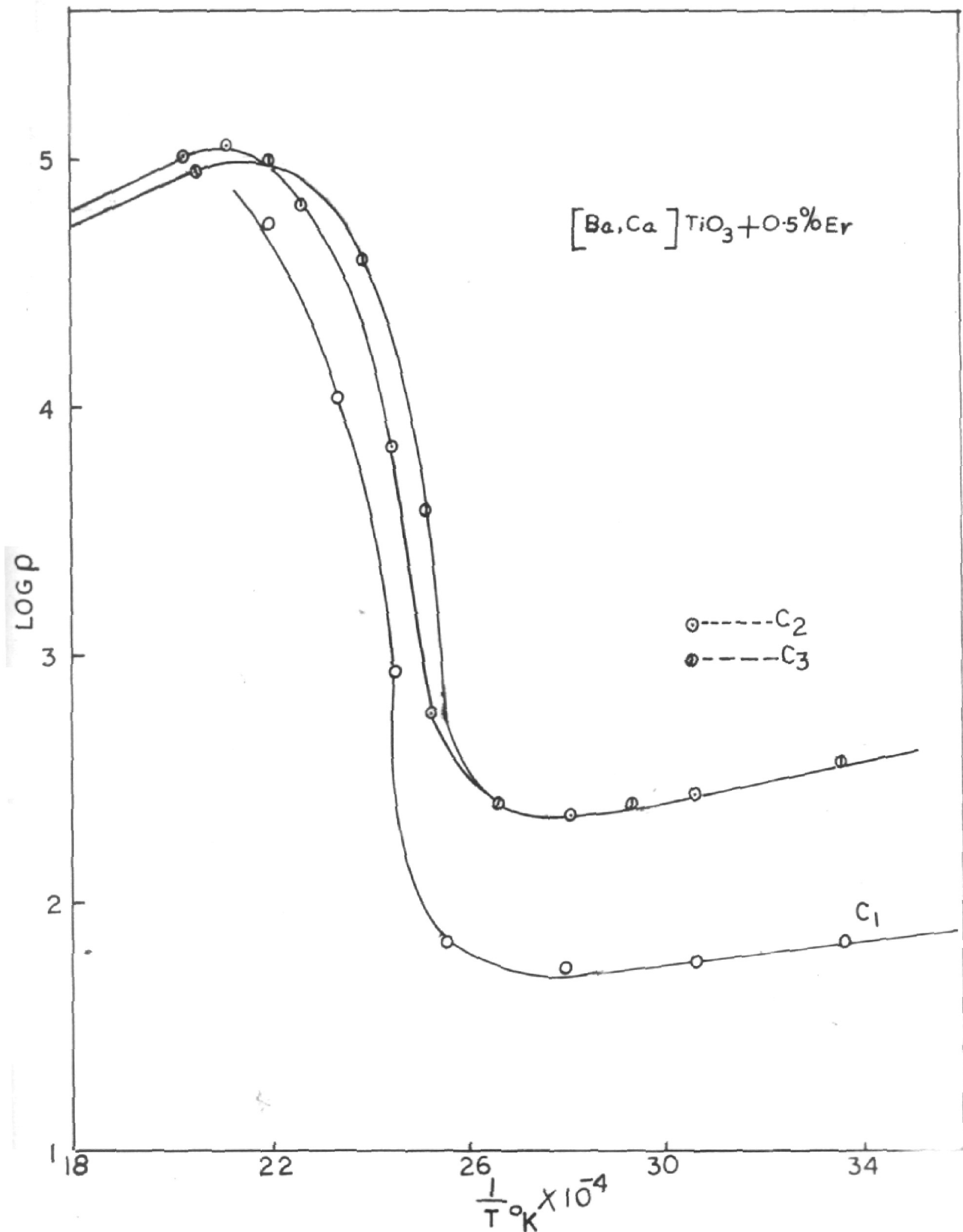

FIG 17. DEPENDENCE OF LOG ρ ON THE INVERSE OF ABSOLUTE TEMPERATURE

The ceramic and electrical data have been given in Table-7. 20 mole % of calcium content is the uppermost limit for semiconductivity.

The effect of partial substitution of barium by calcium on the resistivity temperature property can be understood by a comparison between Fig.16 and the plot of x = 0.5 % from Fig.11. The following points are noticeable.

1) The nature of resistivity temperature characteristics is quite similar in both cases.

2) Slight rise in the Curie temperature takes place due to the calcium content.

3) The activation energy is increased as calcium percentage is increased.

Thus above experimental findings regarding the PTCR behaviour of the three systems lead us to the conclusion that whereas the strontium content does affect the PTCR anomaly behaviour, calcium does not affect it.

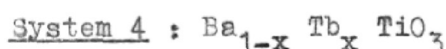

System 4 : $Ba_{1-x} Tb_x TiO_3$

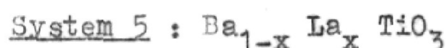

System 5 : $Ba_{1-x} La_x TiO_3$

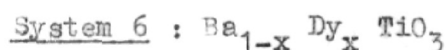

System 6 : $Ba_{1-x} Dy_x TiO_3$

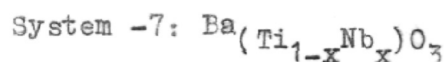

System -7: $Ba(Ti_{1-x}Nb_x)O_3$

Table No.8

Ceramic and Electric Data of Compositions in the system $Ba_{1-x}Tb_xTiO_3$

Sample	Chemical Formula	Firing Temp. °C	Soaking time (hr)	Colour	Curie point °C	Resistivity at 25 C (Ω.cm)	Temp. of α_{max} °C	max Temp. coefficient of ρ (α_{max})	ΔE_1 (eV)	ΔE_2 (eV)
T_1	$Ba_{.9995}Tb_{.0005}TiO_3$	1400	1 hr	Gray	-	$>10^8$	-	-	-	-
T_2	$Ba_{.999}Tb_{.001}TiO_3$	"	"	Yellow	-	$>10^8$	-	-	-	-
T_3	$Ba_{.9985}Tb_{.0015}TiO_3$	"	"	Yellowish gray	-	$>10^8$	-	-	-	-
T_4	$Ba_{.998}Tb_{.002}TiO_3$	"	"	Blue	~120	1.05×10^3	≃122	52.53	0.026	0.13
T_5	$Ba_{.9975}Tb_{.0025}TiO_3$	"	"	Dark blue	~120	931.5	≃118	64.42	0.039	-
T_6	$Ba_{.997}Tb_{.003}TiO_3$	"	"	* "	~120	114.0	≃122	60.77	0.022	0.023
T_7	$Ba_{.9965}Tb_{.0035}TiO_3$	"	"	Blue	~120	1.26×10^3	≃120	14.16	0.065	-
T_8	$Ba_{.996}Tb_{.004}TiO_3$	"	"	Bluish gray	-	25.0×10^3	-	-	-	-

Table No.9

Ceramic and Electric Data of Compositions in the system $Ba_{1-x}La_xTiO_3$

Sample No.	Chemical formula	Firing Temp. ^oC	Soaking time (hr.)	Colour	Curie point ^oC	Resistivity at 25 ^oC (Ω.cm)	Temp. of α_{max} ^oC	max temp. coefficient of ρ α_{max} %/^oC	ΔE_1 (eV)	ΔE_2 (eV)
L_1	$Ba_{0.9995}La_{0.0005}TiO_3$	1400	2	Greenish yellow	-	75.0×10^6	-	-	-	-
L_2	$Ba_{0.999}La_{0.001}TiO_3$	"	"	"	-	"	-	-	-	-
L_3	$Ba_{0.9985}La_{0.0015}TiO_3$	"	"	Gray	-	"	-	-	-	-
L_4	$Ba_{0.998}La_{0.002}TiO_3$	"	"	Green Gray	-	"	-	-	-	-
L_5	$Ba_{0.9975}La_{0.0025}TiO_3$	"	"	Bluish gray	~110	18.2×10^3	~110	10.5	0.009	0.042
L_6	$Ba_{0.997}La_{0.003}TiO_3$	"	"	Dark blue	~110	46.8×10	~113	90.0	0.044	0.33
L_7	$Ba_{0.9965}La_{0.0035}TiO_3$	"	"	Grayish blue	~118	16.2×10^3	~118	21.5	0.07	-
L_8	$Ba_{0.996}La_{0.004}TiO_3$	"	"	Gray	-	$>10^6$	-	-	-	-

Table No.10

Ceramic and Electric Data of Compositions in the system $Ba_{1-x}Dy_xTiO_3$

Sample	Chemical Formula	Firing Temp °C	Soaking time (hr)	Colour	Curie point °C	Resistivity at 25°C (Ω.cm)	Temp. of α_{max} °C	max Temp. coefficient of ρ α_{max} %/°C	ΔE_1 (eV)	ΔE_2 (eV)
D_1	$Ba_{0.9995}Dy_{0.0005}TiO_3$	1350	2 hrs	Yellow	-	$>5.0 \times 10^6$	-	-	-	-
D_2	$Ba_{0.999}Dy_{0.001}TiO_3$	"	"	Grayish yellow	-	"	-	-	-	-
D_3	$Ba_{0.9985}Dy_{0.0015}TiO_3$	"	"	"	-	"	-	-	-	-
D_4	$Ba_{0.998}Dy_{0.002}TiO_3$	"	"	Light Blue	≃120	35.1×10^3	≈122	17.9	0.056	0.198
D_5	$Ba_{0.9975}Dy_{0.0025}TiO_3$	"	"	Blue	≈120	1.1×10^3	≃124	26.0	0.053	-
D_6	$Ba_{0.997}Dy_{0.003}TiO_3$	"	"	Dark Blue	≃120	173.7	≃125	38.9	0.039	-
D_7	$Ba_{0.9965}Dy_{0.0035}TiO_3$	"	"	Greenish blue	≃120	109.3×10^3	≃130	5.8	0.119	-

Table No.11

Ceramic and Electric Data of Compositions in the system $Ba(Ti_{1-x}Nb_x)O_3$

Sample	Chemical Formula	Firing Temp °C	Soaking time (hr)	Colour	Curie point °C	Resistivity at 25°C (Ω.cm)	Temp. of α_{max} °C	max Temp. coefficient of ρ α_{max} %/°C	ΔE_1 (eV)	ΔE_2 (eV)
N_1	$Ba(Ti_{0.9995}Nb_{0.0005})O_3$	1350	2 hrs	Ivory	-	$>54 \times 10^6$	-	-	-	-
N_2	$Ba(Ti_{0.999}Nb_{0.001})O_3$	"	"	Gray	-	"	-	-	-	-
N_3	$Ba(Ti_{0.9985}Nb_{0.0015})O_3$	"	"	Gray	-	"	-	-	-	-
N_4	$Ba(Ti_{0.998}Nb_{0.002})O_3$	"	"	Bluish Gray	$\simeq 120$	6.4×10^3	$\simeq 117$	11.3	0.039	-
N_5	$Ba(Ti_{0.9975}Nb_{0.0025})O_3$	"	"	Dark Blue	$\simeq 115$	34.0×10	$\simeq 120$	23.1	0.019	-
N_6	$Ba(Ti_{0.997}Nb_{0.003})O_3$	"	"	"	$\simeq 120$	36.8×10	$\simeq 120$	7.0	0.023	-
N_7	$Ba(Ti_{0.9965}Nb_{0.0035})O_3$	"	"	"	$\simeq 115$	80.0	$\simeq 116$	4.7	0.013	-
N_8	$Ba(Ti_{0.996}Nb_{0.004})O_3$	"	"	Gray	-	$>50 \times 10^6$	-	-	-	-
N_9	$Ba(Ti_{0.9955}Nb_{0.0045})O_3$	"	"	Gray	-	"	-	-	-	-

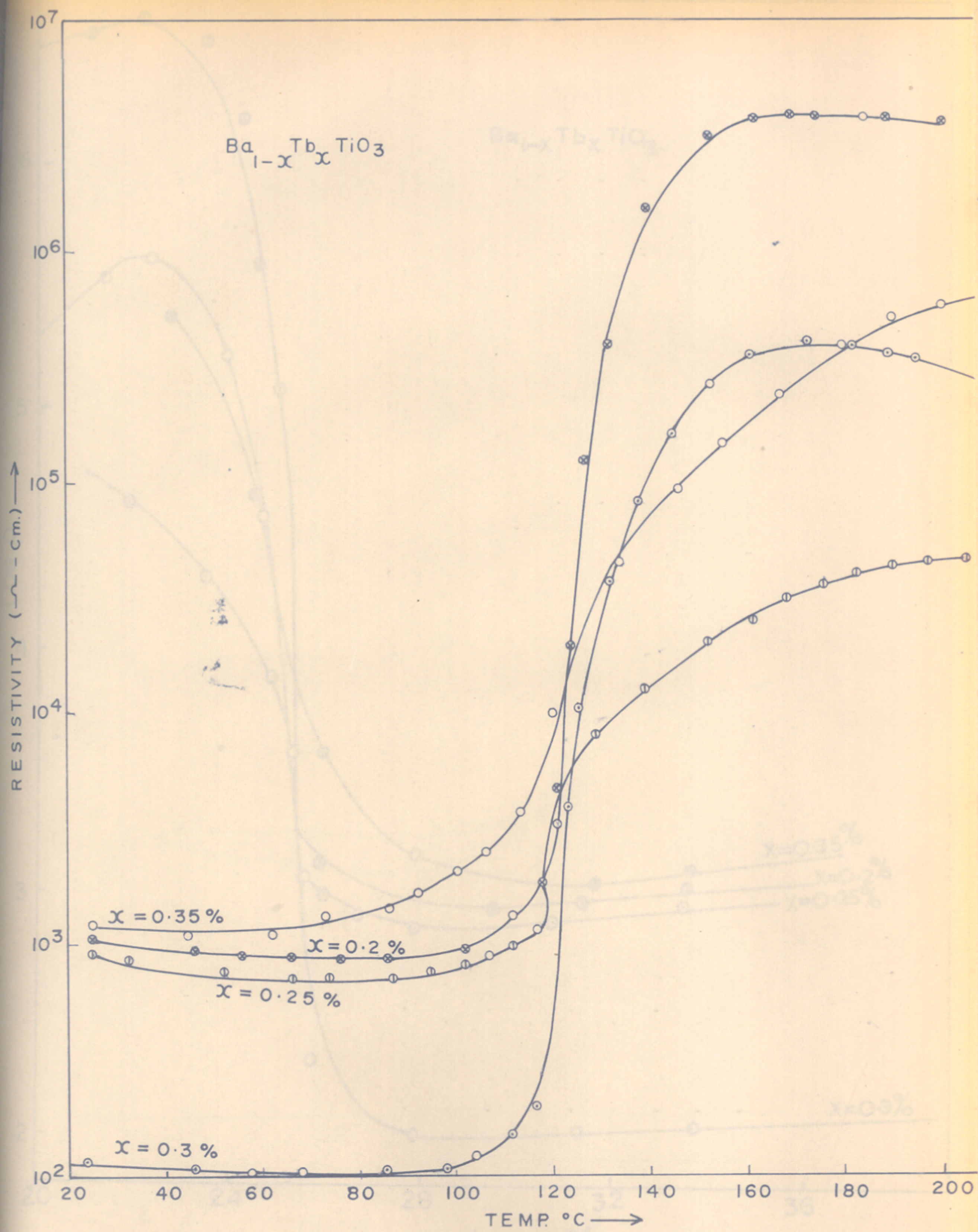

Fig.18. Dependence of resistivity-temp. characters on the content of Terbium

18

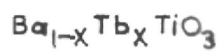

6

5

LOG ρ

4

3

2

$X = 0{\cdot}35\%$

$X = 0{\cdot}2\%$

$X = 0{\cdot}25\%$

$X = 0{\cdot}3\%$

20 24 28 32 36

$\frac{1}{T°K} \times 10^{-4}$

FIG. 19. DEPENDENCE OF LOG ρ ON THE INVERSE OF ABSOLUTE TEMPERAT

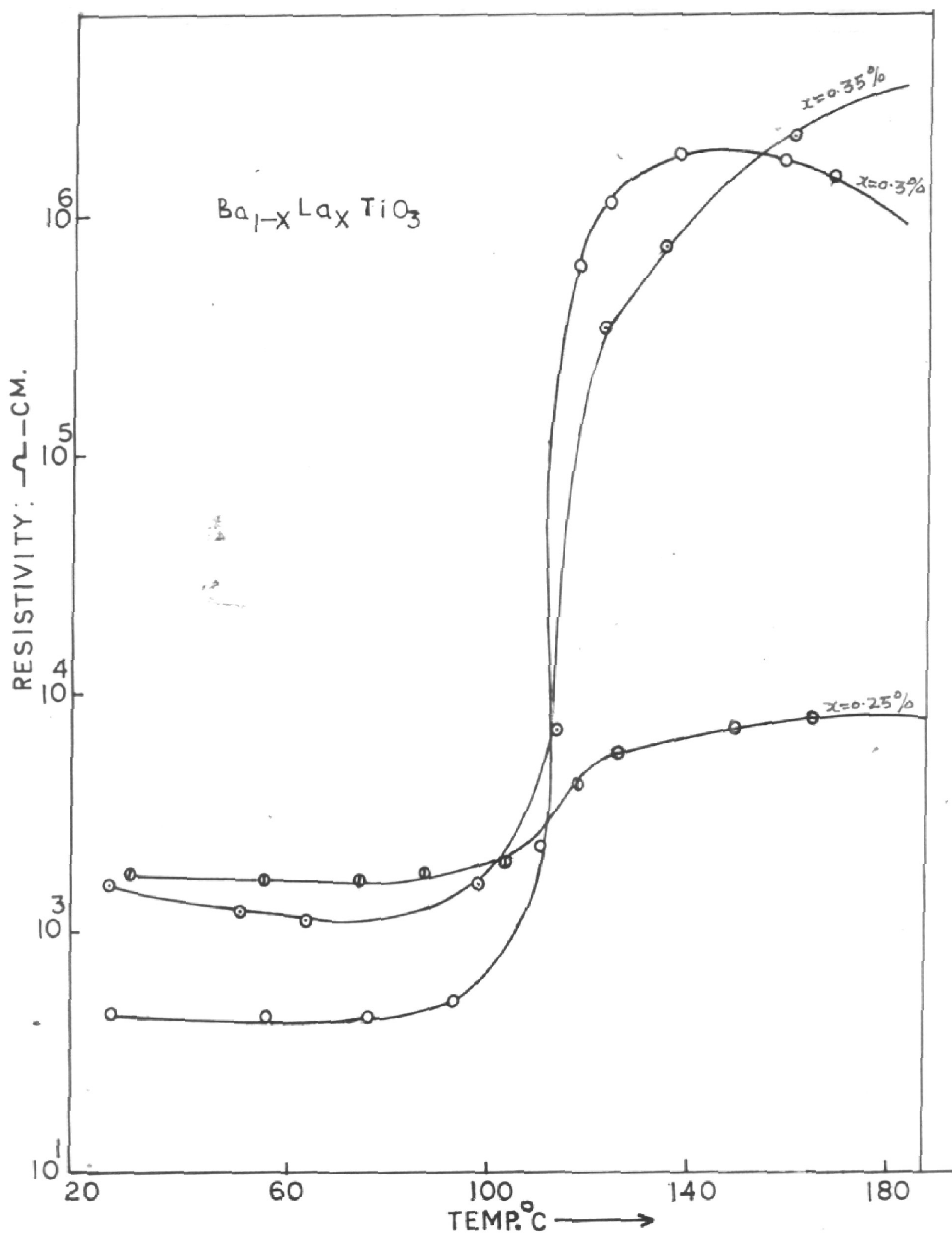

FIG 20. DEPENDENCE OF RESISTIVITY TEMP. CHARACTER ON THE CONTENT OF LANTHANUM.

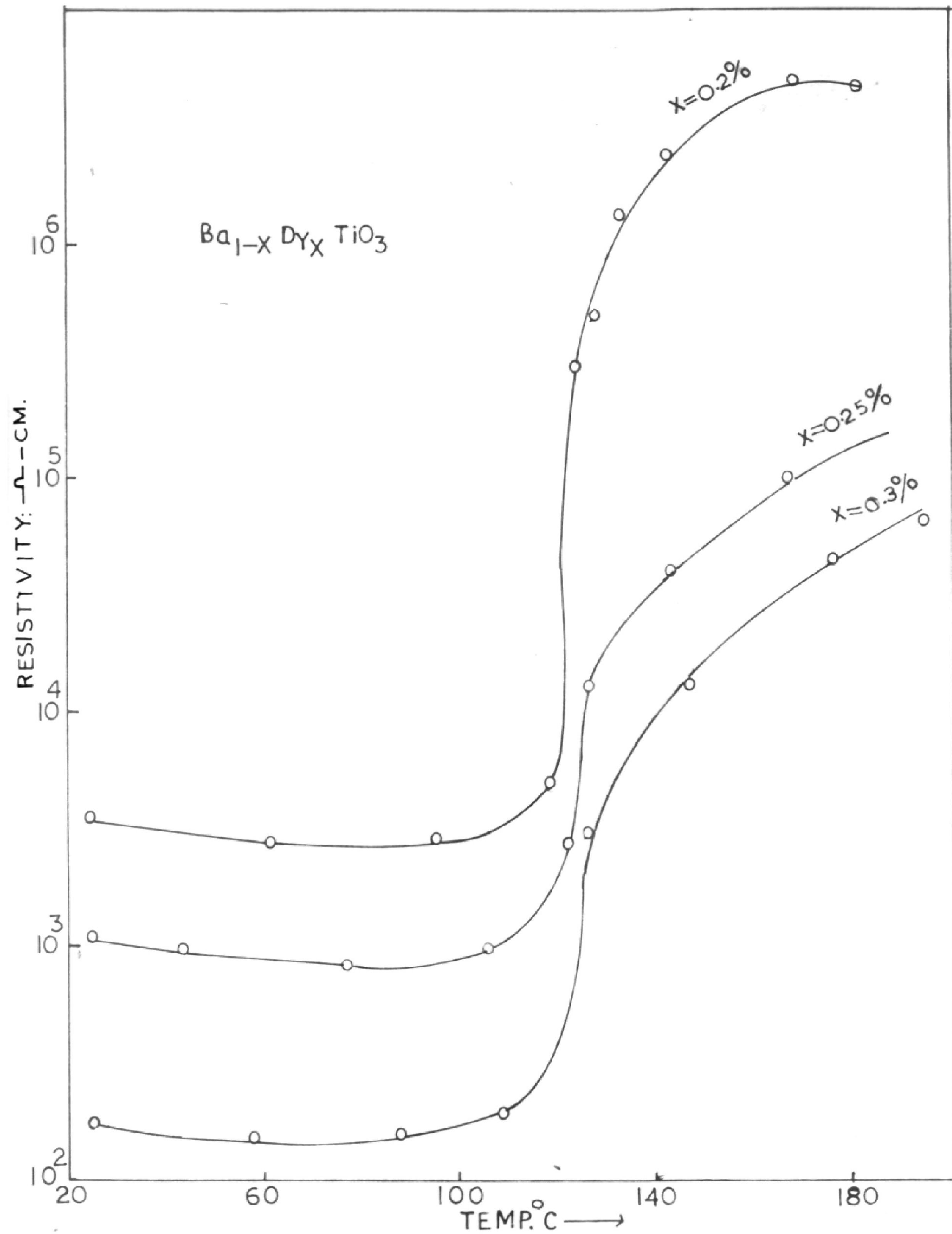

FIG. 21. DEPENDENCE OF RESISTIVITY TEMP. CHARACTERS ON THE CONTENT OF DYSPROSIUM.

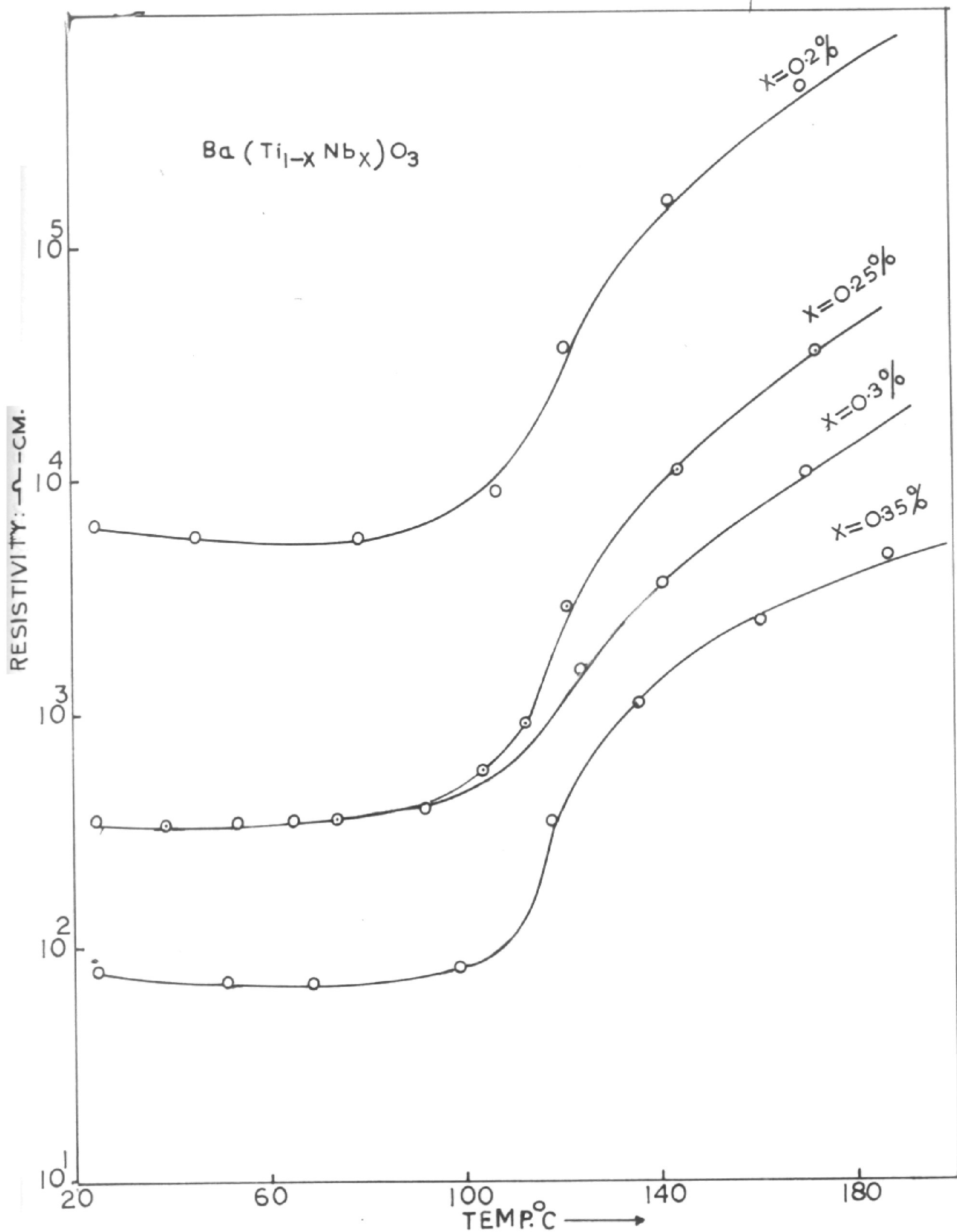

FIG.22. DEPENDENCE OF RESISTIVITY-TEMP. CHARACTERS ON THE CONTENT OF NEOBIUM.

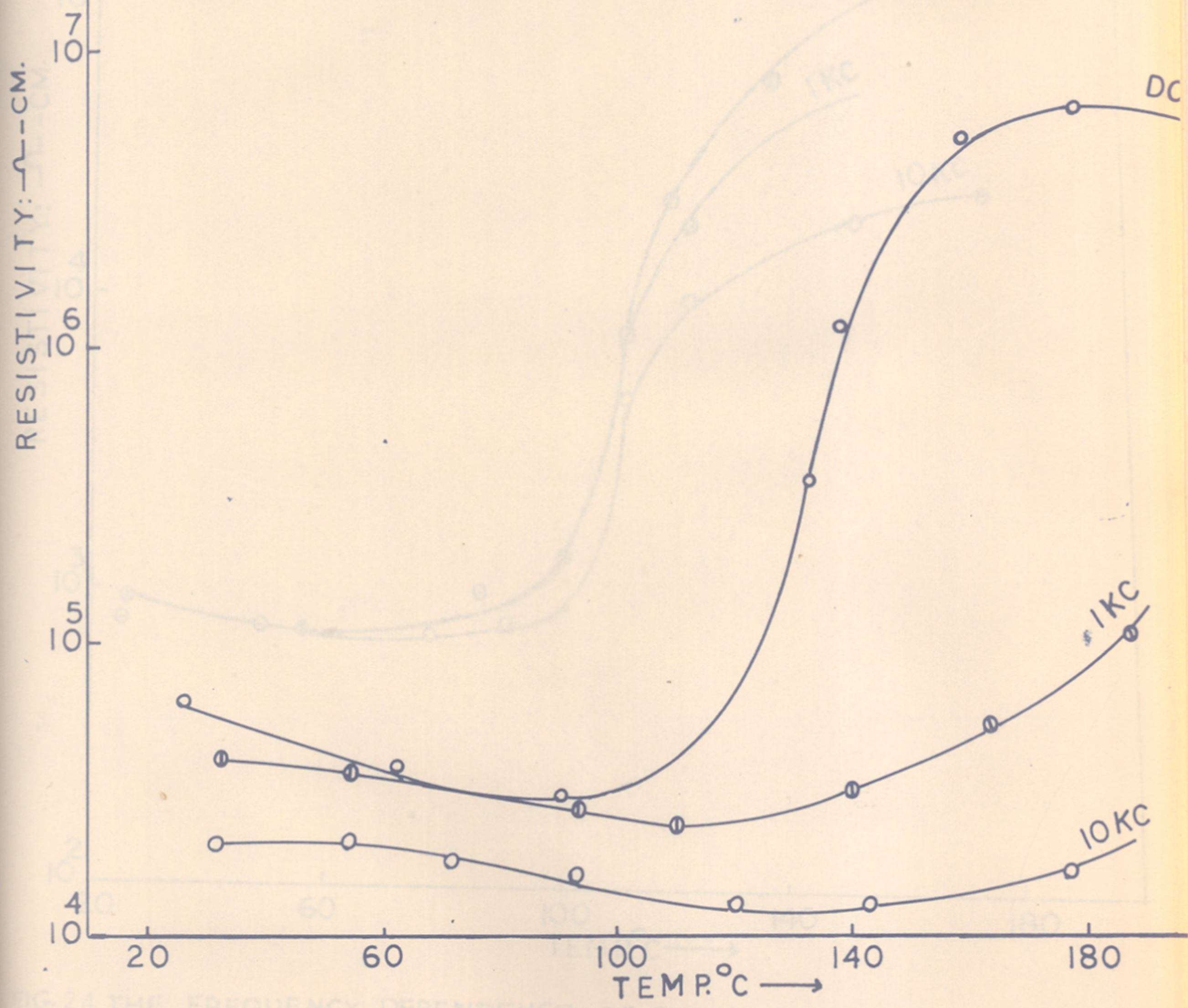

FIG. 23. THE FREQUENCY DEPENDENCE OF RESISTIVITY–TEMP. CHARACTERS.

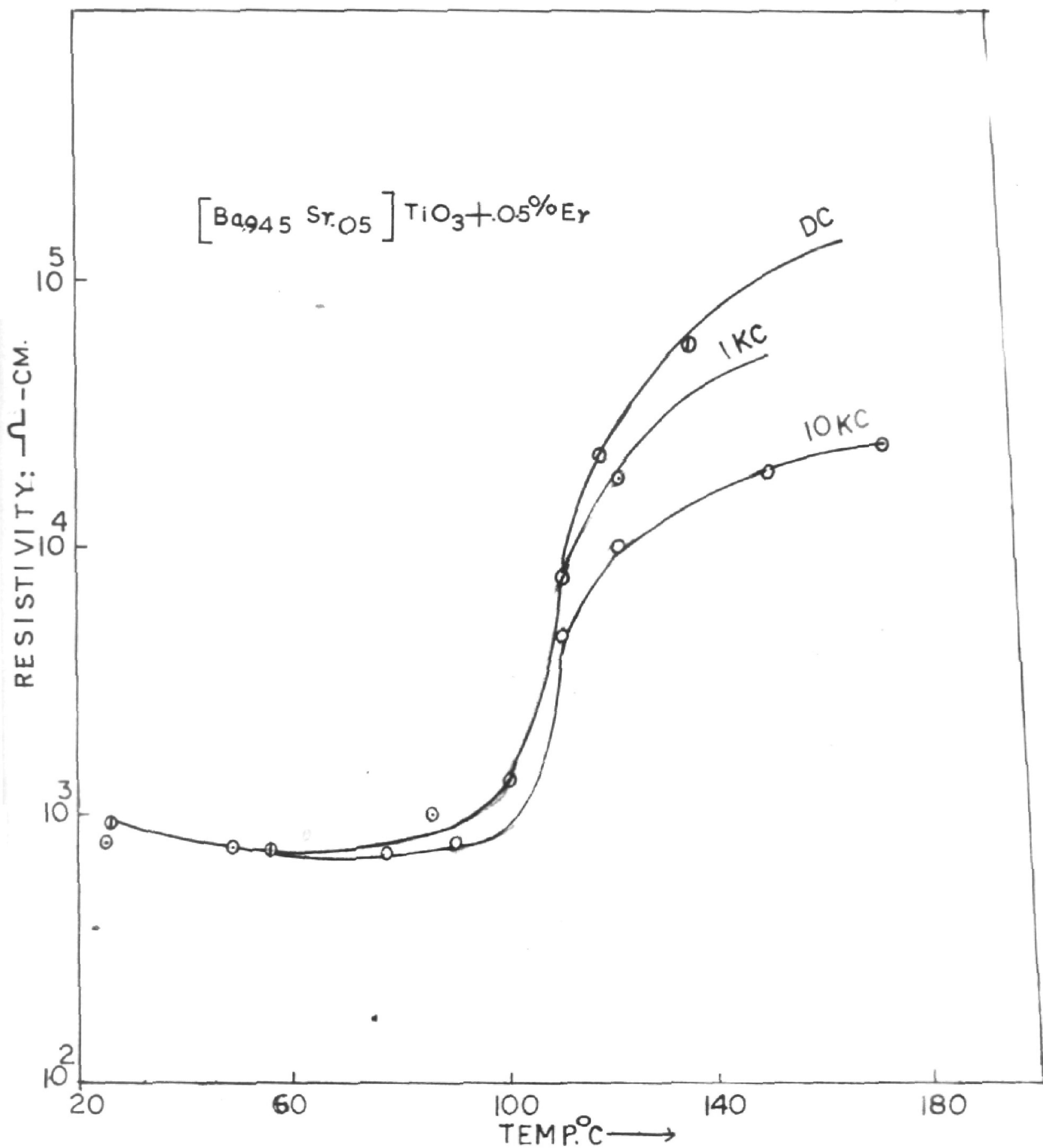

FIG. 24. THE FREQUENCY DEPENDENCE OF RESISTIVITY–TEMP. CHARACTERS.

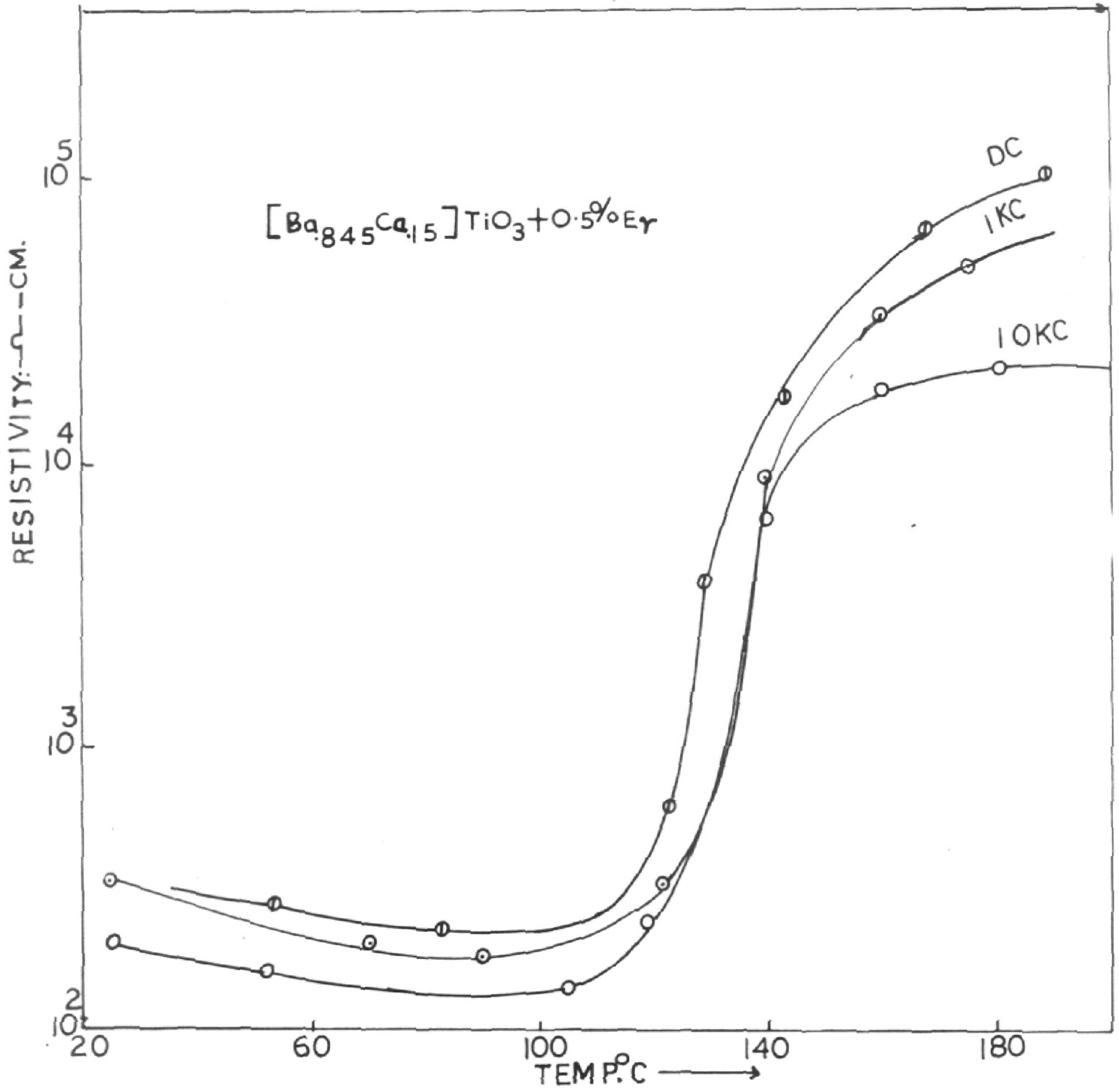

FIG 25. THE FREQUENCY DEPENDENCE OF RESISTIVITY TEMP. CHARACTERS

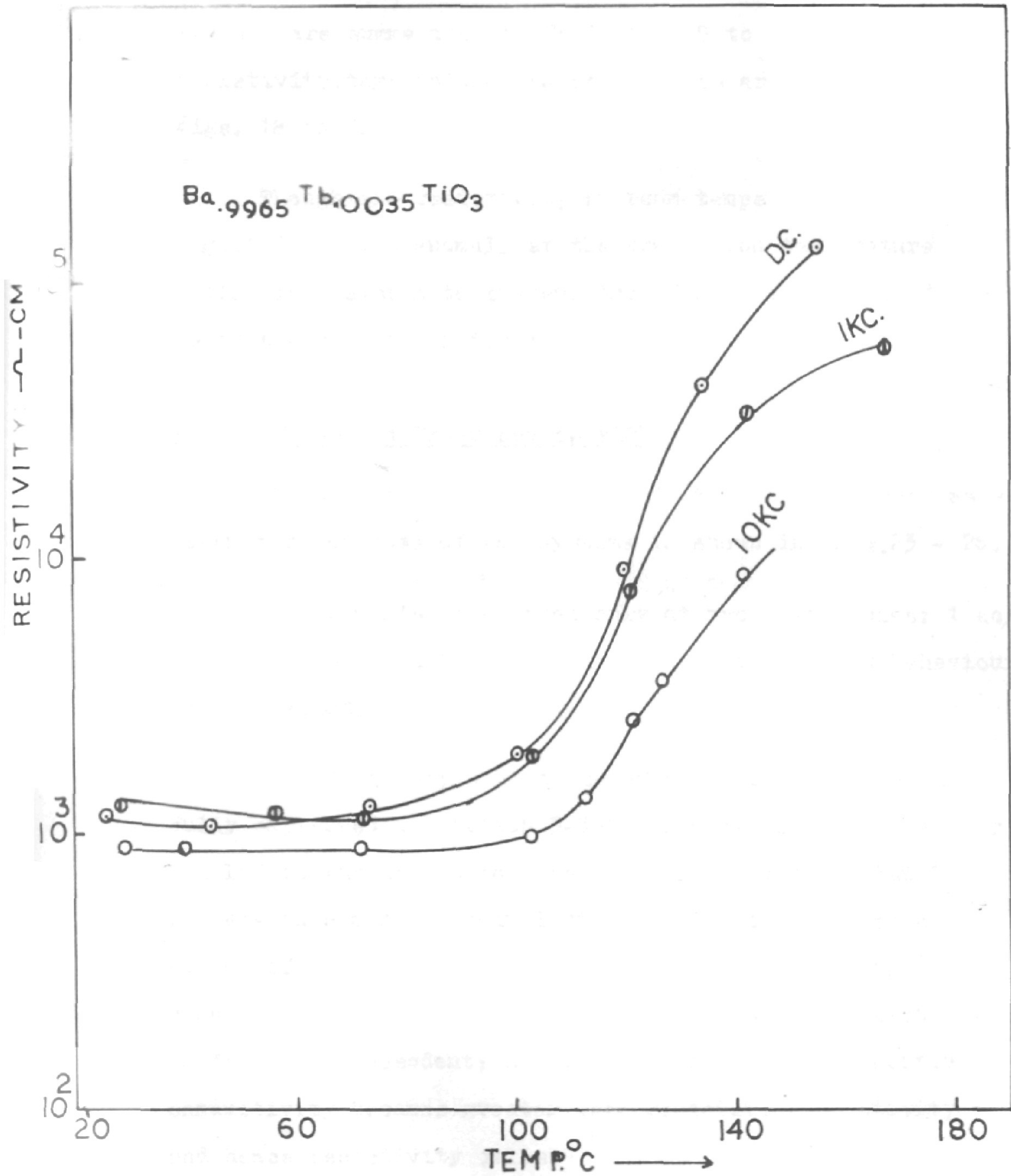

FIG. 26. THE FREQUENCY DEPENDENCE OF RESISTIVITY–TEMP. CHARACTERS.

Ceramic and electrical properties of the above systems are summarised in Table Nos. 8 to 11 and their resistivity_temperature characteristics are shown in Figs. 18 to 22.

Though the resistivity at room temperature and the magnitude of its anomaly at the transition temperature differ from system to system, the PTCR behaviour is identical as in the case of system-1.

3.2.3: Effect of Frequency on PTCR:

The temperature dependence of ρ with frequency as a parameter for some of the systems is shown in Figs. 23 - 26.

Measurements were taken only at two frequencies: 1 kc/Sec and 10 kc/Sec. With increasing frequency the PTCR behaviour is suppressed.

This frequency dependence of resistivity has been fully explained in section 3-3-2. The dispersion behaviour has led to the assumption that the semiconducting $BaTiO_3$ behaves in a manner equivalent to a circuit composed of a number of parallel resistive and capacitive elements connected in series. Therefore the change in resistivity is frequency dependent; as frequency increases capacitive conductivity becomes greater than resistive conductivity and hence resistivity falls.

3.3 A.C.CHARACTERISTICS

3.3.1 Variation of Dielectric Constant (ϵ) with Temperature.

As mentioned in Chapter-1 (Sec 1.6(2)) that the resemblance between the temperature dependence of dielectric constant of undoped $BaTiO_3$ measured for high field ($\sim$ 3 kV/cm) and logarithm of the resistivity in semiconducting $BaTiO_3$, led Heywang to relate the conductivity in semiconducting $BaTiO_3$ to a potential barrier. The barrier height is a function of the dielectric constant of the system. On the other hand some investigators believe that the ferroelectric character of $BaTiO_3$ is responsible for PTCR behaviour. Saburi's hopping mechanism is based on the local field at Ti ions which is a function of dipole interaction and spontaneous polarization.

Here the dielectric behaviour of both doped and undoped $BaTiO_3$ especially with regard to its temperature variation has been investigated. Applied field for both was $\sim$ 10 v/cm (a.c.). The resistance and capacitance of semiconducting samples were measured in parallel and from their geometry corresponding values of resistivity and dielectric constant were calculated.

By definition the dielectric constant of the material is given by

$$\epsilon = C_x/C_o \tag{3.8}$$

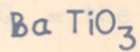

FIG.27. TEMPERATURE DEPENDENCE OF DIELECTRIC CONSTANT AT 1 KC/S

where C_x = the capacitance of the sample and C_o = the air capacitance, the gap and surface area of contact electrodes being the same in both cases.

Now

$$C_o = \epsilon_o A/L \qquad (3.9)$$

ϵ_o = dielectric constant of vacuum

A = the surface area (cm^2)

L = thickness (cm)

Substituting for ϵ_o

$$C_o = 0.0835 \; A/L \; (\mu\mu f \text{ - } cm) . \qquad (3.10)$$

Therefore (3.8) gives

$$\epsilon = \frac{11.30 \; L}{A} C_x \qquad (3.11)$$

The plot of dielectric constant of the undoped $BaTiO_3$ versus temperature has been shown in Fig.27. The behaviour is similar to that reported by McQuarrie[15] and von Hippel.[16] Above 120°C the dielectric constant obeys the Curie-Weiss law as given by

$$\epsilon = C/(T - \theta) \qquad (3.12)$$

where C = Curie constant ($\sim 1.5 \times 10^5$ degrees).

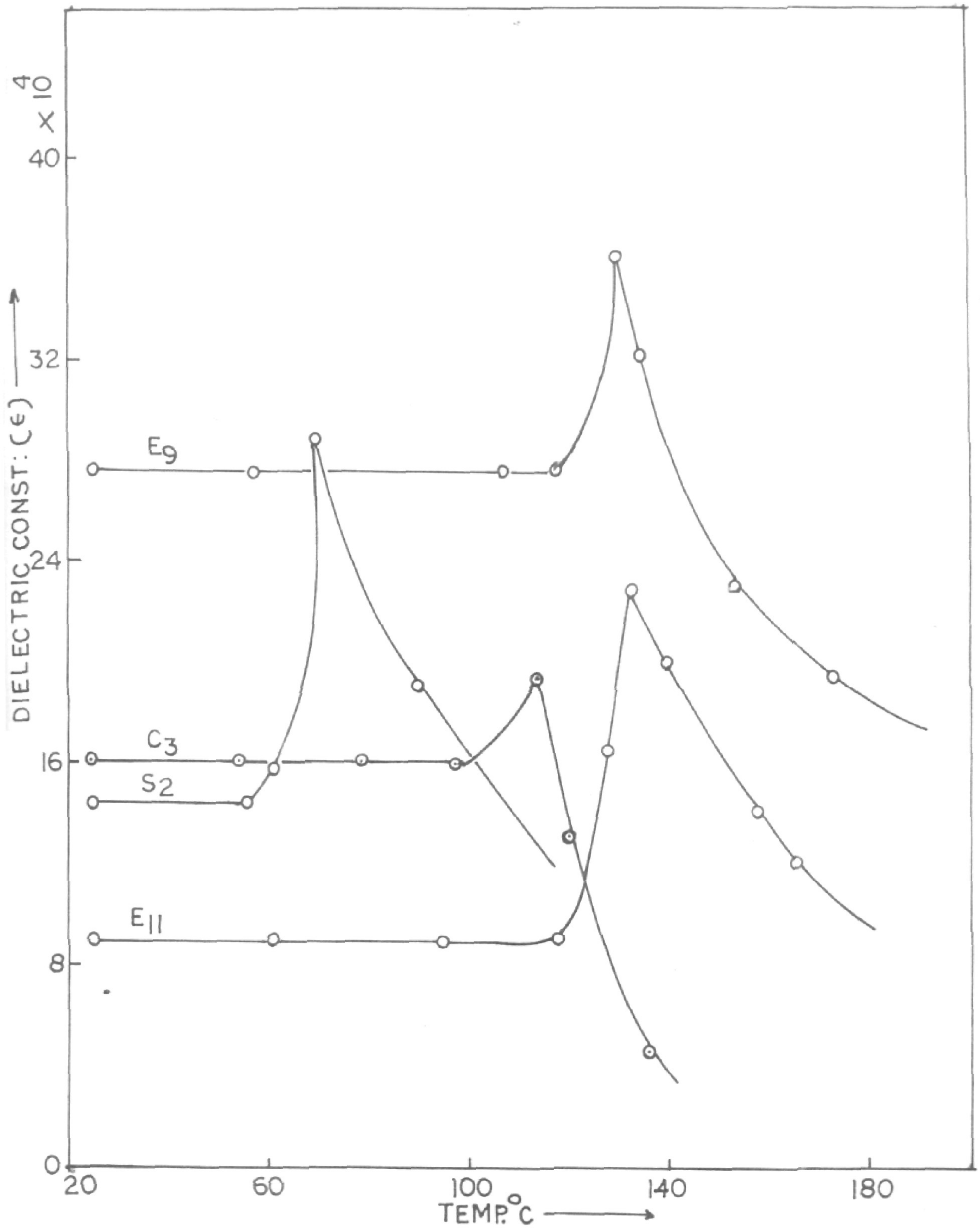

FIG. 28. TEMPERATURE DEPENDENCE OF DIELECTRIC CONST. AT 1KC/S

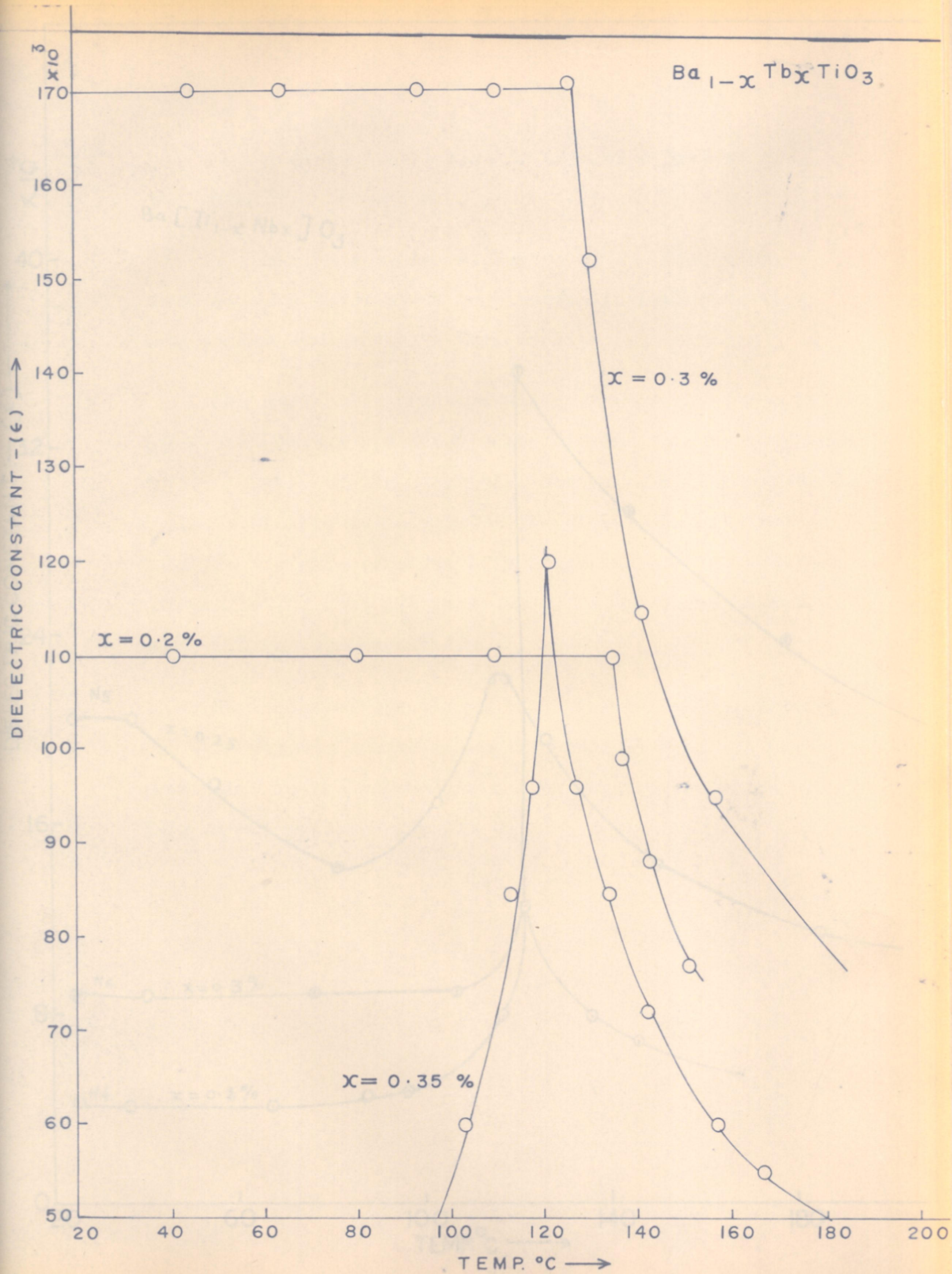

Fig. 29. Temperature dependence of dielectric constant at 10 Kc

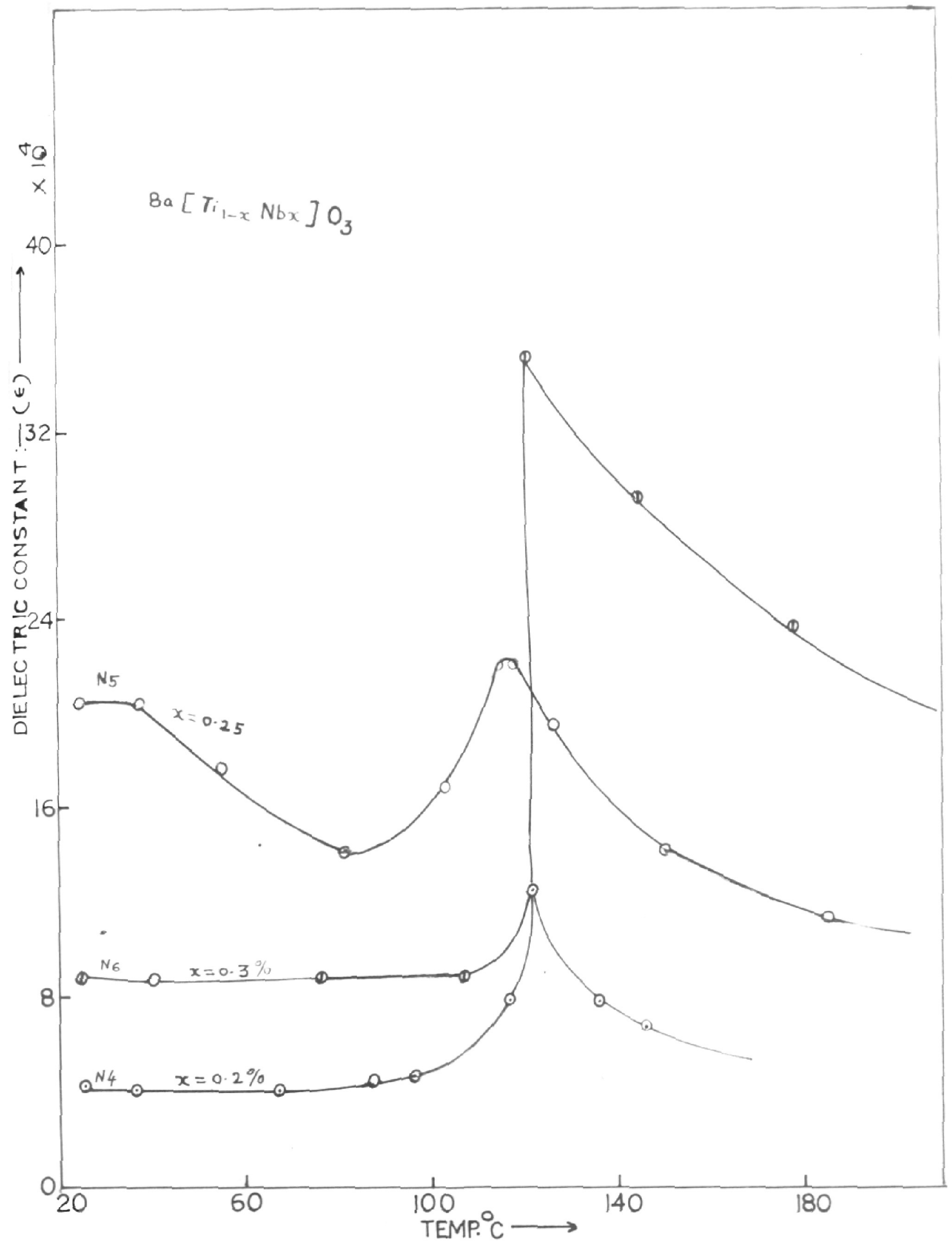

FIG. 30. TEMPERATURE DEPENDENCE OF DIELEC. CONST AT 1KC/S

Θ the Curie point, lies in the neighbourhood of the transition temperature.

For comparison, the variation of the dielectric constant as a function of temperature in semiconducting samples has been shown in Fig. 28-30.

The dielectric constant has a sharp peak at the Curie point, the height and exact shape of peak depends very much on the texture of the material. However, in this region (i.e. above the Curie point) the dielectric constant exhibits the same response with temperature as it does for undoped $BaTiO_3$, but its value is 10 to 100 times higher, depending on the composition.

Now consider the region below the Curie temperature. The apparent dielectric constant decreases from its high peak value to the volume dielectric constant which is independent of temperature.

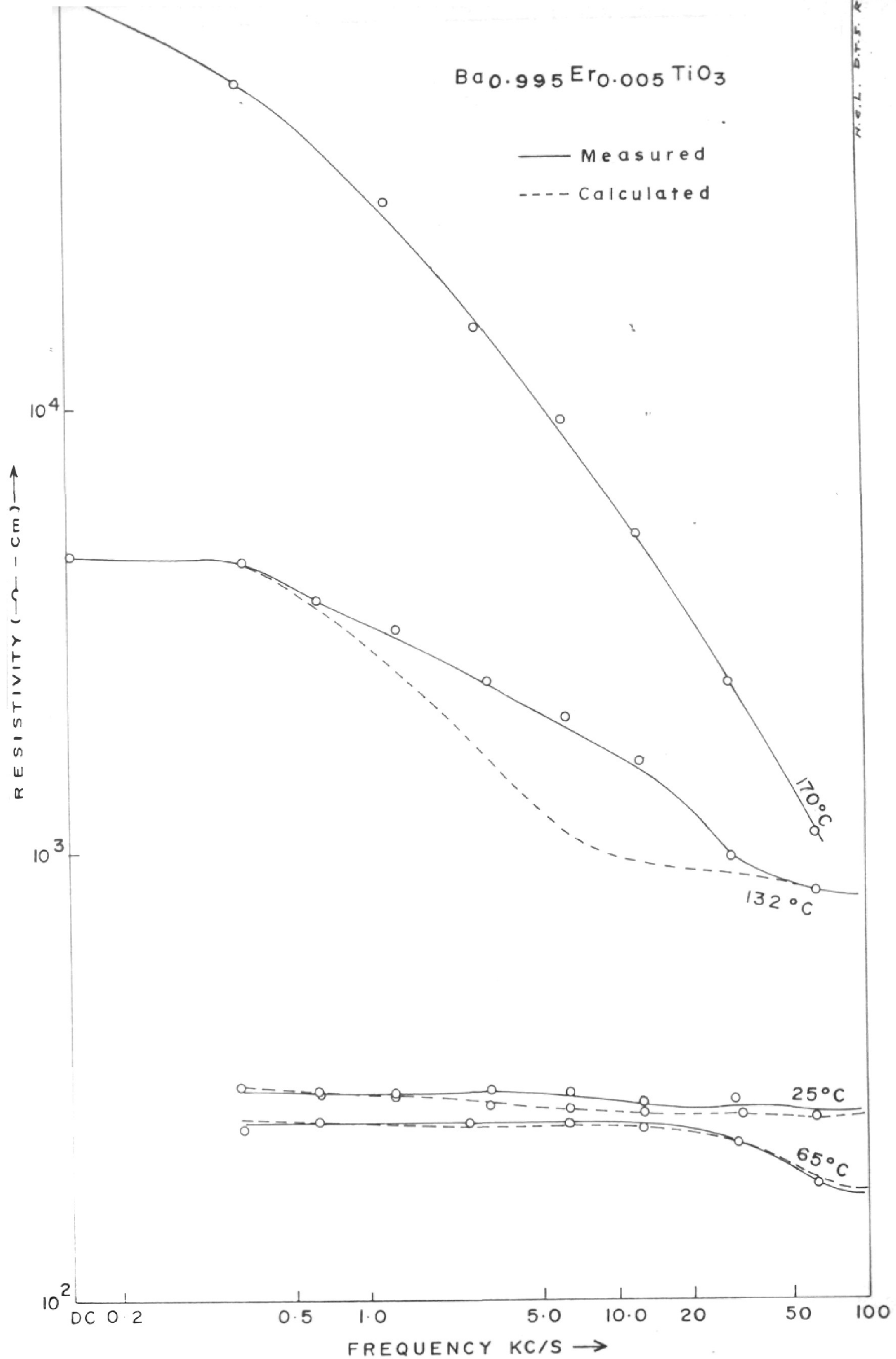

Fig. 31 Resistivity as function of frequncy at various temperatures.

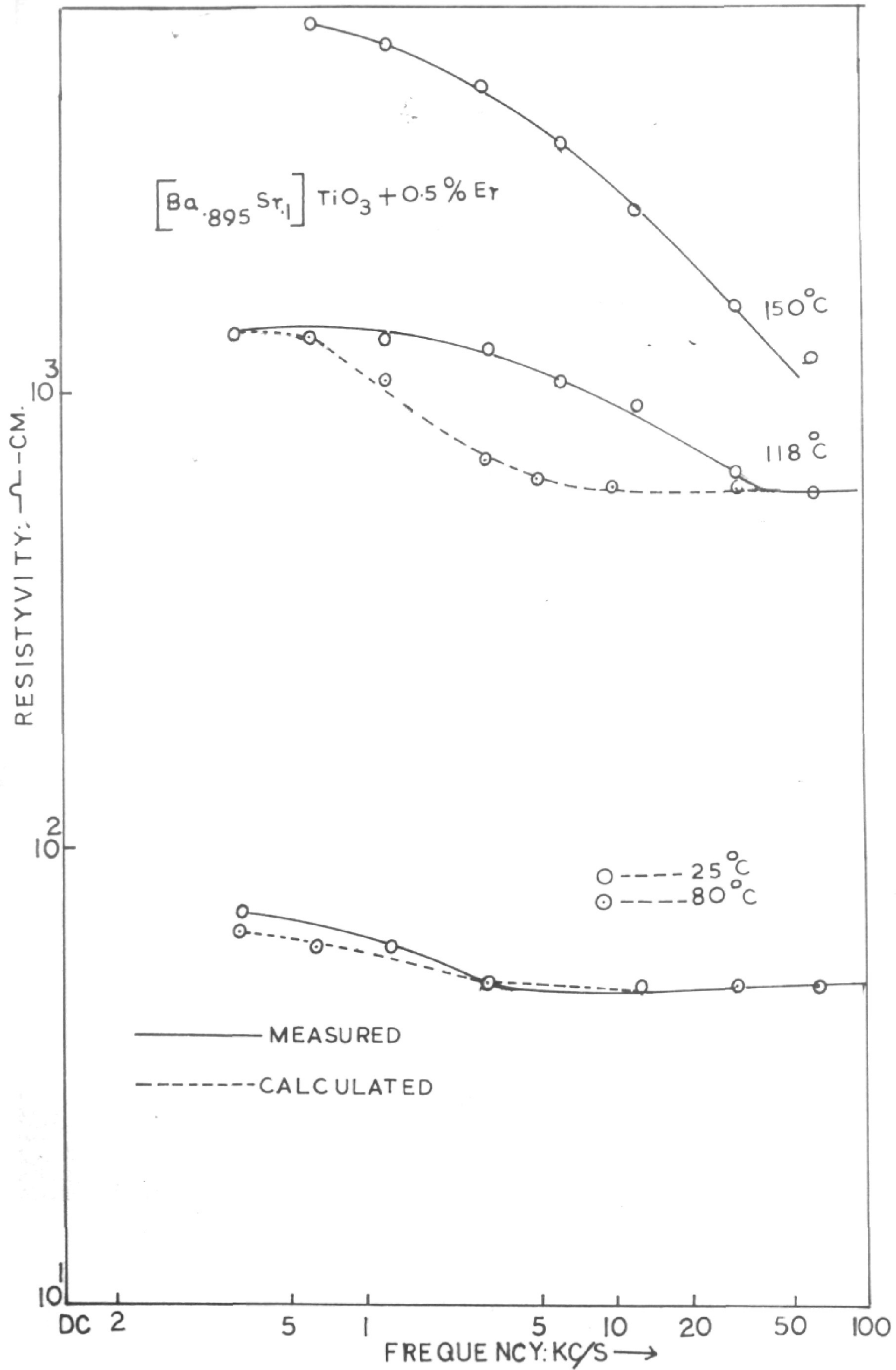

FIG. 32. DISPERSION OF RESISTIVITY.

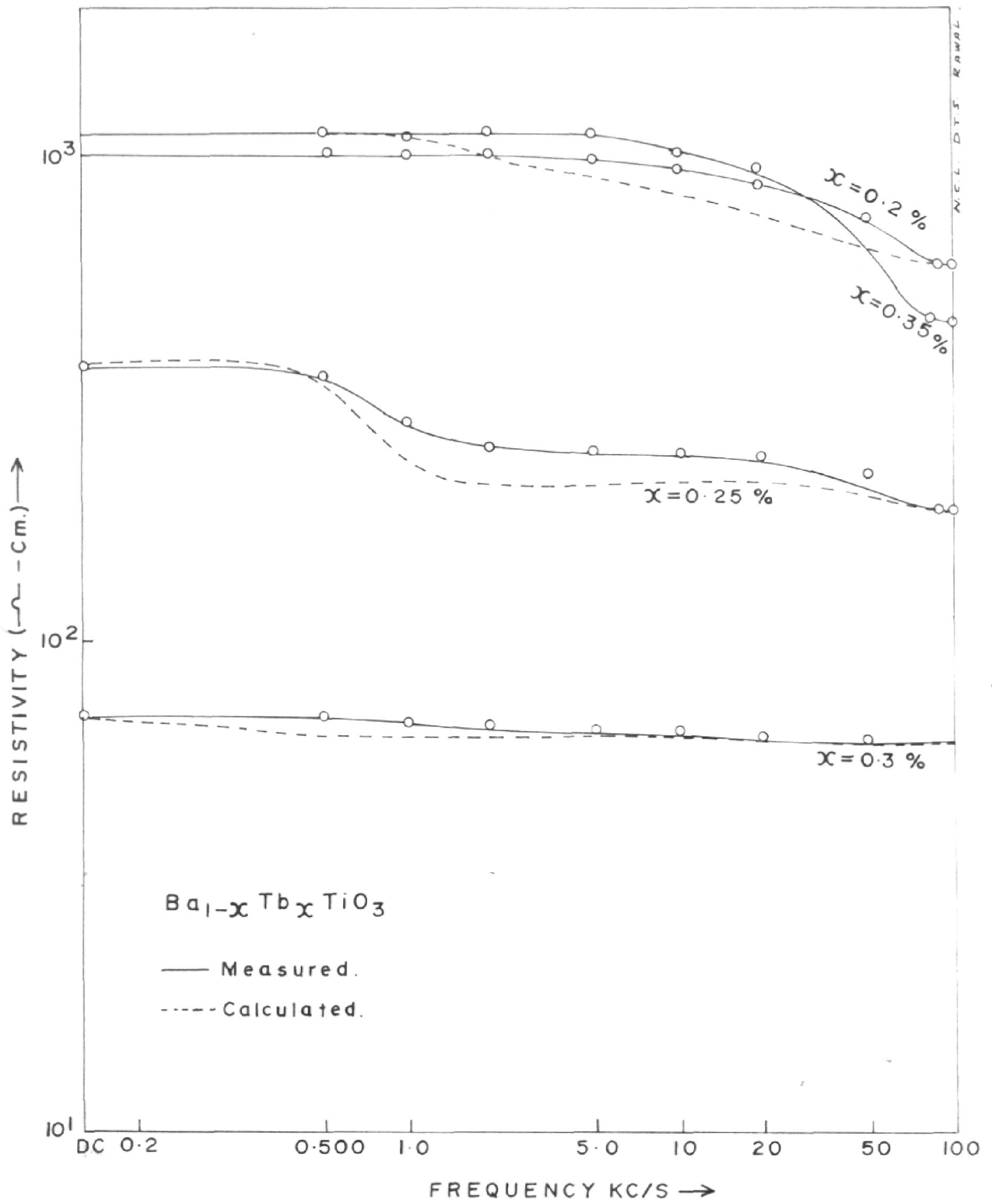

Fig. 33 Resistivity as a function of frequency at room temp.

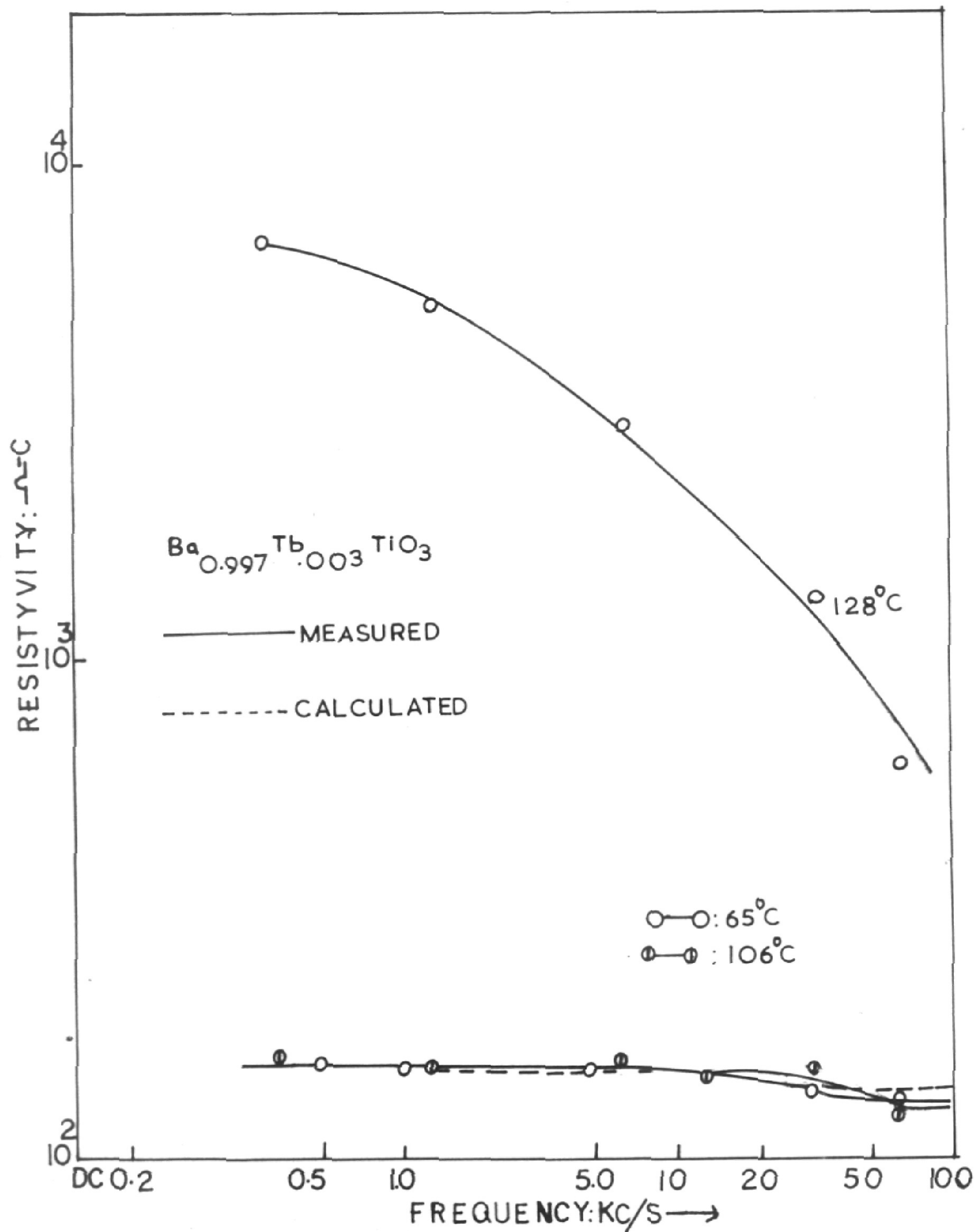

FIG. 34. DISPERSION OF RESISTIVITY

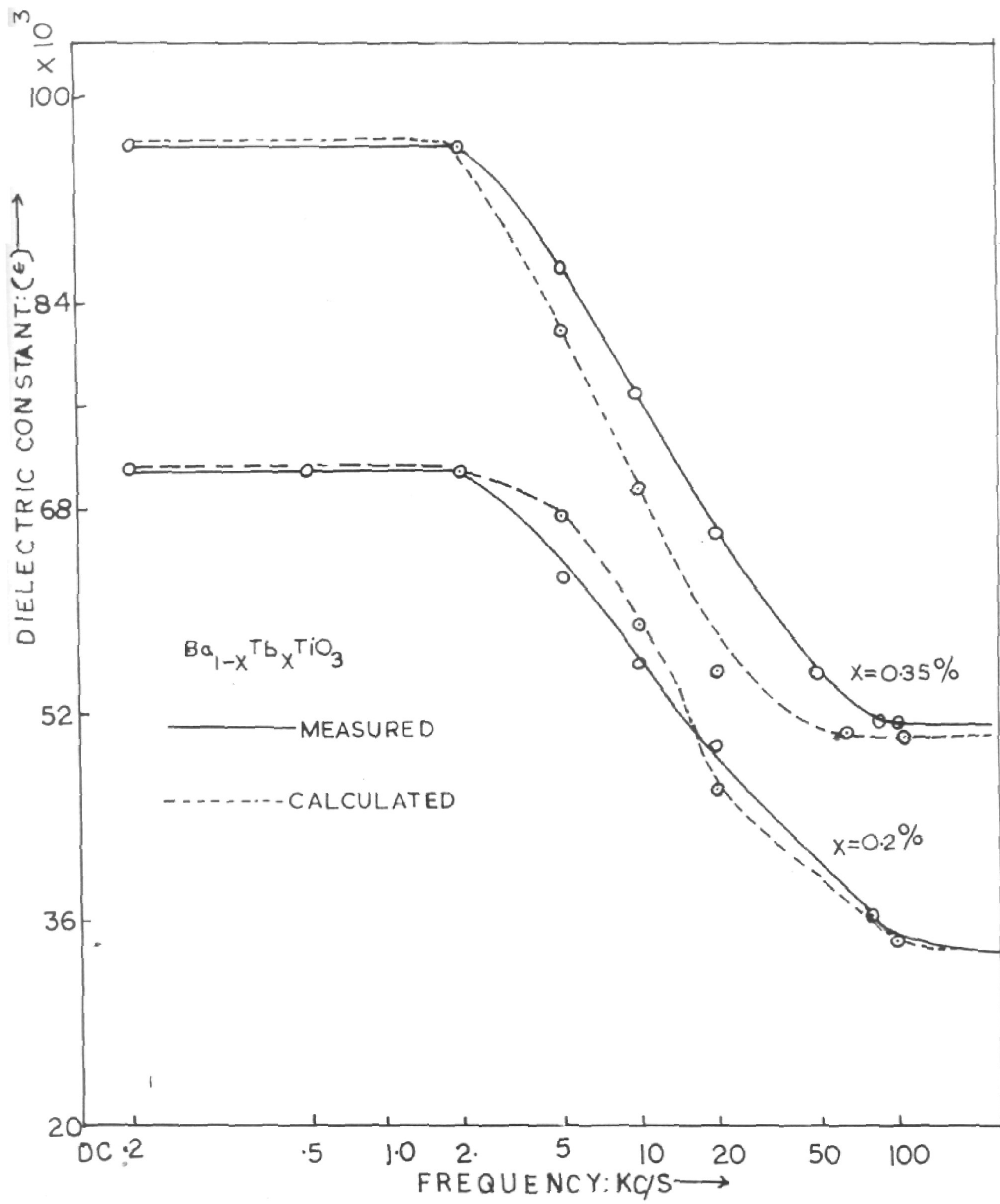

FIG 35 DISPERSION OF DIELECTRIC CONSTANT

3.3.2 Dispersion of resistivity and dielectric constant at audio frequencies:

Analysis of the electrical properties of semiconducting $BaTiO_3$ has been approached by taking into account the study of the dispersion phenomenon.[17-19] In fact Heywang's grain boundary model and Peria's stress-strain model are based on above considerations. Koops[20] observed this phenomenon earlier in nickel zinc ferrite.

Figs. 31-35 depict the dispersion in the dielectric constant and the resistivity. These effects have been interpreted by Koops as the result of an inhomogeneous dielectric structure discussed by Maxwell.[21]

According to Koops, a good phenomenological theory of the dispersion can be given on the assumption that R and C , the parallel resistance and capacitance of the material, result from an equivalent circuit as shown in fig. 3.1 in in which R_1, R_2, C_1, C_2 are constants. Since electrode

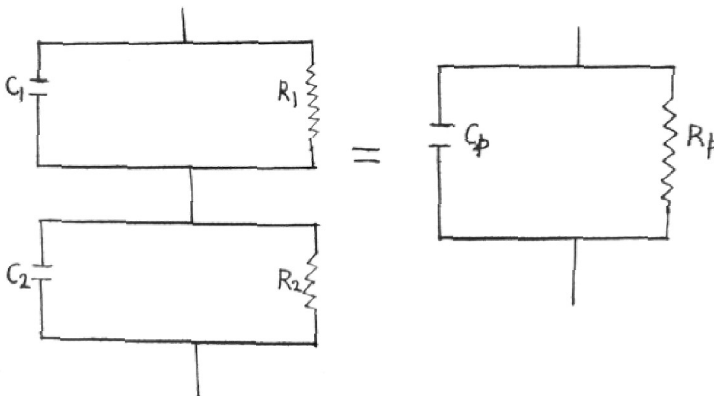

Fig.(3.1): If the right hand circuit is equivalent to the left hand one with C_1, C_2, R_1, R_2 constants, then C_p, R_p are not constants with respect to frequency, but obey dispersion formulae.(After Koops)

contacts are ohmic, there does not exist any barrier layer between the material and electrodes. A.C. theory predicts that R_p and C_p then obey dispersion formulas given in (3.13) and (3.14). This is equivalent to a solid state model consisting of relatively good conducting grains separated by poor conducting layers. The dispersion equations that Koops derived from a consideration of Fig.3.1 are represented by

$$\rho_p = \rho_p^{\infty} + \frac{\rho_p^{0} - \rho_p^{\infty}}{1 + \tau_p^{2}\omega^{2}} \qquad (3.13)$$

with

$$\left.\begin{aligned} \rho_p^{\infty} &= \frac{\rho_1 \rho_2 (\epsilon_1 + x\epsilon_2)^2}{\rho_1^2 \epsilon_1^2 + x\rho_2^2 \epsilon_2^2} \\ \rho_p^{0} &= x\rho_1 + \rho_2 \\ \tau_p &= \epsilon_0 \left(\frac{\rho_1 \rho_2 (\rho_1 \epsilon_1^2 + x\rho_2 \epsilon_2^2)}{x\rho_1 + \rho_2} \right)^{\frac{1}{2}} \end{aligned}\right\} . \qquad (3.14)$$

Similarly,

$$\epsilon_p = \epsilon_p^{\infty} + \frac{\epsilon_p^{0} - \epsilon_p^{\infty}}{1 + \tau_\epsilon^{2}\omega^{2}} , \qquad (3.15)$$

etc.

where

ρ_p = parallel resistivity

ϵ_p = parallel dielectric constant

$\rho_p^{\infty}, \epsilon_p^{\infty}$ = high frequency values of ρ_p and ϵ_p respectively

$\rho_p^{0}, \epsilon_p^{0}$ = low frequency values of ρ_p and ϵ_p respectively

τ_ρ, τ_ϵ = relaxation constants for ρ and ϵ respectively

ω = angular frequency

Let x be the ratio of the thickness of the layers to the thickness of the grains, and ρ_1, ρ_2, ϵ_1 and ϵ_2 denote the resistivity and relative dielectric constant of the layers and grains respectively. Suppose $x \ll 1$.

If the measured ρ_p and ϵ_p are to fit the dispersion equations (3.13) and (3.14), it is necessary to make an additional assumption. Let this be

$$\epsilon_1 = \epsilon_2 \qquad (3.16)$$

This assumption is based upon the knowledge that the true dielectric constant of various oxides is almost the same.

Since $x \ll 1$ and $\rho_1 \gg \rho_2$ equations (3.14) are reduced to

$$\left.\begin{aligned} \rho_p^{\infty} &= \rho_2 \\ \rho_p^{0} &= x\rho_1 + \rho_2 \\ \tau_\rho &= \epsilon_0 \, \epsilon_2 \, [\rho_1^2 \rho_2 / (x\rho_1 + \rho_2)]^{1/2} \\ \rho_p &= \rho_2 + \frac{x\rho_1}{1 + \tau_\rho^2 \, \omega^2} \end{aligned}\right\} \qquad (3.17)$$

Table No.12

Measured and Derived values used in calculating theoretical resistivity and dielectric constant Vs frequency curves of Figs. 32-35

Sample No.	Temp. °C	$\rho_p^{\infty} = \rho_2$ Ω cm	ρ_p^{0} Ω cm	$\epsilon_1 = \epsilon_2 = \epsilon_{\infty}$	$X\rho_1$	τ_p sec.	τ_f sec.
E_{10}	25	2.6×10^2	3.06×10^2	4.3×10^4	46.0	0.8×10^{-4}	
E_{10}	65	2.07×10^2	2.5×10^2	3.3×10^4	43.0	0.2×10^{-3}	
E_{10}	132	8.0×10^2	4.3×10^3	3.9×10^4	37.0	0.2×10^{-3}	
S_2	25	4.9×10	72.0	2.8×10^4	23.0	0.5×10^{-3}	
S_2	118	6.0×10^2	1.4×10^3	7.6×10^4	0.8×10^3	0.8×10^{-4}	
T_4	25	5.9×10^2	10^3	3.4×10^4	4.1×10^2	0.3×10^{-4}	1.13×10^{-5}
T_5	25	189.0	350.0	2.6×10^4	161.0	0.1×10^{-2}	
T_6	25	63.0	72.0	3.1×10^4	9.0	10^{-3}	
T_6	65	132.0	150.0	4.9×10^4	18.0	0.4×10^{-4}	
T_7	25	4.5×10^2	1.1×10^3	5.1×10^4	6.5×10^2	0.3×10^{-4}	1.4×10^{-5}

and

$$
\left.
\begin{aligned}
\epsilon_p^{\infty} &= \epsilon_2 = \epsilon_1 \\
\epsilon_p^{o} &= \epsilon_2 \cdot \frac{x\rho_1^2 + \rho_2^2}{(x\rho_1 + \rho_2)^2} \\
\tau_\epsilon &= \epsilon_0 \, \epsilon_2 \cdot \frac{\rho_1 \cdot \rho_2}{x\rho_1 + \rho_2}
\end{aligned}
\right\} \qquad (3.18)
$$

In figures 31 - 35, experimental as well as calculated values are shown. Investigations were carried out at different temperatures through the PTCR range. Dashed lines were obtained by equations (3.17) and (3.18) using the value for ρ_1, ρ_2, τ_ρ, ϵ_2 etc. summarised in Table No. 12. The agreement between calculated and experimental values below the Curie point is good.

A sharp rise in the resistivity at low frequencies (ρ_p^{o}) occurs above the Curie-point and as the frequency is increased the values are lowered and tend to a constant value (ρ_p^{∞}). From equation (3.17) it follows that if the change in ρ_2 $(= \rho_p^{\infty})$ is small, the sharp rise in ρ_p^{o} must result from the increase in $x\rho_1$ and since x is $\ll 1$, ρ_1 must be high. This is in agreement with the model proposed.

The deviation between calculated and measured curves is greater for temperature above the Curie-point. These deviations may be accounted for by postulating that the variations in the properties and the thickness of layers give rise to a number of relaxation times.

3.4 Thermoelectric Effect

Since Hall data were not readily attainable for semiconducting $BaTiO_3$ due to its thermal noise, spurious piezoresistance signal and very small Hall voltage, thermoelectric power measurements were utilized here to determine the nature of the majority carriers and their concentration.

Seebeck was first to discover this effect. He found that an electromotive force is developed when two wires of different metals are joined together and their two ends are maintained at two different temperatures. The Seebeck coefficient (α) is defined as

$$\alpha = dV_{1-2} / dT \qquad (3.19)$$

where

dV_{1-2} = e.m.f. across the junction (thermo e.m.f.)

dT = temperature difference.

If the polarity is as shown in Fig.3.2 the absolute thermoelectric power of 1 is greater than 2.

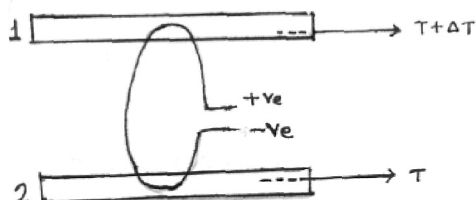

Fig. 3.2

The Seebeck effect may be thought of as a diffusion process. The electrons or holes from the hot end have higher kinetic energy as compared to those from the cold end and hence electric current is produced.

For monovalent metals, quantum theory yields the following relationship for α[22]

$$\alpha = \frac{\pi^2 k^2 T}{3e} \left[\frac{1}{E_f} + \left(\frac{1}{l} \frac{dl}{d\epsilon} \right) \right] \tag{3.20}$$

where

k = Boltzmann's constant

T = absolute temperature

e = electronic charge

E_f = chemical potential of electrons which in case of metals is equal to the Fermi level energy.

l = mean free path length of electrons with a kinetic energy.

For semiconductors with two types of carriers α is given by

$$\alpha = \frac{k}{6} \left\{ \mu_e n_e \left[A + \ln \frac{2(2\pi m_e^* kT)^{3/2}}{h^3 n_e} \right] - \mu_h n_h \left[A + \ln \frac{2(2\pi m_h^* kT)^{3/2}}{h^3 n_h} \right] \right\} , \tag{3.21}$$

where 6 = electrical conductivity, μ_e and μ_h are electron and hole mobilities respectively. A is a constant and depends

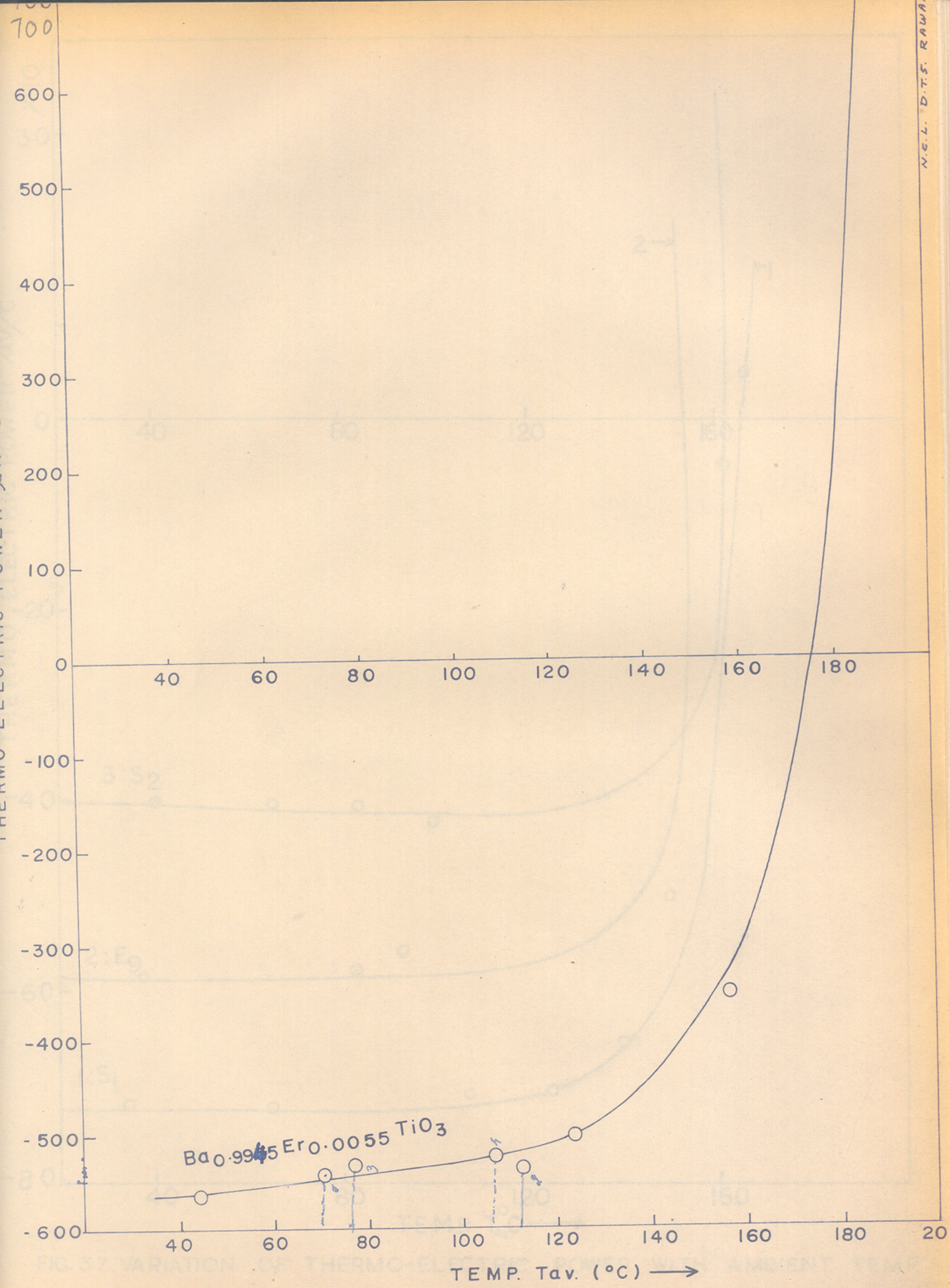

Fig. 36 Variation of thermo-electric power with ambient temperatures

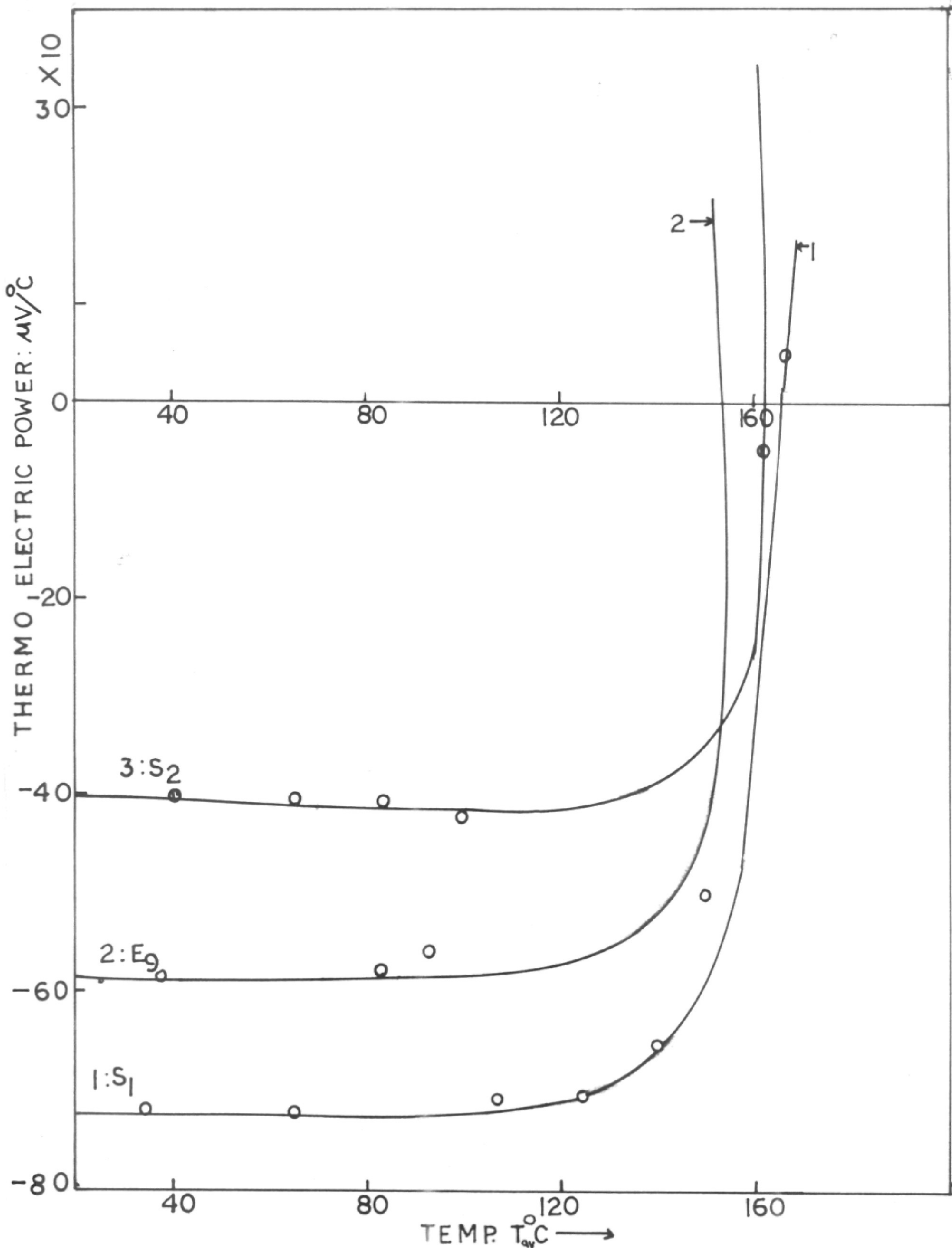

FIG. 37. VARIATION OF THERMO-ELECTRIC POWER WITH AMBIENT TEMP.

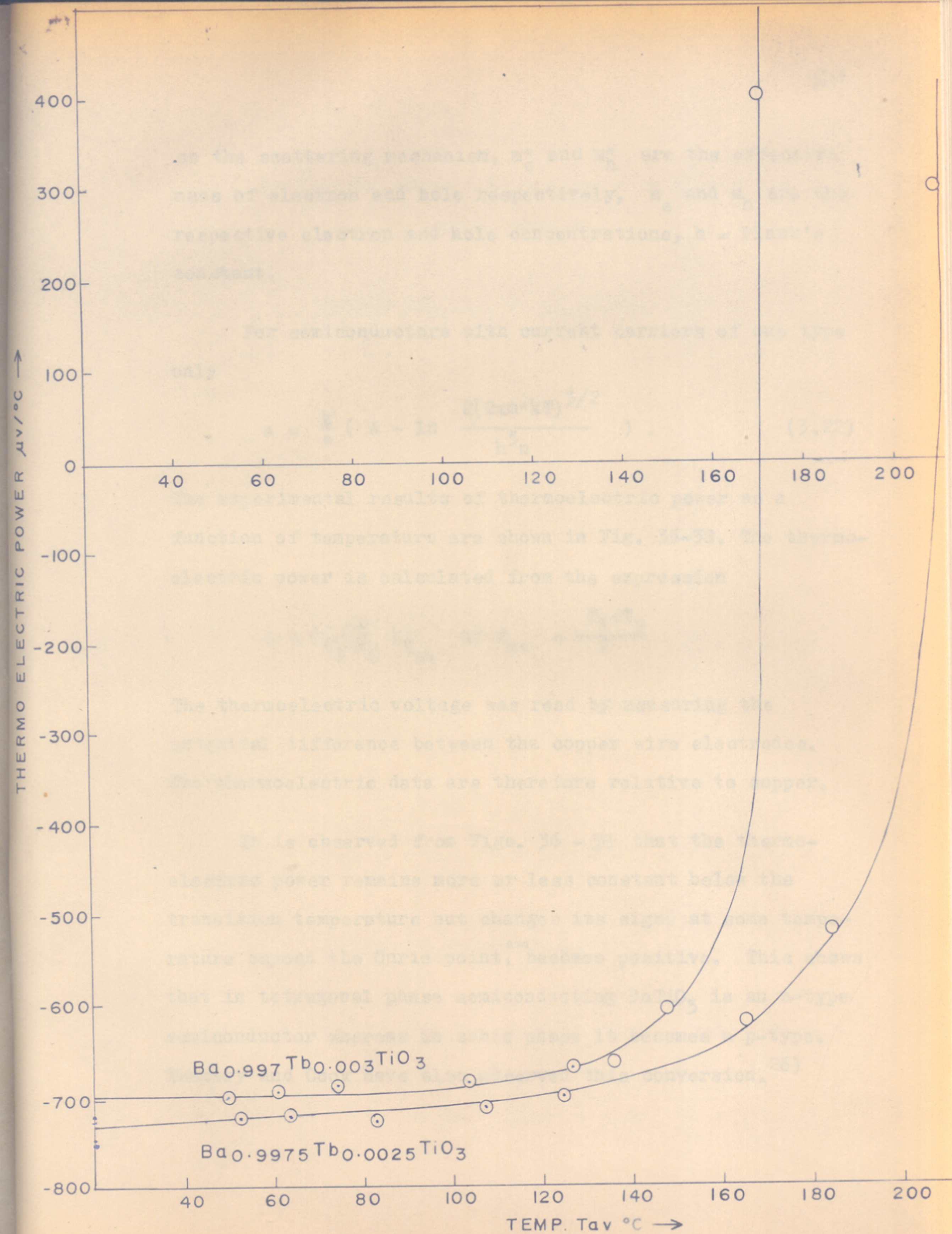

Fig.38. Variation of thermo-electric power with ambient temperatures

on the scattering mechanism, m_e^* and m_h^* are the effective mass of electron and hole respectively, n_e and n_h are the respective electron and hole concentrations, h = Plank's constant.

For semiconductors with current carriers of one type only

$$\alpha = \frac{k}{e} \left(A + \ln \frac{2(2\pi m^* kT)^{3/2}}{h^3 n} \right) . \qquad (3.22)$$

The experimental results of thermoelectric power as a function of temperature are shown in Fig. 36-38. The thermoelectric power is calculated from the expression

$$\alpha = \left(\frac{\Delta E}{T_1 - T_2} \right)_{T_{av}} \quad \text{at } T_{av} = \frac{T_1 + T_2}{2}$$

The thermoelectric voltage was read by measuring the potential difference between the copper wire electrodes. The thermoelectric data are therefore relative to copper.

It is observed from Figs. 36 - 38 that the thermoelectric power remains more or less constant below the transition temperature but changes its sign at some temperature beyond the Curie point, and becomes positive. This shows that in tetragonal phase semiconducting $BaTiO_3$ is an n-type semiconductor whereas in cubic phase it becomes a p-type. Tennery and Cook have also observed this conversion.[26]

Table - 13

Carrier Concentration Calculated by thermo e.m.f. measurements

System: $Ba_{0.9955}Er_{0.0045}TiO_3$

Temperature °C	37.5	54.0	73.0	113	126
Carrier concentration $(n_c) \times 10^{18}$	1.45	0.89	1.47	1.4	1.8

System: $Ba_{0.9945}Er_{0.0055}TiO_3$

Temperature °C	70.0	77.3	107.0	112.0
Carrier concentration $(n_c) \times 10^{17}$	6.98	8.1	10.1	8.9

System: $Ba_{0.9975}Tb_{0.0025}TiO_3$

Temperature °C	52.5	64.5	83.0	107.5	125.5
Carrier Concentration $(n_c) \times 10^{17}$	0.79	0.87	0.87	1.1	1.4

Table 13 (continued)

System: $Ba_{0.997}Tb_{0.003}TiO_3$

Temperature °C	50.0	62.0	75.0	104.0	127.5
Carrier concentration (n_c) x 10^{17}	1.03	1.2	1.3	1.5	2.02

System: $(Ba_{0.945}Sr_{0.05}Er_{0.005})TiO_3$

Temperature °C	51.0	65.5	80.0	108.0	125.0
Carrier concentration (n_c) x 10^{17}	0.89	0.85	1.07	1.2	1.3

System: $(Ba_{0.895}Sr_{0.10}Er_{0.005})TiO_3$

Temperature °C	41.0	65.0	84.5	106.0	122.0
Carrier concentration (n_c) x 10^{18}	3.00	3.6	3.4	3.08	2.50

The formula used to calculate the value of n_c was derived from equation (3.22). Taking the value for A = 2.5 and rearranging the terms, equation (3.22) becomes

$$\log n_c = 3/2 \log T - 0.005\, \alpha + 16.76 \qquad (3.23)$$

(in C.G.S.units)

The value of n_c lies between 10^{17} to 10^{18} / cm^3. The order of n_c thus obtained is similar to that reported by Saburi[54] and Ikushima et al[47] (cf. chapter-1)

The values of carrier concentration (n_c) in the ferroelectric region, are listed in table No.13. From the data obtained it can be concluded that the carrier concentration remains constant upto a certain higher range beyond the transition temperature.

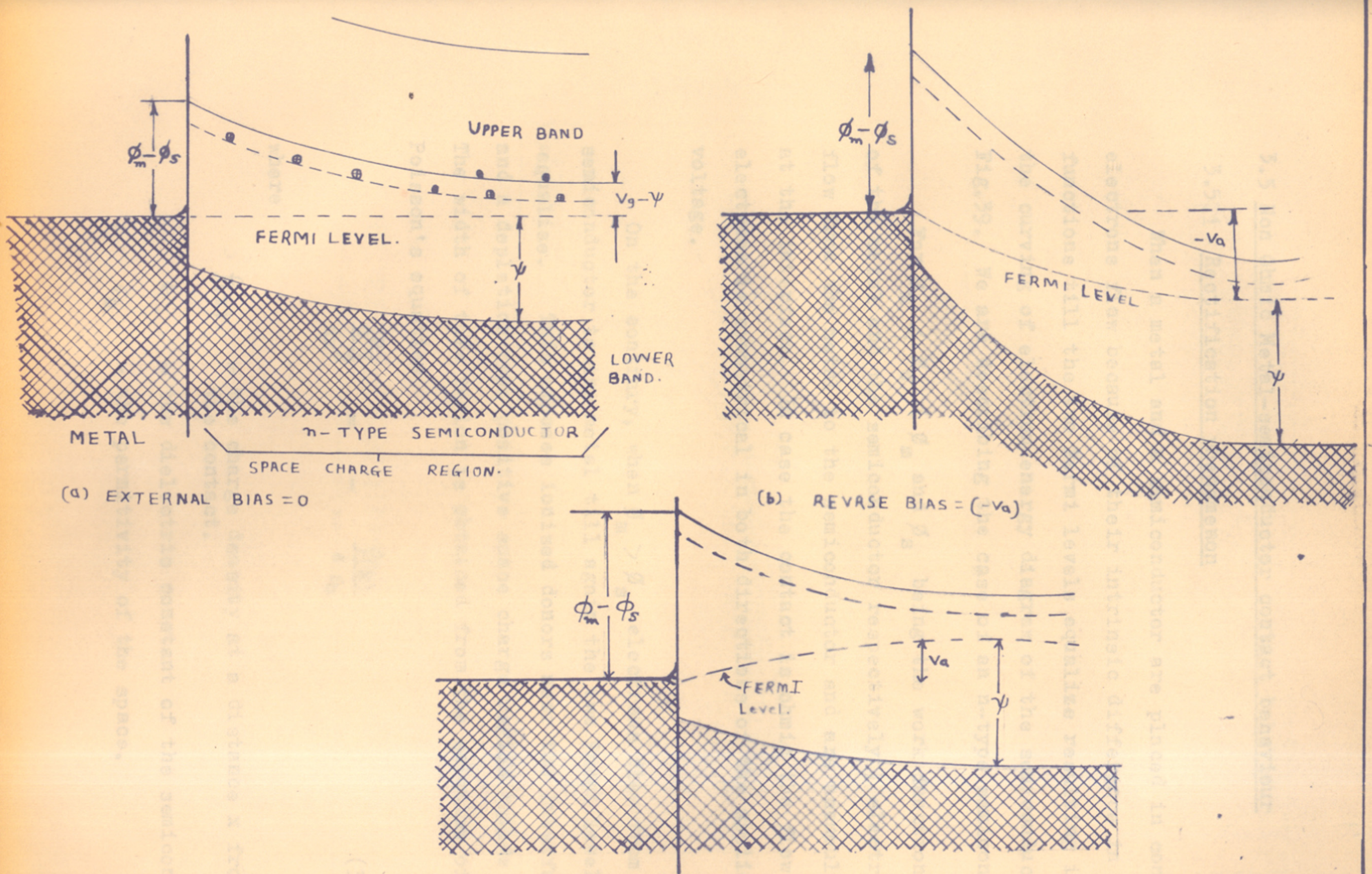

Fig. 39 THE ENERGY LEVEL PROFILES FOR A METAL-TO-n-TYPE SEMICONDUCTOR

3.5 Non Ohmic Metal-semiconductor contact behaviour

3.5.1 Rectification phenomenon

When a metal and a semiconductor are placed in contact, electrons flow because of their intrinsic difference in work functions till the two Fermi levels equalize resulting in the curving of electron energy diagram of the semiconductor Fig.39. We are describing the case of an n-type semiconductor.

For $\phi_m < \phi_s$ (ϕ_m and ϕ_s being the work functions of the metal and the semiconductor respectively) electrons flow from the metal to the semiconductor and are accumulated at the interface. In case the contact is ohmic the flow of electrons is symmetrical in both directions of the applied voltage.

On the contrary, when $\phi_m > \phi_s$ electrons flow from the semiconductor to the metal till again the two Fermi levels equalise. This exposes ionised donors near the interface and a depletion type positive space charge region builds up. The width of this region is obtained from the solution of Poisson's equation

$$\frac{d^2V}{dx^2} = - \frac{\rho(x)}{\epsilon \epsilon_0} \qquad (3.24)$$

where

$\rho(x)$ = the charge density at a distance x from the contact.

ϵ = the dielectric constant of the semiconductor

ϵ_0 = the permitivity of the space.

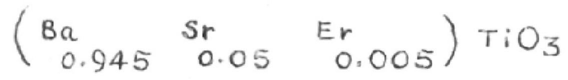

Ag : (In-Hg) Electrodes.

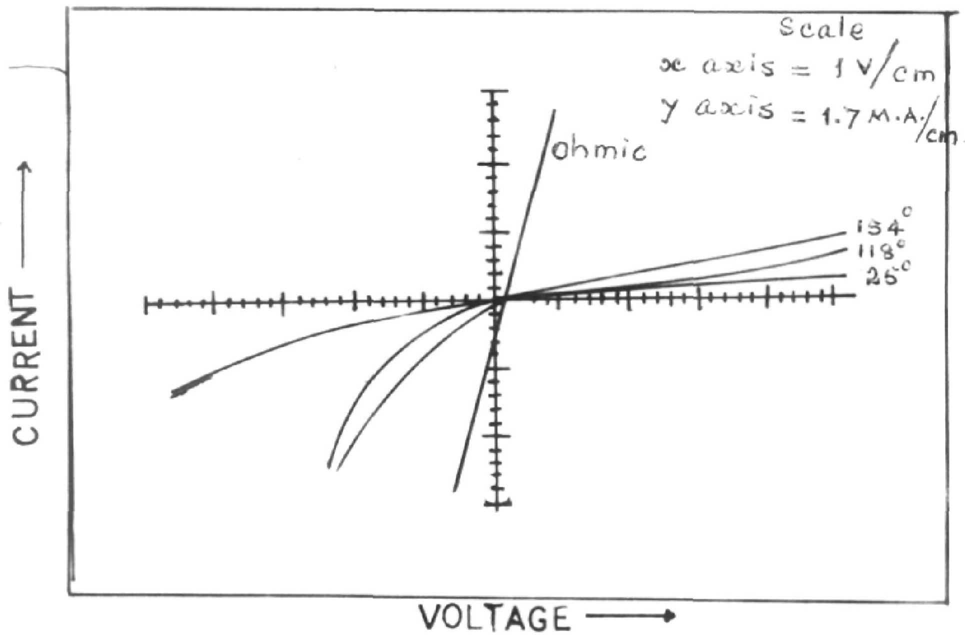

FIG. 40: RECTIFICATION PHENOMENON.

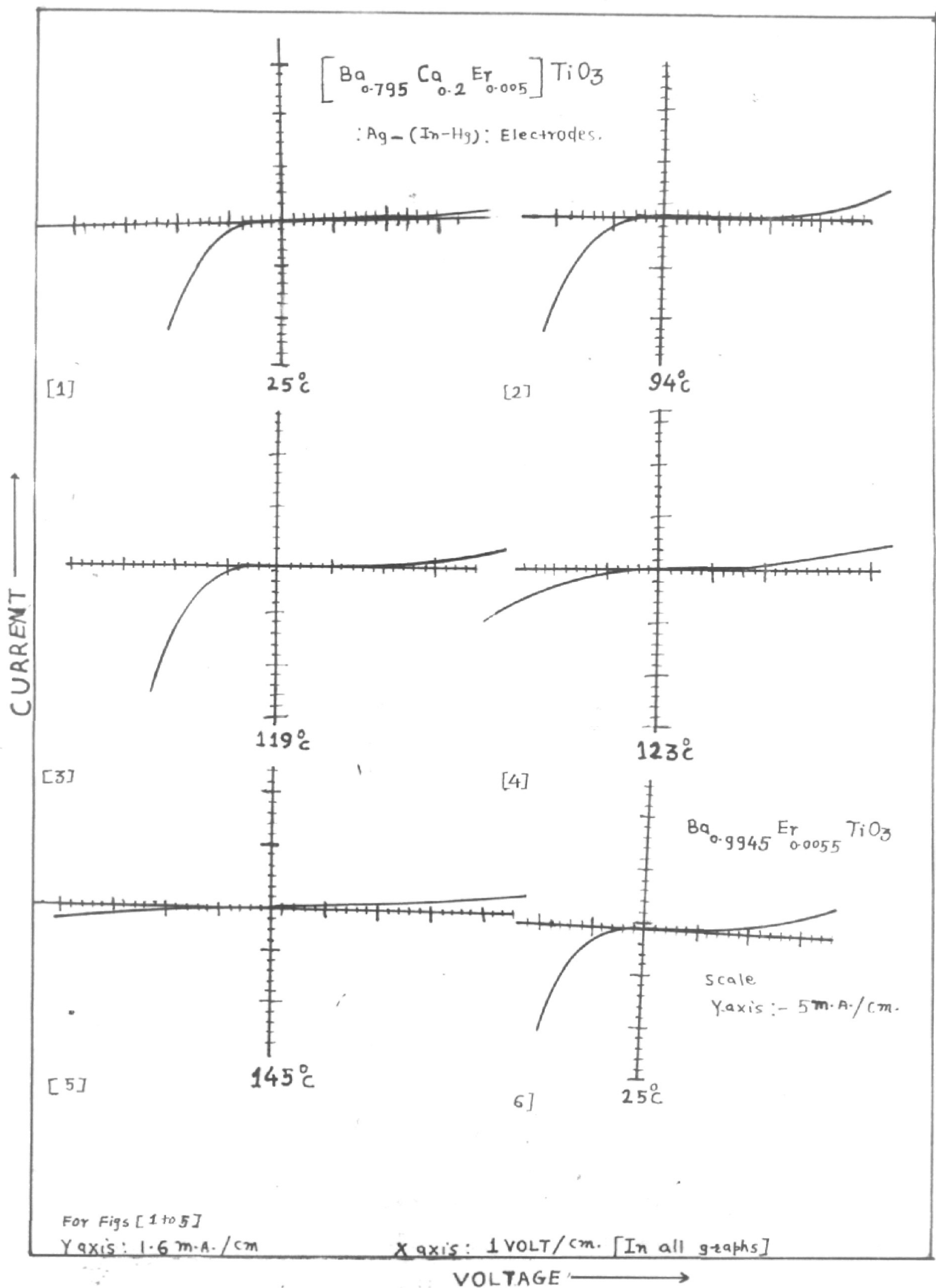

FIG. 41. RECTIFICATION PHENOMENON

Considering the simple case where the space charge region is only due to the ionised donors, the depletion region width x_d is obtained by solving (3.24),

$$x_d = \left[\frac{2\epsilon\epsilon_0 (V + V_B)}{qN} \right]^{1/2} \qquad (3.25)$$

where

V = applied voltage

V_B = diffusion voltage given by $\phi_m - \chi$ (χ being the electron affinity)

N = ionised donor density

q = electronic charge.

The diffusion potential V_B offers a barrier to the flow of electrons from the semiconductor to the metal. If a positive potential is applied to the semiconductor Fig.39-b, the electrons have to cross the contact potential barrier,

$$\phi = \phi_m - \phi_s \qquad (3.26)$$

On the other hand for a negative voltage V applied to the semiconductor Fig.40-C, the barrier to electron flow reduces to V_B-V resulting in an easy flow direction (forward bias). In the former case the system is said to be under reverse bias. This phenomenon is known as the rectifying property of the semiconductor.

An overall voltage current characteristic for typical compositions of semiconducting $BaTiO_3$ is shown in Fig.40-41.

The easy (or forward-bias) direction occurs upon the application of a negative voltage to the In-Hg (Ohmic) contact of semiconductor and the difficult (or backward-bias) direction occurs when the applied potential becomes positive. This is in accordance with the above expectation. Therefore, it is confirmed that the semiconducting $BaTiO_3$ is an n-type semiconductor.

The theory of Schottky field emission predicts a current dependence given by

$$J = AT^2 \exp \left(\frac{-\phi}{kT} \right) \exp \left[\frac{q}{2kT} \left(\frac{qE}{\pi \epsilon \epsilon_0} \right)^{1/2} \right] , \qquad (3.27)$$

where

A = Richardson constant

ϕ = metal semiconductor work function i.e. barrier height

k = Boltzmann constant

q = electronic charge

T = absolute temperature

E = contact field in V/cm

ϵ = relative permittivity in the space charge region.

For Au-CdS diode, Zuleeg and Muller[23)] have shown that the current density J reduces to

$$J = J_0 \exp (1.47 \times 10^{-2} (E/\epsilon)^{1/2} \text{ at } 300^\circ k , \qquad (3.28)$$

where

$$j_0 = AT^2 \exp (- \phi / kT)$$

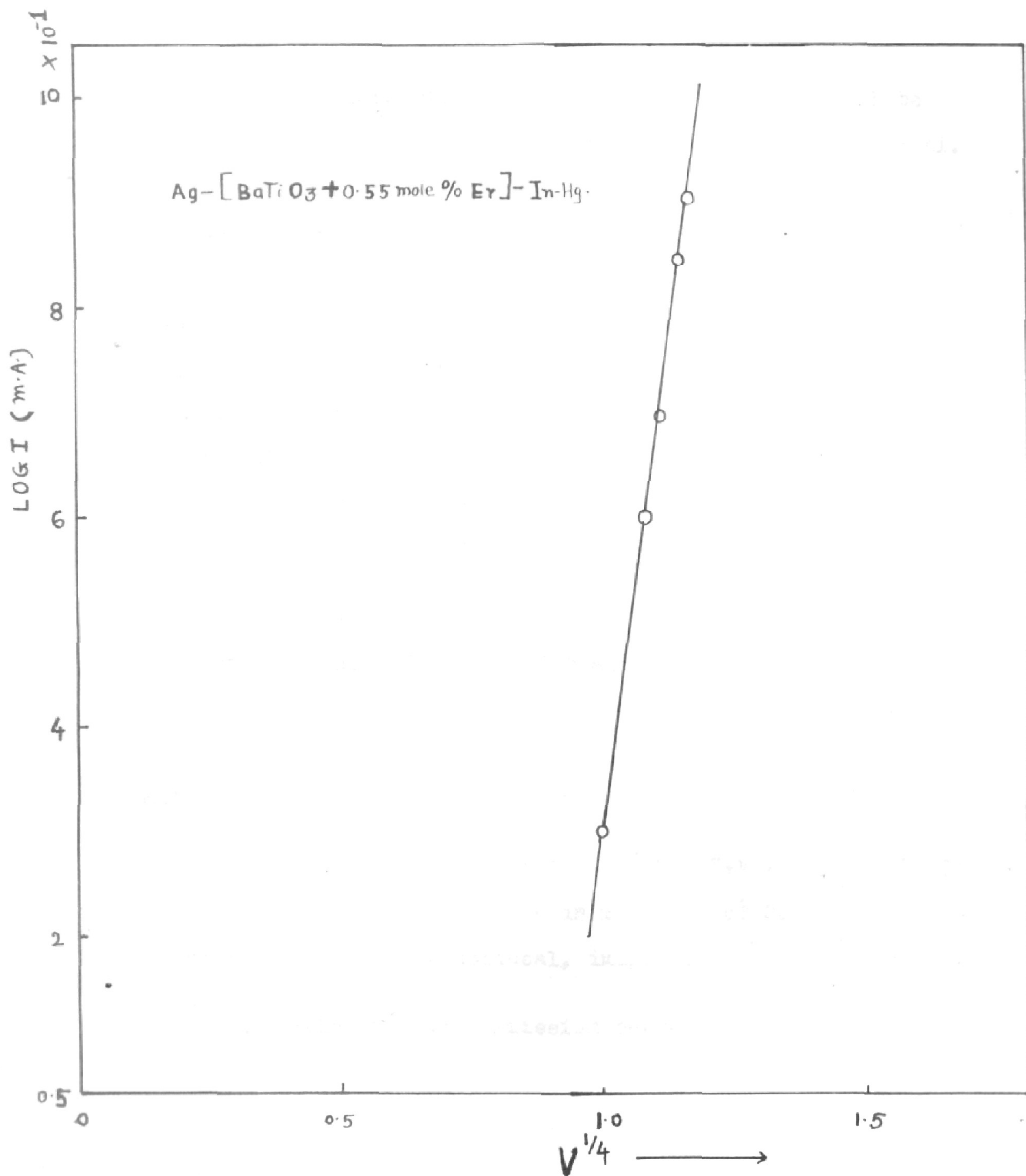

Fig. 42 LOG. PLOT OF FORWARD BIASED CURRENT Vs. THE FOURTH ROOT OF APPLIED VOLTAGE.

The electric field strength (E) at the contact will be a function of the space charge configuration in the crystal. If the interior of the crystal is charge free or if the surface space charge layer is of Mott type[24)] then E should be directly proportional to the average field. Physical reasons that E may not have exactly the value of the average field have been discussed by Muller[25)]. Briefly, these reasons stem from a nonideal surface, from an inaccurate knowledge of the emitting surface-area. These effects act to make the contact field appear to be larger than the field calculated for the idealised situation.

It is possible to formulate an expression for the contact field as a function of bias from considerations of the nature of the barrier layer formed at the junction between the metal and the semiconductor. According to Zuleeg and Muller[23], for a Schottky barrier

$$J = J_o \exp [\ 3.45 \times 10^{-4} \beta^2 N_d (V+V_B)^{\frac{1}{4}}], \qquad (3.29)$$

(in the case of CdS),

where β accounts for a nonideal, image-force emission condition.

Thus Schottky field emission current requires that the plot log J Vs $V^{\frac{1}{4}}$ should be linear.

Figure 42 shows a representative graph. The values are obtained from the interpolation of Fig.41-6 and listed in table No.14. It indicates that under forward bias conditions, Schottky emission takes place.

The effect of temperature on rectification phenomenon has also been studied. Figs. 40-41 show that upto the Curie point (T_c) the nature of voltage - current characteristics remains the same. Above T_c rectification rapidly vanishes and Schottky field emission current is decreased. These results stemp from resistivity anomaly above the transition temperature.

Table No.14

Voltage - current values interpolated from Fig.41-(6)

(Forward bias)

Current (J) (M.A.)	Voltage (V) (volts)	log J $\times 10^{-1}$ M.A.	$V^{\frac{1}{4}}$
2.0	1.0	3.010	1.0
4.0	1.4	6.021	1.086
5.0	1.5	6.990	1.109
7.0	1.7	8.451	1.140
8.0	1.8	9.031	1.157

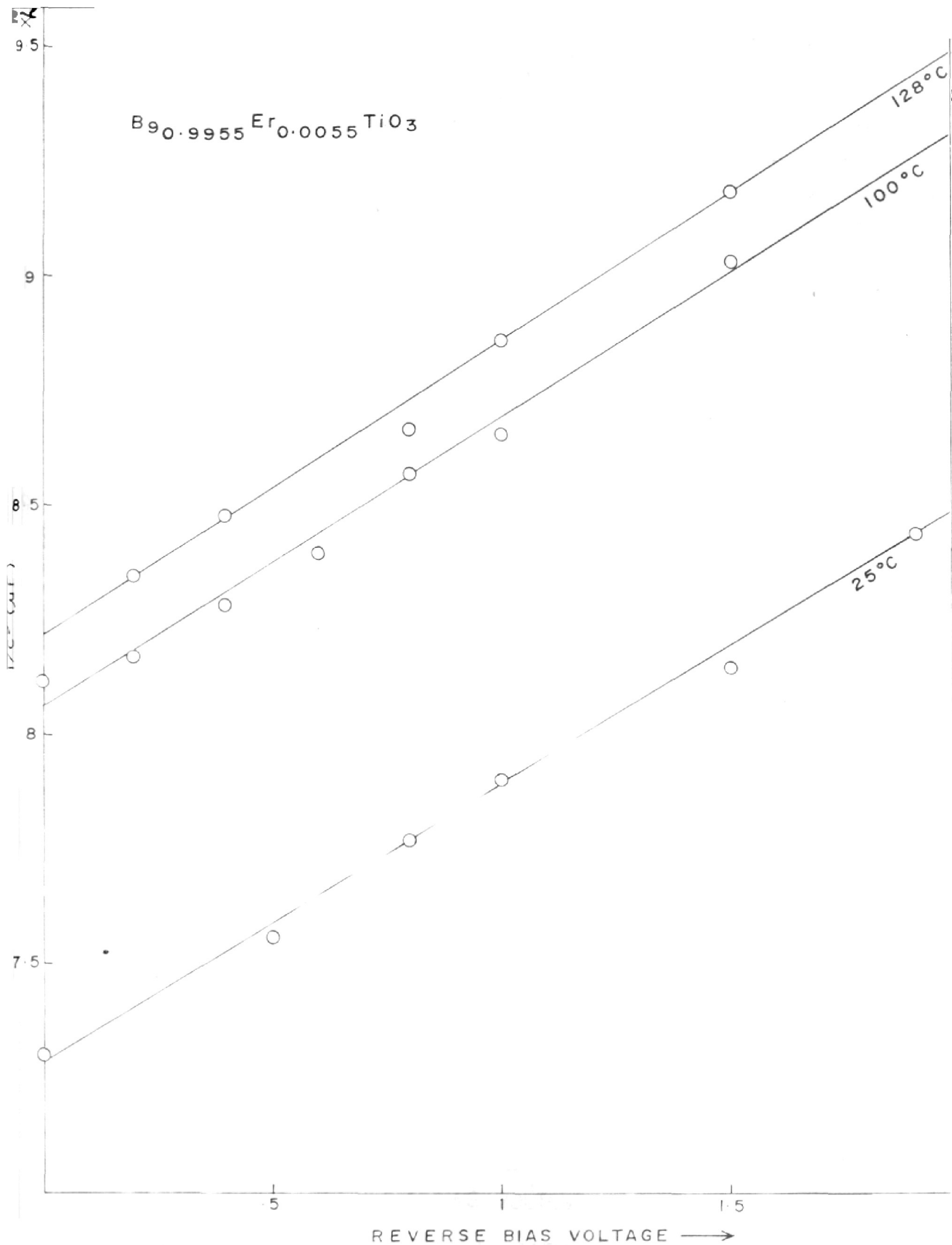

Fig. 43 Bias voltage dependence of Barrier layer Capacitance.

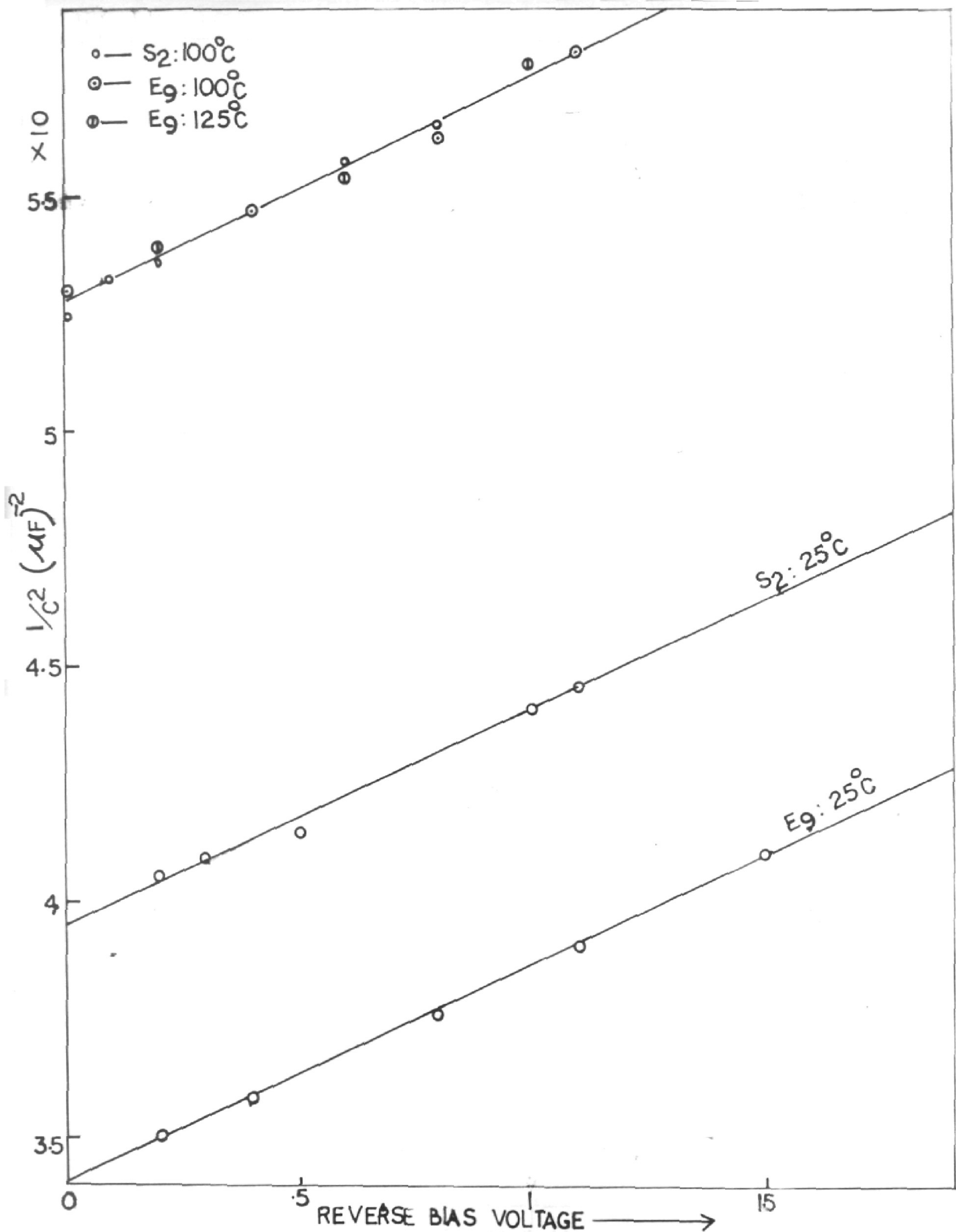

FIG. 4.4. BIAS VOLTAGE DEPENDENCE OF BARRIER-LAYER CAPACITANCE.

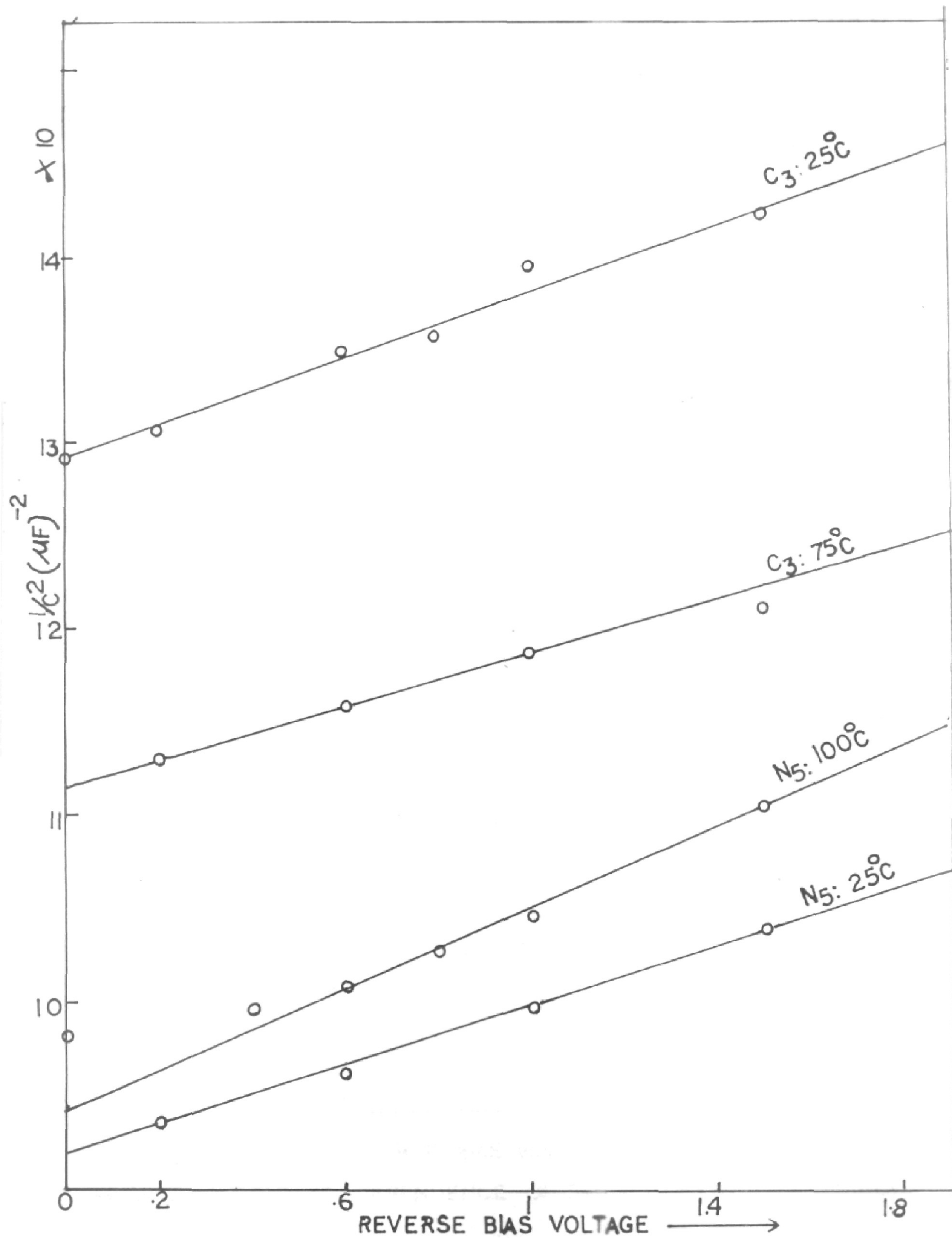

FIG.45. BIAS VOLTAGE DEPENDENCE OF BARRIER-LAYER CAPACITANCE.

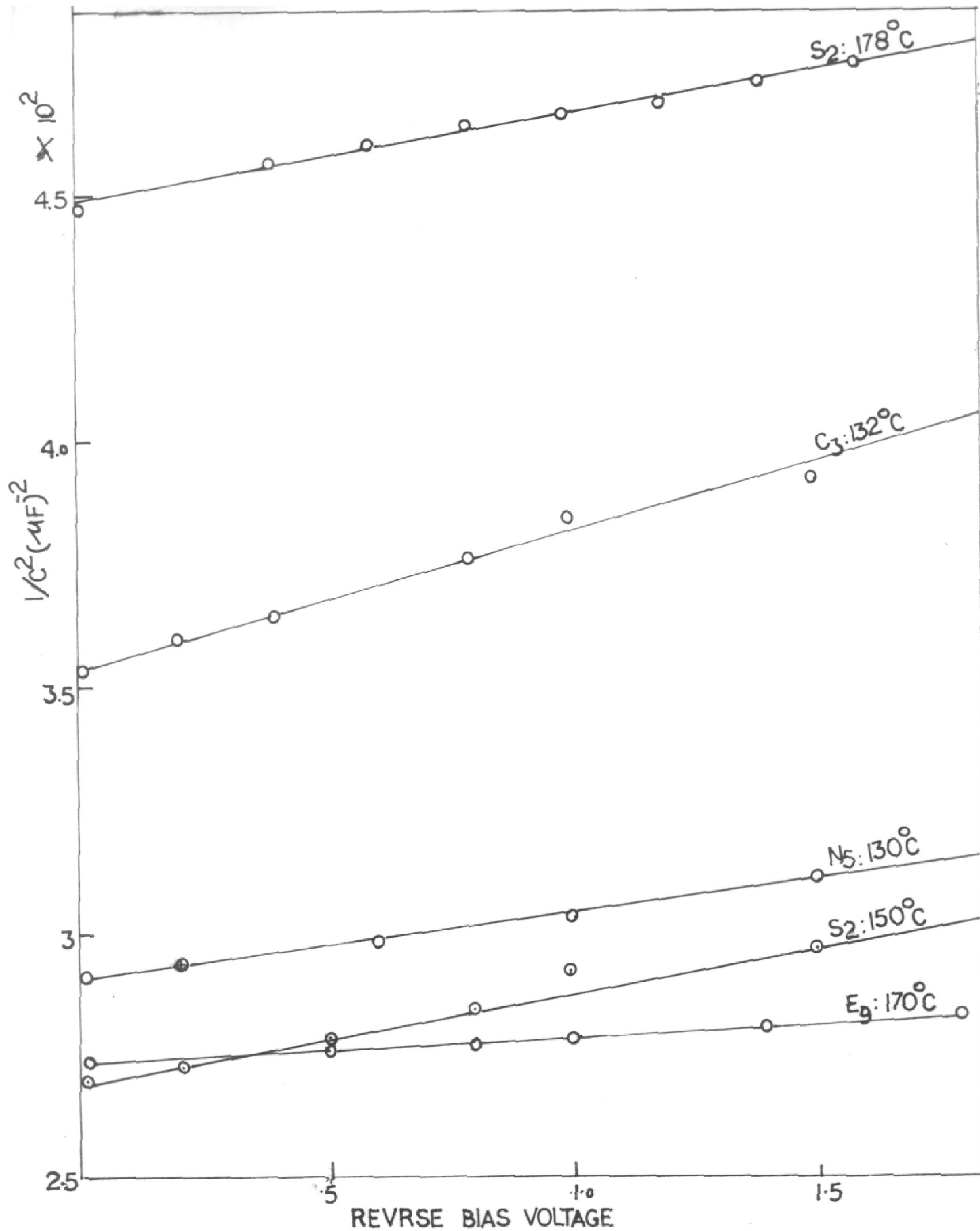

FIG. 46. BIAS VOLTAGE DEPENDENCE OF BARRIER-LAYER CAPACITANCE.

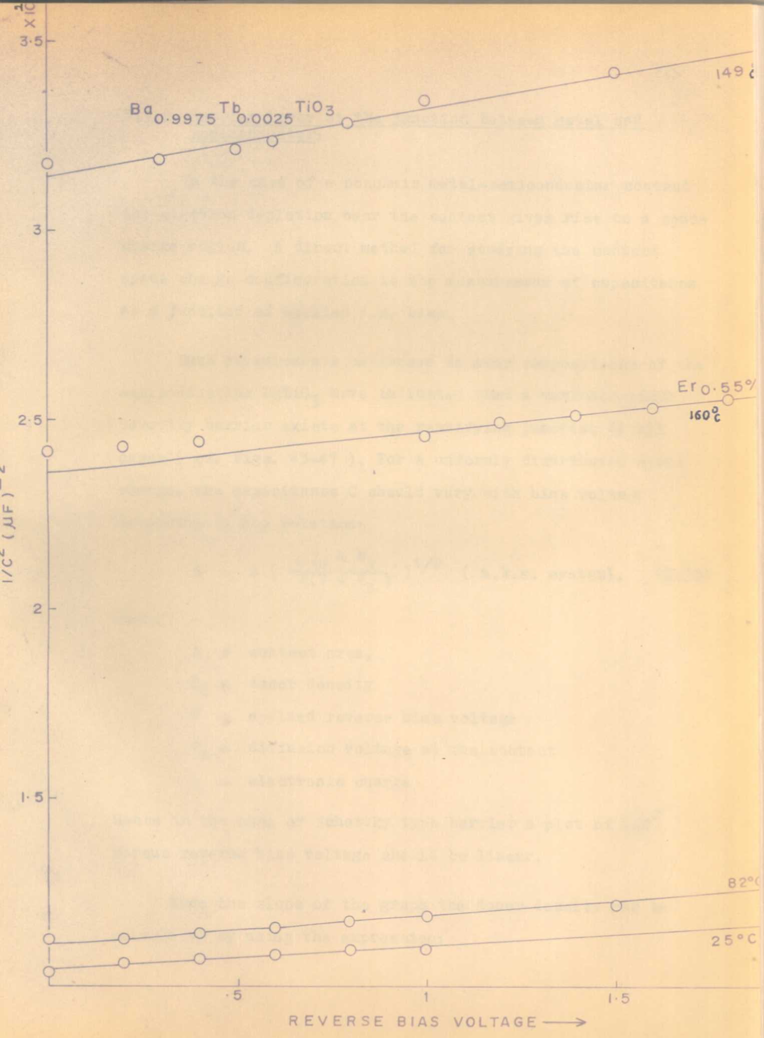

Fig. 47. Bias voltage dependence of Barrier layer Capacitance

3.5.2 Barrier layer at the junction between metal and semiconductor:

In the case of a nonohmic metal-semiconductor contact the electron depletion near the contact gives rise to a space charge region. A direct method for studying the contact space charge configuration is the measurement of capacitance as a function of applied d.c. bias.

Such measurements performed on many compositions of the semiconducting $BaTiO_3$ have indicated that a variable-width Schottky barrier exists at the rectifying junction in all cases (cf. Figs. 43-47). For a unformly distributed space charge, the capacitance C should vary with bias voltage according to the relation:

$$C = A \left(\frac{\epsilon \epsilon_0 \, q \, N_d}{2(V + V_B)} \right)^{1/2} \quad \text{(m.k.s. system)}, \qquad (3.30)$$

where

A = contact area,

N_d = donor density

V = applied reverse bias voltage

V_B = diffusion voltage at the contact

q = electronic charge

Hence in the case of Schottky type barrier a plot of $1/C^2$ versus reverse bias voltage should be linear.

From the slope of the graph the donor density can be calculated by using the expression:

Table No.15

Donor Density calculated by Barrier Layer Capacitance Measurements

Sample No.	Carrier Concentration (n_c) — Below transition temperature					Above transition temperature								
	25°C	75°C	82°C	100°C	125°C	128°C	130°C	132°C	149°C	150°C	160°C	170°C	178°C	190°C
E_9	1.83×10^{17}	-	-	1.83×10^{17}	1.75×10^{17}	-	-	-	-	-	-	9.86×10^{16}	-	-
E_{11}	4.29×10^{16}	-	-	4.13×10^{16}	-	2.27×10^{16}	-	-	-	-	1.53×10^{16}	-	-	-
T_5	3.97×10^{16}	-	2.97×10^{16}	-	-	-	-	-	1.69×10^{16}	-	-	-	-	-
N_5	1.5×10^{16}	-	-	1.5×10^{16}	-	-	9.76×10^{15}	-	-	-	-	-	-	1.59×10^{15}
S_2	2.66×10^{16}	-	-	2.66×10^{16}	-	-	-	-	-	1.07×10^{16}	-	-	1.09×10^{16}	-
C_3	1.88×10^{16}	1.88×10^{16}	-	-	-	-	-	1.45×10^{16}	-	-	1.13×10^{16}	-	-	-

Table No.16

Carrier concentration by thermo e.m.f. and Barrier layer Capacitance

System	Carrier concentration by (n_c)	
	Thermo e.m.f. (mean value)	Barrier capacitance Value at 25°C
$Ba_{0.9955}Er_{0.0045}TiO_3$	1.2×10^{18}	1.83×10^{17}
$Ba_{0.9945}Er_{0.0055}TiO_3$	8.5×10^{17}	4.29×10^{16}
$Ba_{0.9975}Tb_{0.0025}TiO_3$	9.55×10^{16}	3.97×10^{16}
$Ba(Ti_{0.9975}Nb_{0.0025})O_3$	3.1×10^{17}	1.5×10^{16}
$(Ba_{0.795}Ca_{0.2}Er_{0.005})TiO_3$	2.5×10^{17}	1.88×10^{16}
$(Ba_{0.895}Sr_{0.10}Er_{0.005})TiO_3$	3.1×10^{17}	2.66×10^{16}

$$N_d = \frac{2}{A^2 \, q \in \in_o \, m} , \qquad (3.31)$$

where m = slope.

Values of N_d thus obtained at various temperatures are given in table No.15.

This study leads to the conclusion that the carrier-concentration remains almost the same throughout the temperature range of PTCR.

For comparison, the values calculated from thermo e.m.f. and barrier layer capacitance measurements are listed in the table No.16. Values obtained from barrier layer capacitance measurements are near about 10 times less than those obtained by thermo e.m.f. measurements. An inaccurage knolwedge of the emitting surface area and the formation of a non ideal Schottky barrier at the metal - semiconductor junction may be considered as possible reasons for this deviation.

REFERENCES:-

1. F.A.Kroger, G.Diemer and H.A.Klassens; Phys Rev. 103, 279 (1956).
2. H.A.Sauer and S.S.Flaschen. Proc. 7th electron. Components symp, Washington, D.C.(N.Y.) pp. 41-46 May (1956).
3. S.S.Flaschen and L.G.VanUitert, J Appl,phys. 27, 190 (1956).
4. D.R.Turner and H.A.Sauer, J.electrochem.soc. 107, 250 (1960).
5. H.A.Sauer and J.R.Fisher, J.Am.cer.soc 43, 297 (1960).
6. V.J.Tennery and R.L.Cook, J.Am.Cer.Soc 44, 187 (1961).
7. W.D.Johnston and D Sestrich, J.Inorg. and Nucl. Chem. 20, 32 (1961).
8. J.Kainz, Ber Deut. Keram Ges. 35, 69 (1958).
9. Ichiro Ueda and Seiji Ikegami, J.phys.soc. Japan. 20, 546 (1965).
10. G.H.Jonker, Solidstate electronics 7, 895 (1964).
11. P.W.Haayman, R.W.Dam and H.A.Klassens, German Pat 929,350 June (1955).
12. R.H.Dungan, D.F.Kane, and L.R.Bickford, J.Am. cer. soc. 35, 318 (1952).

13. Malcolm McQuarrie, J.Am. cer.soc. 38, 444 (1955).

14. R.C.Devries and R.Roy, ibid, 38, 142 (1955).

15. Vgl.Z.B.Mequarrie, Bull.Am.cer.soc. 34, 256 (1955).

16. A.Von Hippel, "Dielectrics and waves" pp 205, John Wiley and sons. Inc. (N.Y.) (1954).

17. W.T.Peria, W.R.Bratschun and R.D.Fenity, J.Am.cer.soc. 44, 249 (1961).

18. W.Heywang, J.Am. cer.Soc. 47, 484 (1964).

19. J.B.MacChesney and J.F.Potter, (ibid) 48, 81 (1965).

20. C.G.Koops, Phys, rev 83, 121 (1951).

21. J.C.Maxwell, "Electricity and magnetism." London, Oxford Univ. press. Vol. 1, sect 328.

22. A.F.Ioffe, "Physics of Semiconductors" pp 305, Infosearch Ltd London (1960).

23. R.Zuleeg and R.S.Muller, Solidstate electronics 7, 575 (1964).

24. H.K.Henisch, "Rectifying semiconductor contacts" Oxford Univ. press, London (1957).

25. R.S.Muller, J.Appl. Phys. 34, 2401 (1963).

26. Victor J. Tennery and R.L.Cook, J.Am. cer.soc 44, 187 (1961).

C H A P T E R - 4

CHAPTER - 4

A THEORETICAL ANALYSIS OF RESISTIVITY ANOMALY

4.1 INTRODUCTION

In this chapter, we shall give an alternative mechanism of the resistivity anomaly in semi-conducting ferro-electrics (e.g. $BaTiO_3$ doped with various impurities). The central theme of the formulation resides in the idea of carrier scattering by spatial polarization fluctuations. The mechanism envisaged is operative in addition to the usual thermal scattering wherein the carriers are scattered by quanta of lattice-vibration modes (phonons). In some earlier work (Shukla and Sinha[1]), it was shown that owing to electron-vibration coupling permanent dipole moments are formed in the elementary octahedra comprising TiO_6 in $BaTiO_3$ near the Curie temperature. These eventually get ordered below this temperature in the ferro-electric state, the instability of the transverse optical mode affecting this transition. Further, some recent neutron scattering data on $BaTiO_3$ suggest (Blume and Yamada[2]) that just above the Curie temperature the long-range order breaks down but the permanent dipoles persist. In a way, this amounts to order-disorder transition wherein there is short-range order even beyond the transition temperature.

The present theoretical model takes full cognizance of this experimental fact. Thus in the completely ordered phase, the carriers will see the ideally periodic array of dipoles and will not suffer any scattering apart from the phonon processes. However, above the transition temperature there will be scattering due to 'broken' translation symmetry of the dipoles. We shall see that the final mathematical expression reflects the above situation automatically. In the present treatment, the carriers are assumed to have itinerant character as exemplified by Bloch electrons. There is no difficulty in extending it to localised carriers which are apt to show a hopping type motion, possibly phonon assisted (Sinha and Sinha[3]). We have taken the former picture in view of the fact that there is strong evidence of band type conduction in $SrTiO_3$ semi-conductors (Frederikse _et al._[4]).

4.2 Mathematical Formulation

For this purpose, we consider a system of free carriers moving in the periodic potential of atoms and a system of point electric dipoles. Above the Curie temperature, the orientation of the dipoles in certain short-range region (henceforth referred to as 'pockets') may be the same, but they differ from pocket to pocket.

The Hamiltonian for such a system can be written as

$$H = H_e + H_D + H_{eD} + H_{ep} + H_p + \ldots , \quad (1)$$

where H_e is the electronic part of the Hamiltonian and has the explicit form

$$H_e = \sum_i - \frac{\hbar^2 \nabla_i^2}{2m} + \sum_i V(r_i) \equiv \sum_i H_e(i). \quad (2)$$

Here the first term represents the kinetic energy operator of the electrons and the second term the potential energy in the periodic field of atoms; m is the mass of the electron, $-\hbar^2 \nabla_i^2 = p_i^2$ - the square of the momentum operator and $\underline{r}_i$ is the electronic coordinate. The single-electron eigenfunctions are given by

$$H_e(i)\, \varphi_{\underline{k}t} = E_{\underline{k}t}\, \varphi_{\underline{k}t} , \quad (3)$$

where $\underline{k}$ is the wave-vector and t the band index, $E_{\underline{k}t}$ is the corresponding energy eigen-value. $\varphi_{\underline{k}t}$ has the usual Bloch form

$$\varphi_{\underline{k}t} = \frac{1}{\sqrt{\Omega}}\, u_{\underline{k}t}\, e^{i\underline{k}\cdot\underline{r}} , \quad (4)$$

where Ω is the normalization volume, $u_{\underline{k}t}$ is a periodic

function. As we shall confine our attention to one band only (the conduction band), we shall drop the band index henceforth. Also in the effective mass (m^*) approximation

$$E_k = \hbar^2 k^2/2m^* \tag{5}$$

H_D is the Hamiltonian for the system of interacting dipoles. Its explicit form will not be needed in the present formulation. Likewise, H_p and H_{ep} are the pure phonon and electron-phonon interaction terms. We shall not require their explicit forms as their contributions are already known. H_{eD} is the Hamiltonian for electron-dipole interactions with the form,

$$H_{eD} = -\sum_{li} \frac{e\underline{\mu}_l \, (\underline{r}_i - \underline{R}_l)}{\epsilon_{eff} \left|\underline{r}_i - \underline{R}_l\right|^3} , \tag{6}$$

where e is the electronic charge, $\underline{\mu}_l$ the electric dipole moment vector of the lth dipole whose vector coordinate is $\underline{R}_l$, ϵ_{eff} is an effective dielectric constant of the medium. This takes care of the dielectric polarization induced by the excess carriers produced by the dopants.

For subsequent calculations, it is convenient to recast the interaction term (cf. equation (6)) in terms of Fourier components. Its form in the reciprocal space representation can be shown to be

$$H_{eD} = \frac{i}{\hbar} \sum_{l,i,\lambda} \frac{4\pi e}{\epsilon_{eff}} \frac{(\underline{\mu}_l \cdot \underline{\lambda})}{\lambda^2} \exp[-i\underline{\lambda} \cdot (\underline{r}_i - \underline{R}_l)] , \qquad (7)$$

where $\underline{\lambda}$ is a vector in the reciprocal space. Now the resistivity is related to the relaxation time $\langle \tau \rangle$ averaged over the thermal distributions. Or more explicitly

$$\rho = \frac{m^*}{ne^2 \langle \tau \rangle} , \qquad (8)$$

where n is the number of carriers per unit volume and

$$\langle \tau \rangle = \frac{2}{3k_B T} \cdot \frac{\int E_k \tau(E_k)\, e^{-E_k/k_B T}\, N(E_k)\, dE_k}{\int e^{-E_k/k_B T}\, N(E_k)\, dE_k} \qquad (9)$$

where k_B is the Boltzmann constant, $N(E_k)$ is the density of states and for (5) takes the form

$$N(E_k) = \frac{1}{2\pi^2} \left(\frac{2m^*}{\hbar^2} \right)^{3/2} E_k^{1/2} \qquad (10)$$

In the above $\tau(E_k)$ is the relaxation time which depends on energy E_k. We shall now derive its explicit form for interaction term given in (7). For this purpose we shall require the scattering matrix element

$$\left|\left\langle \underline{k}' \left| H_{eD}^{(i)} \right| \underline{k} \right\rangle\right| \equiv \int \psi_{k'}^{*} \, H_{eD}^{(i)} \psi_{\underline{k}} \; d\Omega \qquad (11)$$

$$= \sum_{l} \frac{i}{\Omega} \frac{4\pi e}{\epsilon_{eff}} \frac{(\underline{\mu}_l \cdot \underline{\lambda})}{\lambda^2} \, e^{-i\underline{\lambda}\cdot\underline{R}_l} \, \delta_{\underline{k}-\underline{k}', \underline{\lambda}+\underline{g}} \qquad \ldots\ldots (12)$$

where in getting (12) we make use of the function (4). The Krönecker $\delta_{\underline{k}-\underline{k}', \underline{\lambda}+\underline{g}}$ indicates the interference condition $\underline{k} - \underline{k}' = \underline{\lambda} + \underline{g}$ in the scattering process for an electron with wave vector $\underline{k}$ to $\underline{k}'$. We shall confine ourselves to elastic and normal processes i.e. $|\underline{g}| = 0$, $\underline{g}$ being the reciprocal lattice vector. Also $|\underline{k}| = |\underline{k}'|$. Now the relaxation frequency $1/\tau_{\underline{k}}$ is given by (Wilson[5])

$$\frac{1}{\tau_{\underline{k}}} = \frac{k^2}{\pi\hbar} \left(\frac{\partial k}{\partial E_k} \right) \Omega \int \left|\left\langle \underline{k}' \middle| H_{eD}^{(i)} \middle| \underline{k} \right\rangle\right|^2 (1 - \cos\theta) \sin\theta \, d\theta \qquad \ldots\ldots (13)$$

In writing (13) we have assumed complete isotropy i.e. the matrix element $\langle \underline{k}' | H_{eD}^{(i)} | \underline{k} \rangle$ depends only on the magnitude of $\underline{k}$ and angle between $\underline{k}$ and $\underline{k}'$. The quantity $\left|\langle \underline{k}' | H_{eD}^{i} | \underline{k} \rangle\right|^2$ can be re-written as (cf. (12))

$$\left| \langle \underline{k}' | H_{eD}^{(i)} | \underline{k} \rangle \right|^2$$

$$= \frac{16\pi^2 e^2}{\Omega^2 \epsilon_{eff}^2} \left(\sum_{l} (\underline{\mu}_l \cdot \underline{\lambda}) e^{i\underline{\lambda}\cdot\underline{R}_l} \right) \left(\sum_{l'} (\underline{\mu}_{l'} \cdot \underline{\lambda}) e^{-i\underline{\lambda}\cdot\underline{R}_{l'}} \right)$$

$$= \frac{16\pi^2 e^2 \mu^2}{\Omega^2 \epsilon_{eff}^2 \lambda^2} \left\{ \left(\sum_{m} \cos\theta_m \, e^{i\underline{\lambda}\cdot\underline{R}_m} \right) \left(\sum_{\Delta} e^{i\underline{\lambda}\cdot\underline{\Delta}} \right) \right\}$$

$$* \left\{ \left(\sum_{m'} \cos\theta_{m'} \, e^{-i\underline{\lambda}\cdot\underline{R}_{m'}} \right) \left(\sum_{\Delta'} e^{-i\underline{\lambda}\cdot\underline{\Delta}'} \right) \right\}, \quad \ldots\ldots\ldots\ldots (14)$$

where we have assumed that the magnitude of the dipoles $|\mu_l| = |\mu_l'| = \mu$. Here m and m' span the centres of the pockets assumed to be spherical and of mean radius Λ. $\underline{\Delta}$ and $\underline{\Delta}'$ refer to the position vectors of dipoles inside a pocket.

In the paraelectric phase (i.e. beyond the Curie temperature) the direction of the macroscopic polarization varies randomly from one pocket to another. We shall, therefore, use random phase approximation in dealing with the product in (14). Thus only diagonal terms will survive. After some mathematical computation this reduces to

$$\left| \langle \underline{k}' | H_{eD}^{i} | \underline{k} \rangle \right|^2 = \frac{16\pi^2 e^2}{\epsilon_{eff}^2} \left(\frac{N_d}{\Omega^2} \right) \nu_d \, \frac{\mu^2}{\lambda^2} \, F(x) , \qquad (15)$$

where

$$F(x) = 3 \left(\frac{x \cos x - \sin x}{x^3} \right)^2 \qquad (16)$$

with $x = \lambda \Delta$, N_d is the total number of dipoles in the crystal and ν_d = the average number of dipoles per pocket.

In deriving the above, we have used the relation $\left(\cos^2 \theta_m\right)_{av} = 1/3$ and the long wavelength approximation i.e. $\lambda \Delta < 1$.

Substituting (15) in (13) and noting that

$$\partial k / \partial E_{\underline{k}} = m^* / \hbar^2 k \quad \text{and} \quad \lambda^2 = |\underline{k} - \underline{k}'|^2 = 4k^2 \sin^2 \theta/2$$

we get

$$\frac{1}{\tau_{\underline{k}}} = \frac{16\pi^2 e^2 \mu^2 \; \nu_d n_d m^*}{\pi \; \epsilon_{eff}^2 \; \hbar^3} \times \frac{1}{2k} \int_0^{\pi} F(x) \sin \theta \, d\theta \qquad \ldots\ldots\ldots (17)$$

which on integration reduces to

$$1/\tau_{\underline{k}} \approx \frac{16}{3} \; \frac{\pi e^2 \mu^2 \nu_d n_d m^*}{\epsilon_{eff}^2 \; \hbar^3} \; \frac{1}{k} \left(1 - \frac{\Delta^2 k^2}{10} \right), \qquad (18)$$

where n_d is the number of dipoles per unit volume.

As we are using the long-wavelength expression

$$\tau_{\underline{k}} \approx \frac{3 \epsilon_{eff}^2 \hbar^3}{16\pi e^2 \mu^2 \nu_d n_d m^*} k \left(1 + \frac{\Delta^2 k^2}{10}\right) \qquad (19)$$

On making use of the relation (5) we get

$$\tau(E_k) = B\left[\left(\frac{2m^*}{\hbar^2} \right)^{1/2} E_k^{1/2} + \frac{\Lambda^2}{10} \left(\frac{2m^*}{\hbar} \right)^{3/2} E_k^{3/2} \right], \qquad (20)$$

where

$$B = \frac{3\, \epsilon_{eff}^2\, \hbar^3}{16\pi e^2 \mu^2\, \nu_d n_d m^*} \qquad (21)$$

Substituting (10) and (20) in (9) we get

$$\langle \tau_{av} \rangle = \frac{\frac{2B}{3k_BT} \int_0^\infty E_k^{3/2} \left[\left(\frac{2m^*}{\hbar^2}\right)^{1/2} E_k^{1/2} + \frac{\Lambda^2}{10} \left(\frac{2m^*}{\hbar^2}\right)^{3/2} E_k^{3/2} \right] e^{-E_k/k_BT}\, dE_k}{\int_0^\infty e^{-E_k/k_BT}\, E_k^{1/2}\, dE_k}$$

$$= \frac{2B}{3k_BT} \frac{\left[(k_BT)^{3/2} \left(\frac{2m^*}{\hbar^2}\right)^{1/2} \Gamma(3) + \frac{\Lambda^2}{10} \left(\frac{2m^*}{\hbar^2}\right)^{3/2} (k_BT)^{5/2}\, \Gamma(4) \right]}{\Gamma(3/2)} \qquad \ldots\ldots (22)$$

where $\Gamma(n)$ is the usual gamma function. Finally, with the help of (22) and (6), the contribution to resistivity due to polarization fluctuation is

$$\rho_{pf} \approx \frac{\sqrt{2}\, \pi^{3/2} (m^*)^{3/2}\, \nu_d n_d \mu^2}{(k_BT)^{1/2}\, n\, \epsilon_{eff}^2\, \hbar^2} \frac{1}{\left[1 + \frac{\Lambda^2}{L_T^2}\right]}, \qquad (23)$$

where L_T represents wavelength of the thermal electrons given by

$$L_T^2 = \frac{\pi\hbar^2}{2m^* k_B T} \qquad (24)$$

It is expected that the pocket of short range order will have dimension smaller than L_T. Thus

$$\rho_{pf} = \frac{\sqrt{2}\, \pi^{3/2}\, (m^*)^{3/2} \nu_d n_d \mu^2}{(k_B T)^{1/2} m^* \epsilon_{eff}^2\, \hbar^2} \exp\left[- \frac{\Lambda^2}{L_T^2} \right] \qquad (25)$$

The exponential function in (25) is a sort of space-correlation function and reflects the stochastic assumption made. The total resistivity, inclusive of the lattice (phonon) scattering is given by (recalling Matthiessen's rule[5])

$$\rho_t = \rho_T + \rho_{pf} \qquad (26)$$

where ρ_T is the usual resistivity due to thermal scattering and its temperature dependence will be governed by the mode of phonon scattering i.e. one phonon or two phonon processes (Krishnamurthy and Sinha[6)]). Whatever may be the details of this, this will not give rise to PTCR anomaly.

4.3 Estimates and discussion

Below the transition temperature the entire resistivity contribution comes from ρ_T (the phonon part). The reason is that in the ordered phase when $\cos \theta_1 = \cos \theta_1'$, where

the pockets are very large, the matrix element (cf equation (12)) vanish identically in virtue of lattice summation i.e.

$$(\underline{\mu}.\underline{\Delta}) \sum_{1'} e^{-i\Delta.\underline{R}_1'} = \delta(\underline{\lambda})\ (\underline{\mu}.\underline{\Delta})\ N. \equiv 0 \qquad (27)$$

where $\delta(\underline{\lambda})$ is the Dirac delta function and has the property $\lambda\delta(\lambda) = 0$. At the transition temperature, the long range order falls abruptly and there will be a jump in the resistivity. The magnitude of the jump is controlled by the value of Λ and the ratio (μ/ϵ_{eff}). The dipole moment is related to the dielectric constant (for large value of ϵ) $\epsilon \propto \mu^2$. Thus the dependence of ρ_{pf} on ϵ_{eff} alone is $\rho_{pf} \propto \frac{1}{\epsilon_{eff}}$. This alone cannot explain the jump actually observed and the exponential factor does play a role. As temperature is raised the pocket size (the range of short-range order) will decrease and ρ_{pf} will continue increasing. However, there will be a maximum at some temperature (at some values of Λ), namely

$$\Lambda = L_T \sqrt{\frac{3}{5}} \qquad (28)$$

On the assumption that ν_d = volume of pocket times the number of dipoles per unit volume. The shape of the hump is similar to the experimentally observed results.

We shall now estimate the contribution of ρ_{pf} just beyond the transition temperature (i.e. $400^{\circ}K$ for $BaTiO_3$)

The following values of the parameters involved are taken

$$n_d = 10^{22} \text{ to } 10^{23} \text{ per cm}^3$$

$$n = 10^{17} \text{ to } 10^{18} \text{ per cm}^3$$

$$m^* = \text{electron mass for convenience}$$

$$T = 400^{\circ}K$$

$$\mu = e\,|r| = e\,(0.13) \times 10^{-8} \text{ cm}$$

$$\nu_d = 10^3 \text{ to } 10^4 \text{ per pocket}$$

We are taking the case where $\Lambda < L_T$

$$\epsilon_{eff} = 10^2$$

With this value the resistivity due to dipole fluctuation turns out to be

$$\rho_{pf} \sim 10^3 \text{ to } 10^4 \ \Omega\cdot\text{cm} \tag{29}$$

A typical value of resistivity for the above carrier concentration below the Curie temperature is of the order of 10 $\Omega\cdot$cm which is to be identified with ρ_T. Thus the net increase beyond the transition is

$$\frac{\Delta\rho}{\rho_T} = \frac{\rho_t - \rho_T}{\rho_T} = 10^2 \text{ to } 10^3 \tag{30}$$

This increase is of the right order observed in most of the experimental results.

Now a few comments about this mechanism in relation to experimental results and other theories are in order. In all ferroelectric systems the PTCR anomaly is closely associated with the appearance or disappearance of dipole ordering. Since our theory depends on the polarization fluctuation in space, it is in complete accord with these results. The experimental results of Brown and Taylor[7] on single-domain crystals shows that there is a resistivity rise by a factor of the order of 10^1 to 10^2. Thus the PTCR anomaly is not necessarily associated with the surface states in the grain boundaries in polycrystals. However, it is to be admitted that in polycrystalline samples the effects visualised in the present mechanism will be further enhanced as the pockets (of short range order) become smaller in size.

We have assumed the carrier concentration n to be fairly constant in the temperature range of interest. Of course, at very high temperatures, the number of carriers will increase and the resistivity will start falling as, indeed, observed.

REFERENCES

1) Shukla G.C. and Sinha K.P., J. Phys. Chem. Solids, 27, 1837 (1966)

2) M.Blume and Y. Yamada: Private communication to Dr.K.P.Sinha.

3) Sinha A.P.B. and Sinha K.P., Indian J. Pure Appl. Phys., 1, 286 (1963).

4) A.P.R.Frederikse, J.W.R.Thurber and W.R.Hosler, Phys.Rev., 134A, 442 (1964).

5) A.H.Wilson, 'Theory of Metals' Cambridge Univ. Press, 2nd Ed. (1954).

6) B.S.Krishnamurty and K.P.Sinha, J. Phys.Chem.Solids, 26, 1949 (1965).

7) F.Brown and C.E.Taylor, J.Appl.Phys., 35, 2554 (1964).